A study of the bipolar nebula associated with LKH208

Shirt, Janice Victoria

A Study of the Bipolar Nebula associated with LKHα208

by

Janice Victoria Shirt

A thesis submitted to the University of Durham for the Degree of Doctor of Philosophy

September, 1984

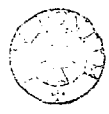

PREFACE

The work described in this text was carried out by the author between 1981 and 1984 whilst a research student at the University of Durham, under the supervision of Dr S.M.Scarrott.

The instrumentation and computer data-reduction techniques were developed by the polarimetry group under Dr Scarrott. The original scattering routines and optimization procedures are the work of R.F.Warren-Smith with some changes having been made by the author in order to accommodate the present data.

The author has undertaken to observe, process and interpret new data of the nebulosity illuminated by the star LKHα208.

ABSTRACT

An investigation of the nebulosity illuminated by the star LKHα208 has been carried out. Observations of the nebulosity were made in four colours. These were used in conjunction with linear polarization measurements for the object to investigate the detailed structure of the nebula.

Numerical modelling of the nebulosity has been carried out. It has been shown that the observations result from the scattering of radiation by dust which is concentrated at the edges of a cavity, the structure of which may be approximated by a paraboloid. The grains comprising the nebula are of high albedo ($>$ 0.8) and low refractive index (1.25 $\pm$ 0.12). It is proposed that icy grain mantles are present in the dust, so yielding these results. The dust grain size distribution takes the form of a power-law distribution such that

$$n(a)=a^{-4.3}$$

where n(a)da is the number density of particles with radii in the range (a, a+da).

CONTENTS

REFLECTION NEBULAE

ILLUSTRATIONS

TABLES

CHAPTER 1

POLARIZED LIGHT

1.1 THE NATURE OF POLARIZED LIGHT

Light is an electromagnetic wave, each elementary wave being described by an electric (E) vector and a magnetic (H) vector which are mutually perpendicular and both perpendicular to the direction of propagation of the wave. Natural incoherent light is unpolarized and consists of a superposition of many such elementary waves, their electric vectors being randomly oriented with no preferential direction (figure 1.1a). If for some reason a beam of light becomes 'polarized' then this means that there is a preferred direction for the electric and

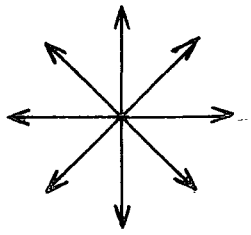

a) Unpolarized light

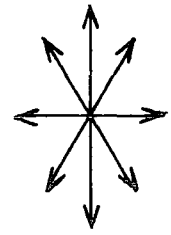

b) Partially, vertically plane polarized light

Figure 1.1
Polarization of a beam of incoherent light

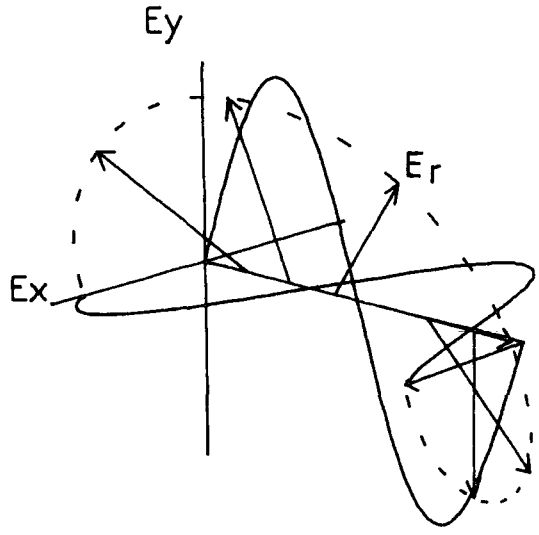

Figure 1.2
Superposition of two elementary waves which have a phase difference between them.

magnetic vectors (figure 1.1b). Since the magnetic vector is always perpendicular to the electric vector, only the electric vector henceforth need be considered.

There are three principal states of polarization : unpolarized, linearly polarized and elliptically polarized. The nature of the latter two can be simply seen by considering the addition of just two elementary waves with $\underline{E}$ vectors perpendicular to each other and with a phase difference between them (figure 1.2). In the simplest case the two $\underline{E}$ vectors may be represented by

$$\underline{E}_x(z,t) = \underline{i}E_{0x}.\cos(kz - \omega t)$$

$$\underline{E}_y(z,t) = \underline{j}E_{0y}.\cos(kz - \omega t + \varepsilon) \qquad .....(1.1)$$

where E_{0x} and E_{0y} are the amplitudes of the waves oscillating in the x and y planes respectively. ε is the relative phase difference between them. k is the constant of propagation and ω is the angular frequency. The resultant wave is given by

$$\underline{E}_r = \underline{E}_x + \underline{E}_y \qquad .....(1.2)$$

and lies in the same plane, perpendicular to the propagation direction. If ε is an even multiple of π then

$$\underline{E}_r = (\underline{i}E_{0x} + \underline{j}E_{0y}).\cos(kz - \omega t) \qquad .....(1.3)$$

or if ε is an odd multiple of π then

$$\underline{E}_r = (\underline{i}E_{0x} - \underline{j}E_{0y}).\cos(kz - \omega t) \qquad .....(1.4)$$

These two cases above, where the waves are either in phase or in anti-phase result in the resultant $\underline{E}$ vector lying in a fixed plane and the wave is said to be linearly polarized.

If ε is arbitrary then it can be shown that

$$(E_y/E_{0y})^2 - 2(E_y.E_x/E_{0y}.E_{0x})\cos\varepsilon + (E_x/E_{0x})^2 = \sin^2\varepsilon \qquad .....(1.5)$$

which is the equation of an ellipse. The resultant vector lies still in the plane perpendicular to the propagation direction and rotates, tracing out an ellipse with time. A special case of elliptical polarization occurs when the amplitudes of the two waves are equal and the phase difference takes values of $\varepsilon = -\pi/2 \pm 2m\pi$ where m = 0,1,2,3, etc. Then

$$E_{0x} = E_{0y}$$

$$\underline{E}_x(z,t) = \underline{i}E_{0x}\cos(kz - \omega t) \qquad .....(1.6)$$

$$\underline{E}_y(z,t) = \underline{j}E_{0y}\sin(kz - \omega t)$$

and $$\underline{E}_r(z,t) = E_{0x}(\underline{i}\cos(kz - \omega t) + \underline{j}\sin(kz - \omega t))$$

which is the parametric equation of a circle. The above combination of the two beams has resulted in right handed

circular polarization, since by convention polarization is right handed if the electric vector rotates clockwise with time, when viewed along the direction of propagation. A phase difference of $\varepsilon = \pi/2 \pm 2m\pi$ will result in left handed polarization.

1.2 STOKES VECTORS OF A SIMPLE WAVE

A more general expression describing the electric vector based on equation 1.1 is

$$\underline{E}_r = \mathrm{Re}[\, E_X \underline{i} + E_Y \underline{j}] \qquad .....(1.7)$$

where

$$E_X = a_X . e^{-i\varepsilon_1} . e^{-ikz+i\omega t}$$

and $$.....(1.8)$$

$$E_Y = a_Y . e^{-i\varepsilon_2} . e^{-ikz+i\omega t}$$

a_X and a_Y are the amplitudes and ε_1 and ε_2 are the phases of the two components of the wave. The Stokes parameters of this wave are described as

$$I = E_X E_X^{\circ} + E_Y E_Y^{\circ}$$

$$Q = E_X E_X^{\circ} - E_Y E_Y^{\circ}$$

$$U = E_X E_Y^{\circ} + E_Y E_X^{\circ} \qquad \text{.....(1.9)}$$

$$V = i[E_X E_Y^{\circ} - E_Y E_X^{\circ}]$$

Simple manipulation leads to

$$I = a_X^2 + a_Y^2$$

$$Q = a_X^2 - a_Y^2$$

$$U = 2a_X a_Y \cos(\delta) \qquad \text{....(1.10)}$$

$$V = 2a_X a_Y \sin(\delta)$$

where $\delta = \varepsilon_1 - \varepsilon_2$

Van de Hulst relates the Stokes parameters to the geometric parameters of an ellipse such that

$$I = a^2$$

$$Q = a^2 \cos 2\beta . \cos 2\chi \qquad \text{....(1.11)}$$

$$U = a^2 \cos 2\beta . \sin 2\chi$$

and

$$V = a^2 \sin 2\beta$$

where a^2 is the intensity of the wave, $\tan\beta$ gives the ratio of the length of the major to the minor axis of the ellipse and is called the ellipticity, and the angle χ gives the orientation of the ellipse with respect to the x axis. These parameters are shown in figure 1.3. A more complete working of the above is found in van de Hulst, 1981.

I, as already stated, measures the intensity of the wave. Q and U describe the state of linear polarization, Q representing the preference of the $\underline{E}$ vector for $\chi = 0$ or the $\pm \pi/2$ directions, and U representing its preference for the $\chi = \pm \pi/4$ directions (figure 1.4). V measures the amount of circular polarization as is clear from a consideration of the parameter β. When $\cos\beta$ equals $\sin\beta$ the ellipticity becomes unity and V = I. Both Q and U become identically zero and the light is completely circularly polarized. Conversely, for completely linearly polarized light, V must be zero such that the ellipticity becomes also zero.

If a plane of reference is chosen other than that used here, then only χ changes, so that I, $(Q^2 + U^2)$ and V are invariant as should be expected.

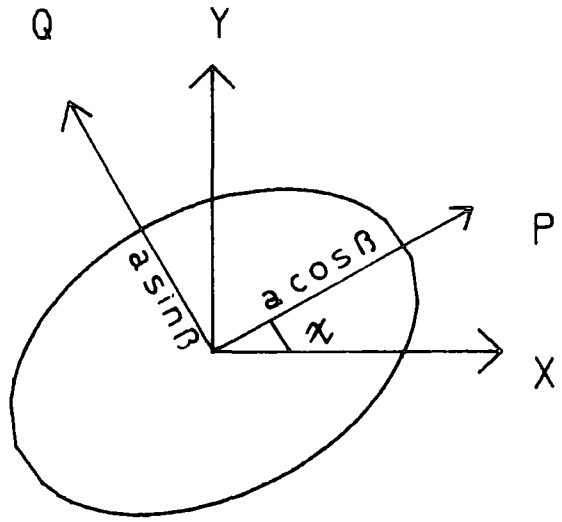

Figure 1.3
Geometric parameters defining the state of polarization of an elliptically polarized wave.P and Q are the principle axes of the ellipse.

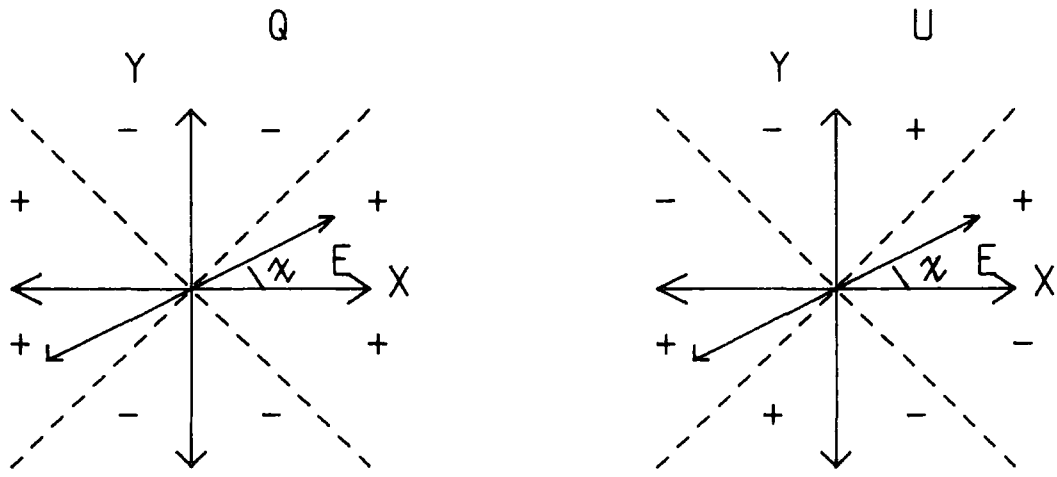

Figure 1.4
The signs of the Stokes parameters Q and U for varying χ

1.3 STOKES PARAMETERS OF INCOHERENT LIGHT

The usefulness of Stokes vectors is seen when the need to analyse incoherent beams of light arises. Here, the phases of the simple waves making up the beam are randomly distributed and interference effects between the beams tend to cancel out so that the resulting Stokes vector of the beam is just simple addition of the Stokes vectors of each individual wave, (van de Hulst, 1981) i.e. for a beam,

$$\begin{aligned} I &= \sum_i I_i \\ Q &= \sum_i Q_i \\ U &= \sum_i U_i \\ V &= \sum_i V_i \end{aligned} \qquad \ldots\ldots(1.12)$$

Since the light being received by a telescope is incoherent the Stokes vectors provide a way of parameterizing the light which is measured.

For an incoherent beam of light it can be shown that

$$I^2 \geq Q^2 + U^2 + V^2 \qquad \ldots\ldots(1.13)$$

the equality only holding if all of the component waves

have the same polarization. The polarized intensity is defined as

$$I_p = (Q^2 + U^2 + V^2)^{1/2} \quad \ldots.(1.14)$$

while the overall degree of polarization is defined as

$$P = (Q^2 + U^2 + V^2)^{1/2}/I = I_p/I \quad \ldots.(1.15)$$

The degree of linear polarization is defined as

$$P = (Q^2 + U^2)^{1/2}/I \quad \ldots.(1.16)$$

with an orientation, θ of the plane of polarization to the x axis of

$$\theta = 0.5 \tan^{-1}(U/Q) \quad \ldots.(1.17)$$

CHAPTER 2

INTERSTELLAR DUST

2.1 INTRODUCTION

Ever since Trumpler presented convincing evidence in 1930 for the widespread existance of dust throughout the plane of the galaxy, astronomers have attempted, with varying degrees of success, to answer several fundamental questions. What is the dust made of ? How is it formed, and how does it interact with the galactic environment ?

A large number of different materials with varying size distributions have been proposed as candidates for the dust and many, fit the observational

data. Overall, all that has been demonstrated is the intractability of the problem we are facing. Even so, steady progress has been made towards developing a comprehensive picture of the physical processes at work in the life cycle of dust grains.

It is clear now, that although the dust has a well defined distribution in the galaxy, the interstellar medium in fact presents a chaotic picture, with dust and gas distributed in clouds of widely varying density, location and physical conditions. Remarkably, there is a large degree of uniformity in the physical properties of the dust.

2.2 EARLY OBSERVATIONS OF INTERSTELLAR DUST

The first hint that the galaxy consisted of more than just stars came two hundred years ago when William Hershel noticed a " hole in the sky ". He was observing part of the Rho Ophiuchi complex and saw regions of the sky apparently devoid of stars. He attributed this to the breaking up of the Milky Way. It was not until 100 years later, with the advent of celestial photography, that a proper interpretation was made. Barnard (1889) attributed the 'holes' to the presence of obscuring dust clouds,which were blocking out the light of background stars.

INTERSTELLAR DUST

Confirmation of the presence of galactic dust came in 1912 when Slipher discovered that the spectrum of the nebulosity in the Pleiades was the same as that of illuminating stars. Until 1930 the question as to whether or not the intervening space between the clouds was empty, remained open.

Trumpler compared luminosity distances to open clusters as derived from their Hertzsprung - Russell diagrams, with distances calculated on the basis of their angular diameters. He was then able to show that the average colour excess of the clusters increased with distance, that is, that starlight becomes progressively more reddened with increasing distance. These results provided convincing evidence for the presence of an absorbing layer of material in the galactic plane.

The colour excess of a star, E(B-V), is the excess of the measured colour index (usually expressed as the (blue-visual) magnitude in the UBV system) over the expected intrinsic value for the star, which is based on its spectral type. Alternatively it is defined as the difference in the extinctions at two wavelengths, λ_1 and λ_2 such that

$$E(\lambda_1 - \lambda_2) = A(\lambda_1) - A(\lambda_2) \qquad .....(2.1)$$

where the extinction $A(\lambda)$ is defined as the difference in the apparent magnitude of the reddened star and an

unreddened star of the same spectral type at the wavelength λ.

Photoelectric photometry brought new discoveries. 1934 saw the discovery of the diffuse interstellar bands by Merrill, which still remain unexplained in detail. Only recently, Herbig (1975) published a list of 39 diffuse absorption features between 4430 Å and 6850 Å, with the strongest of these features being centred on 4430 Å and 6850 Å. They are observed in the spectra of highly reddened stars and Herbig believes that they are interstellar in origin.

New data aquired in the visual (Hall, 1937 : Whitford, 1948) demonstrated that the interstellar extinction is inversely proportional to the wavelength, which implies that the grains responsible for this extinction should have sizes ~ the wavelength of the visible light. Henyey and Greenstein (1941) after studying the light scattered by reflection nebulae, and also the diffuse galactic light, proposed that the grains were strongly forward scattering and of high albedo, the albedo of a particle being defined as the ratio of the scattering cross section to the extinction cross section. Mie scattering calculations are now commonly used to calculate the properties of visual light after interaction with dust grains.

Lindbland (1935) led the field on ideas concerning

the formation of the grains. He suggested that small particles could form by accretion of atoms in space. Van de Hulst (1943, 1949) took the idea of Lindbland and proposed that the three most condensable species, oxygen, carbon and nitrogen, could combine with hydrogen and condense onto a suitable nucleus. (The exact nature of this nucleation process is still a problem). His final mixture was composed of water, ammonia and methane in the form of frozen grains. The mixture became known as 'dirty ice' and the model implied that 1% of the material between the stars should be water. Such a high value for the water content motivated Danielson et al., (1965) and Knacke et al., (1969) to search for the strongest of the ice absorption features which is that at 3 μm. To their surprise, their results in the diffuse interstellar medium were negative and generous estimates could only place the water content at 10% of that expected. Several years later however, the 3 μm feature was observed in the Becklin-Neugebauer object (Gillett et al., 1973) which is a protostellar object in the Orion molecular cloud. The implications of this and many other subsequent observations will be discussed in some detail later.

Exploration of the ultra-violet regime for any uv extinction law was initially severely hampered due to the high absorption of uv radiation by our atmosphere. Ground based observations were misleading, suggesting a

saturation in the extinction at 4 μm^{-1}. This would be expected, irrespective of refractive index, from the large 0.1 μm particles which were assumed to produce the observed visual extinction (van de Hulst, 1957 ; Greenberg and Shah, 1969). However, observations above the atmosphere using rockets (Boggess et al., 1964 ; Stecher 1965) demonstrated a rise in extinction into the uv. Stecher found the first structure in the curve which is now known as the 2175 Å (4.6 μm^{-1}) bump. Observations from the Orbiting Astronomical Observatory, (OAO-2) satellite (Bless and Savage 1970, 1972) confirmed and clarified Stechers results and showed that beyond the bump between 5.8 and 6.2 μm^{-1}, the extinction began to rise again. A wealth of satellite data has shown that this rise continues into the far uv and much attention has been given to the possible origins of these two main features, namely the 2175 Å bump and the far uv rise.

Several averaged and normalized extinction curves showing the features described above, are given in figure 2.1. The references for the various curves are given together with an indication of how many stars were used to derive each curve.

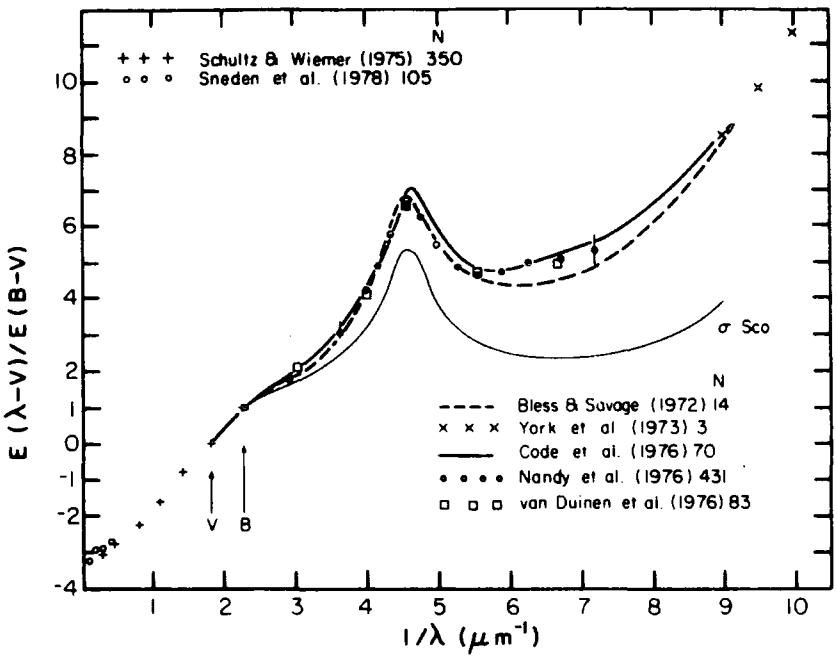

Figure 2.1
Normalized interstellar extinctions plotted against $1/\lambda$. One abnormal uv curve is shown for σ Sco (Bless and Savage, 1972).

(Figure taken from Savage and Mathis, 1979)

2.3 INTERSTELLAR LINEAR POLARIZATION

Interstellar linear polarization was discovered accidentally during searches for intrinsic polarization in early type stellar atmospheres (Hall and Hiltner, 1949). It became clear that whilst extinction may be observed in certain regions without polarization (Hiltner 1956), the converse was not true, thus linking the observed polarization with the dust. That there was a wavelength dependence of the polarization over optical wavelengths, (0.3 - 1.0 μm) was first noted by Gehrels (1960). Optical observations of thousands of early type stars showed that the degree of linear polarization is proportional to the extinction, with a canonical value of 3% per visual magnitude of extinction (Mathewson and Ford, 1970). These observations also revealed a large degree of uniformity in the position angle of the polarization over extensive regions of the sky which implied that not only must the grains be non-spherical, but that they must also be aligned in some way. Grain alignment via their paramagnetic relaxation in an interstellar magnetic field was postulated (Davies and Greenstein 1951) to explain the observed polarizations.

A program to measure the wavelength dependence of

the polarization and its relationship with the interstellar extinction was carried out by Coyne, Gehrels and Serkowski (1974). The resulting curves of polarization against wavelength showed a broad maximum which generally lay somewhere in the visual, with a steep fall off towards the longer wavelengths. The levels of polarization however were found to differ widely from star to star. In spite of this it was shown that for stars which had apparently very different polarizations, curves drawn of P/P_{MAX} against λ_{MAX}/λ, were remarkably uniform as shown in figure 2.2, and followed closely an empirical formula

$$P(\lambda)/P_{MAX} = \exp(-k.\ln^2(\lambda/\lambda_{MAX})) \qquad .....(2.2)$$

where k is found to be 1.5 and λ_{MAX} varies typically from 0.45 μm to 0.8 μm (Serkowski et al., 1975). Theoretical work has shown that P_{MAX} is related to the amount of extinction caused by the dust and the degree of alignment of the grains, while λ_{MAX} probably is related to the average size of the polarizing grains (Huffman, 1977). Serkowski also demonstrated that P_{MAX} was well correlated to the ratios of the colour excesses in the UBVR spectral regions, and that in fact the ratio of total selective extinction, R, which is defined as

$$R=A(V)/E(B-V) \qquad .....(2.3)$$

is related to λ_{MAX} such that

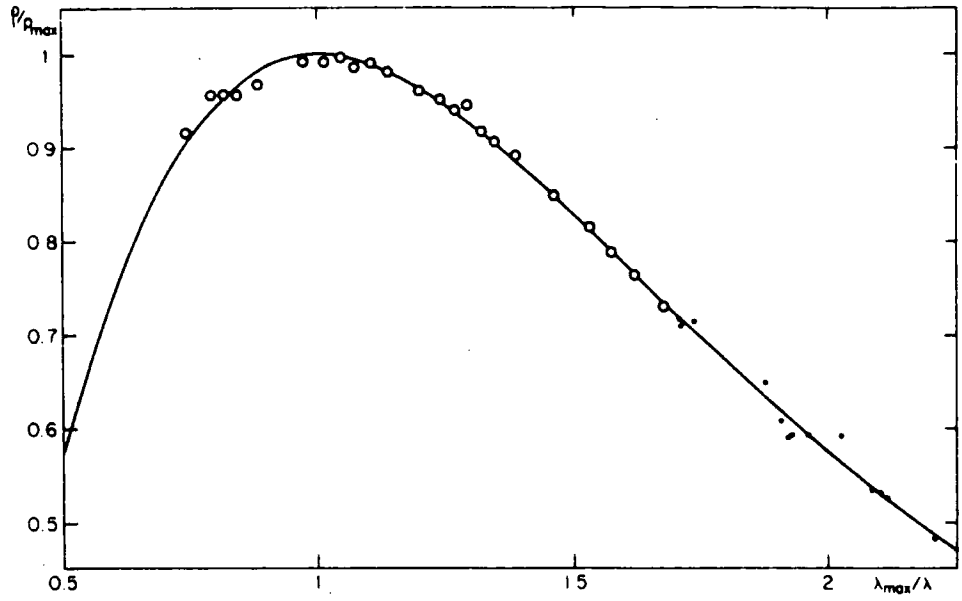

Figure 2.2

The wavelength dependence of interstellar linear polarization. Each open circle is based on 20 stars, while each dot represents observations of individual stars with a particular filter.

(Figure taken from Serkowski et al., 1975)

$$R=5.5\lambda_{MAX} \qquad .....(2.4)$$

Recently, the wavelength dependence of the interstellar polarization has been observed at near infra-red wavelengths (Wilking et al., 1980). When this data was combined with existing optical polarimetry, it was found necessary to modify Serkowski's formula.The data showed a progressive narrowing of the normalized polarization curve as the maximum wavelength increases to near infra-red wavelengths. Wilking allowed the constant k to become a free parameter and so extended Serkowski's formula to the infra-red. He found that k was directly related to λ_{MAX} and that increasing k had the effect of narrowing the curve and visa versa. The wavelength dependence of the interstellar linear polarization from 0.3 - 2.2 μm is now best described by

$$P(\lambda)/P_{MAX} = \exp(-1.17\ \lambda_{MAX}.\ln^2(\lambda_{MAX}/\lambda)) \qquad ....(2.5)$$

Attempts to explain the narrowing of the curve with increasing λ_{MAX}, to actual physical properties of the polarizing grains have met with numerous difficulties. The simplest explanation that could be found, ascribed the variation to either the grains becoming more spherical, as the proportion of large grains present in the dust distribution increases, or that the range of sizes present decreases with an increasing number of large grains.

The physical properties of the grains then have a strong bearing on the interstellar polarization and any interpretation of the extinction curve needs to take note of the constraints placed on them by the interstellar polarization and visa versa.

2.4 ELEMENTAL DEPLETION

Among the initial results from the far ultra-violet spectra obtained by the Copernicus satellite were abundances relative to hydrogen for a number of elements in the interstellar clouds (Rogerson et al., 1973). Analysis of the data which consisted of the interstellar absorption lines of 5 reddened stars (ξ Per, α Cam, λ Ori A, ζ Oph and γ Ara)(Morton et al.,1973), showed that several elements were depleted compared to solar abundances.

Table 2.1 gives the cosmic abundances of the main volatile and refractory elements (Cameron, 1973) and also the fractional amounts of atoms (relative to their cosmic abundance) of the same elements detected in the interstellar gas towards Zeta Ophiuchi (Morton et al., 1974). Note, the extinction spectrum of the Zeta Ophiuchi complex is taken as typical of the interstellar medium.

Clearly this scale of depletion must infer

Table 2.1

Element	Number density relative to H	Fraction of the cosmic abundance detected in the ISM towards ζ Oph
C	3.71×10^{-4}	0.2
N	1.18×10^{-4}	0.2
O	6.76×10^{-4}	0.25
Mg	3.34×10^{-4}	0.03
Si	3.14×10^{-4}	0.03
Fe	2.61×10^{-4}	0.01

something about grain formation. If there had been no previous knowledge of dust then these results would have strongly pointed towards their existence. Since hydrogen was the only molecule detected in high abundance towards Zeta Ophiuchi, and even carbon monoxide, which is the most abundant molecule after hydrogen, could only account for 0.1% of the expected carbon abundance (Morton et al., 1974), it seems unlikely in this case to find the missing mass tied up in molecules. So it was proposed that the heavy elements had been attached to the grains (van de Hulst, 1949 : Spitzer, 1954).

Even today, with the many theories concerning the nature and formation of the grains, there is still difficulty in fully accounting for the missing material. It may be hidden in the large particle end of a power-law distribution of grain sizes, since here the extinction per unit mass is very low, or a large number of as yet unspecified molecules may exist. Another theory is that the material is in the form of comets and the observed depletions may be more closely related to their formation, than that of grains (Greenberg, 1974,1982).

2.5 THE DIFFUSE GALACTIC LIGHT

The attenuation of the light from the stars is achieved through the scattering and absorption of the incident light by intervening material. Investigation of these two processes is yet another way of gaining valuable information concerning the grain material. The scattering of light from dust grains comprising the general interstellar 'haze', gives rise to the diffuse galactic light and its study has been valuable in determining the albedo, a, and the forward scattering (or asymmetry) factor, g, of the interstellar particles. g is given by

$$g = \langle \cos\theta \rangle \qquad .....(2.6)$$

where θ is the scattering angle (measured from the incident direction of the beam). g=0 represents completely isotropic scattering and g=1, completely forward scattering.

Observations of the diffuse galactic light obtained with OAO-2 have enabled Lillie and Witt (1973, 1976) to separate the extinction curve into absorption and scattering components as shown in figure 2.3, which has then allowed the grain albedo and asymmetry factors to be deduced. The values obtained for the albedo and asymmetry

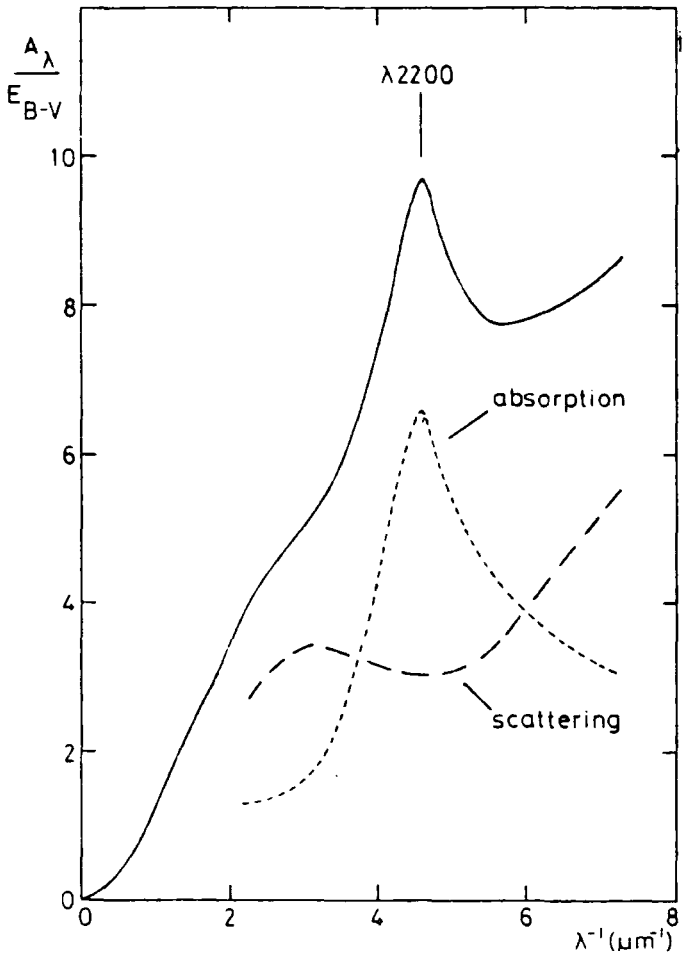

Figure 2.3
The mean observational extinction curve (Savage and Mathis, 1979) showing the contributions from absorption and scattering (Lillie and Witt, 1976)

(Figure taken from Whittet, 1981)

factors at different wavelengths are displayed in figure 2.4. The data clearly shows the extinction bump at 2175 Å to be caused by absorption processes since it coincides with the albedo minimum at a = 0.35 ± 0.05. The albedo increases to 0.7 ± 0.1 at wavelengths beyond 3000 Å and to 0.6 ± 0.05 at wavelengths shorter than 1550 Å. The asymmetry factor lies between 0.6 and 0.9 for the whole wavelength range investigated, indicating that interstellar grains are strongly forward scattering.

The interstellar extinction curve has been of vital importance in furthering our understanding of interstellar dust. The curve will now be discussed in some detail starting with the visible part of the extinction curve and continuing to the uv and ir regions.

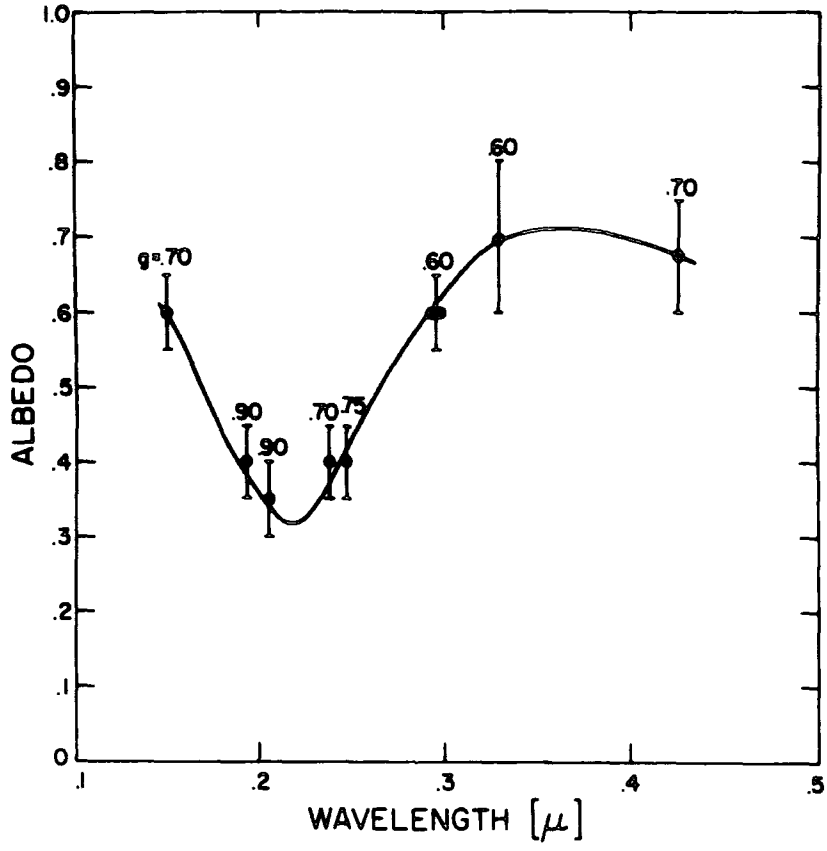

Figure 2.4
The albedo, a, and asymmetry factor, g, plotted as a function of wavelength. The values of g are indicated above the corresponding error bars for a. The uncertainties in g are of the order of ± 0.15.

(Figure taken from Lillie and Witt, 1976)

2.6 STRUCTURE OF THE VISUAL PART OF THE EXTINCTION CURVE

The general form of the visual part of the extinction curve has provided astronomers with information concerning the sizes of interstellar grains. The origin of the diffuse and broad band structures within the curve still remains a point of debate. It seems likely however that they provide information concerning the composition of the grains and the interstellar gas.

The visual extinction is roughly inversely proportional to the wavelength, with the extinction rising slightly towards the blue. It is generally believed that the size of the particles causing the extinction are of the same order as the wavelength of light. Smaller particles would come into the Rayleigh scattering regime where the extinction would follow a λ^{-4} law and much larger particles would lead to a wavelength independent extinction ('grey' extinction). Greenberg (1968) showed that highly absorbing very small grains would have a λ^{-1} law, but Purcell (1969) placed constraints on the mass density of such extinguishing matter that would be needed to produce the observed extinctions. The number of atoms, free molecules and free electrons that would be required was found to be far too high for the interstellar medium,

so this idea was ruled out.

The most notable 'feature' of the curve is an apparent change in the slope of the blue part of the spectrum at 2.3 μm^{-1}. This has been shown quite adequately (Hayes et al., 1973) to be a natural consequence of having a size distribution of grains in the interstellar medium. Really, the general extinction curve in this waveband only tells us information concerning the general size of the grains, since a suitable size distribution usually enables a fit for many different grain materials.

2.6.1 BROAD BAND STRUCTURE IN THE VISUAL EXTINCTION CURVE

Hayes has demonstrated the existence of very broad band stuctures up to 1000 Å wide in the curve. They are shown in figure 2.5. Hayes proposes that grains are responsible for the structures and in particular, that impurities in the grains cause the broad bands. Predicting then that the same structure should be observed in the wavelength dependence of the interstellar polarization, Hayes awaited further observational data. This came in 1974 and is shown in figure 2.6 (Mavko, 1974).

In 1977, Huffman compared the broad band structures with structures in the extinction curves of magnetite, a C1 meteorite (Orgueil) and a C2 meteorite

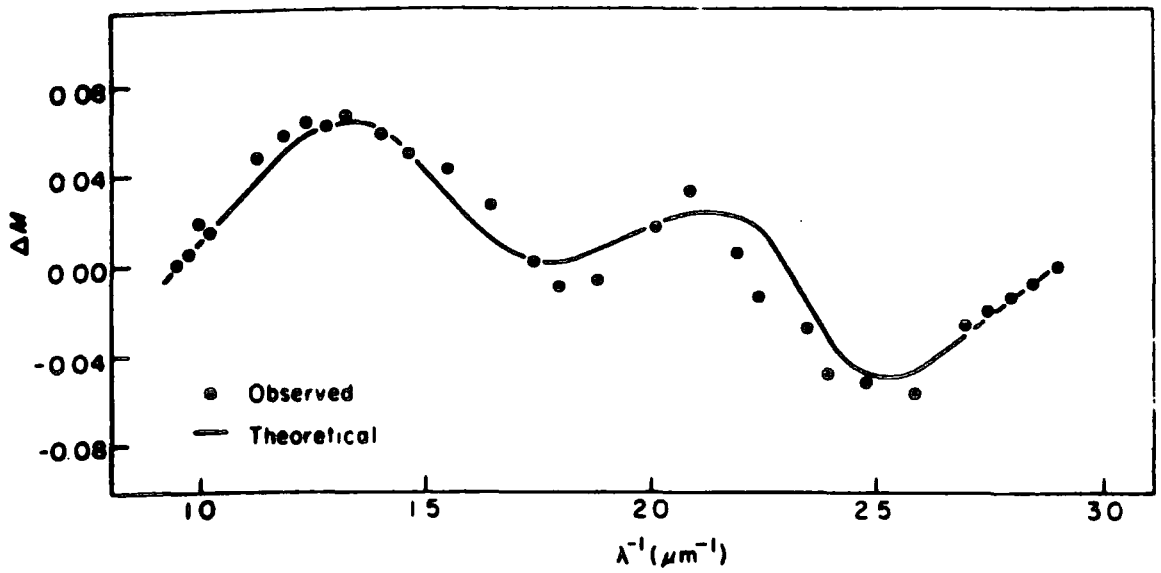

Figure 2.5

Very broad band extinction against $1/\lambda$. The solid line is a theoretical curve of the interstellar extinction derived using an appropriate absorptivity for the grains.

(Figure taken from Hayes et al., 1973)

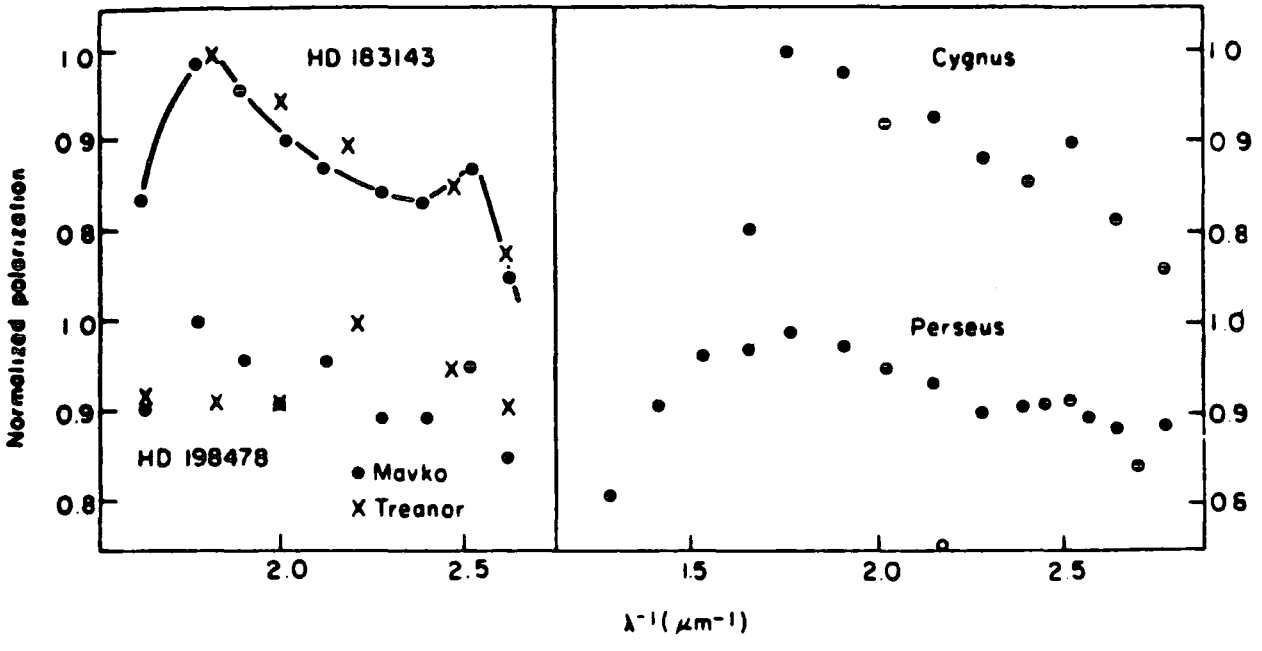

Figure 2.6

A very broad band structure in the linear polarization curves for several stars.

(Figure taken from Mavko et al., 1974)

(Murchison). Both magnetite and orgueil (which contains quite a large amount of magnetite), had broad band structures similar to those in the extinction curve and led Huffman to propose magnetite as responsible for the broad band structure.

2.6.2 THE DIFFUSE ABSORPTION BANDS IN THE VISUAL EXTINCTION CURVE

The origin of the diffuse bands in the visual region remain largely a mystery. Prominent theories are that the bands originate in very small grains (Andriesse, 1977), in impurities in the host particles (Purcell and Shapiro, 1977), in metallic oxide surface transitions (Duley et al., 1979) or in gaseous molecules (Smith et al., 1977).

In order to separate the theories, correlations between diffuse band strengths and various interstellar grain extinction parameters have been eagerly sought. The latter have consisted in the main of the strength of the 2175 Å bump in the uv and the measured colour excesses. Diffuse band strengths are defined

$$E(\lambda-V)/E(B-V) \qquad .....(2.7)$$

where λ is the wavelength of a given diffuse band. The

2175 Å bump strength is defined as

$$E(\lambda_{PEAK})/E(B-V) \qquad .....(2.8)$$

and is the height in magnitudes of the 2175 Å bump peak above a straight baseline drawn between 3000 Å and 1700 Å on a normalized $1/\lambda$ plot.

Many correlations have been found, although some discrepancies exist. Wu, York and Snow (1981) find the strength of the 4430 Å band correlates equally well with the 2175 Å bump strength and the colour excess E(B-V), while Dorschner, Friedman and Gurtler (1977) find the 4430 Å band much better correlated with E(B-V) than with the bump.

A problem with this work is that almost any two parameters will correlate to some degree due to the relatively constant gas to dust ratio throughout the galaxy (Bohlin et al., 1978). Seab and Snow (1984) have tackled this problem and look for correlations after taking account of the above inherent dependence. They find that there are no correlations other than a weak one between the 4430 Å diffuse band and the 2175 Å bump. This would seem to support proponents of a molecular gaseous origin for the 5780 Å and the 6284 Å bands.

Seab and Snow find a complicated correlation pattern between the 4430 Å band and the 2175 Å feature. In regions where the grains possess mantles (Snow and Seab,

1980 ; Goebel, 1983) the observed bump structures and the diffuse band are weaker than normal. The band is strong when observed along lines of sight where the gas and dust temperatures are high. However, in such regions the strength of the 2175 Å feature is shown to vary greatly.

Douglas (1977) showed that semi-detached or impurity isolated carbon chains on a disordered surface would absorb radiation at 4430 Å. This led Seab and Snow to propose that graphite grains are the carriers of the 4430 Å band with the band originating at disordered surfaces in the same way as described by Douglas. They argue that the above mechanism can explain the correlations. In regions where the grains possess mantles it would be expected that the strength of both features would be reduced since the above mechanism would be suppressed by the mantles. In higher temperature regions however, where there are shock waves and other energetic processes increasing the disorder at the grain surfaces, it would be expected that the band strength would be enhanced, without necessarily affecting the bump strength at all.

2.7 STRUCTURE AND INTERPRETATION OF THE ULTRA-VIOLET EXTINCTION CURVE.

The extinction curve in this part of the spectrum has two main features, the extinction bump at 2175 Å and the far uv rise.

2.7.1 THE ULTRA-VIOLET EXTINCTION FEATURE AT 2000 Å

This bump is the most outstanding feature of the entire extinction curve. Its profile is fairly symmetrical with FWHM 480 Å (Savage, 1975), this value being somewhat dependent on the chosen baseline. The strength of the 2175 Å extinction has been shown to be very well correlated with the visual extinction throughout the galaxy, the correlation being demonstrated in figure 2.7. The clear implication then, is that the feature must be interstellar in origin, and that either the same grains are responsible for both extinctions or, if the grains are different, then they must be very well mixed and maintain their relative proportions throughout a large variety of different dusty environments (Savage, 1975 : Nandy et al., 1975 : Dorschner et al., 1977).

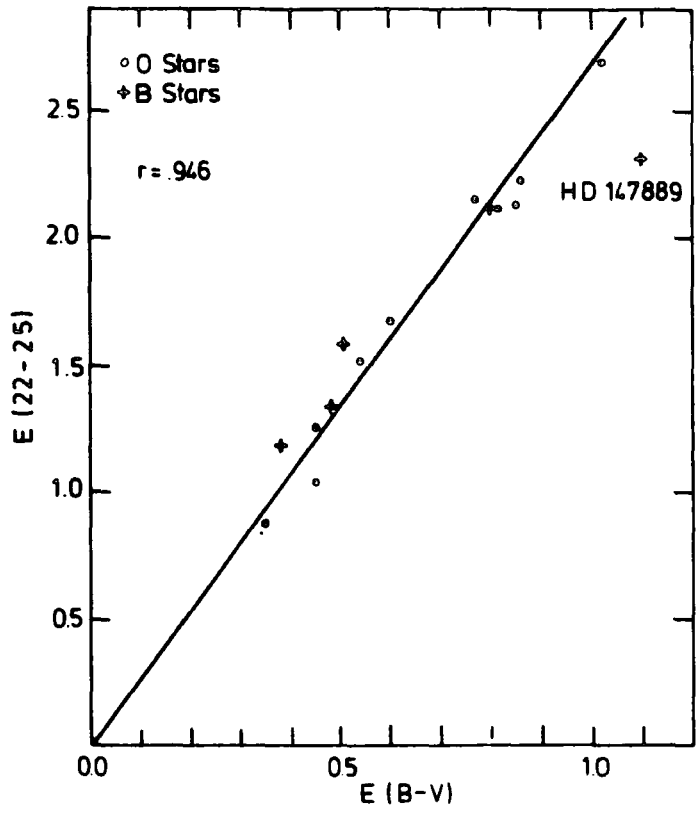

Figure 2.7

Correlation between the 2200 Å feature and the visual reddening; the correlation coefficient is r.

(Figure taken from Greenberg and Chlewicki, 1983)

No theory concerning the origin of the feature is totally secure. Gilra (1972) was the first to propose that very small particles of graphite with sizes ~ 0.01 μm could explain the bump and this theory has with various additions and refinements to the basic model, so far withstood the test of time. Many other candidates such as silicates (orthopyroxene) (Huffman et al., 1971), colour centres in irradiated quartz and absorption by hydrocarbons have been proposed at various times and subsequently shown to be inadequate. The silicates were a good example of how a material can be made to fit the extinction, using Mie calculations and a suitable size distribution, but they were shown to be unlikely by Bless and Savage, 1972). Graphite is still the main contender in attempts to explain this feature.

The major problem with the graphite theories is that the position of the extinction maximum and the shape of the whole feature does not change. This is exemplified in the recent results of Massa et al., (1983). Using the International Ultra-Violet Explorer (IUE), Massa observed stars which were known from ANS (Astronomical Netherlands Satellite) data to have peculiar extinctions. Even for such a set of stars neither the position nor the shape of the 2175 Å feature was found to vary. However, the variation of the complex refractive index of graphite near the resonance, which lies in the region of 2200 Å, is so

pronounced that its wavelength dependence is very sensitive to particle parameters such as size, shape and presence or absence of coatings and this clearly causes problems when trying to explain the invariant features of the interstellar extinction bump. Detailed discussion of this problem is found in a review article by Savage (1975).

The above problem led Mathis et al. (1977) to propose theoretical grain mixtures of combinations of graphite, enstatite, olivine, silicon carbide, iron and magnetite, using up to three at a time, to explain the extinction curve from the ir through to the uv. Cosmic abundances of the various elements were used as constraints on the possible distributions of the materials. Their grains were found to require a power-law distribution of sizes to obtain the best fits. All of the possible mixtures needed graphite to reproduce the bump. The good fits obtained by many combinations in the visual, served to demonstrate that in this band, the extinction is relatively insensitive to the refractive index. They finally proposed a mixture of graphite and silicates, with a size distribution as :

$$n(a) \propto a^{-\theta} \qquad .....(2.9)$$

where n(a)da is the number density of particles with radii in the range (a, a+da), and 0.005 μm < a > 1 μm. The power

index, q, varied between 3.3 and 3.6 for spheres. The graphite made a large contribution to the 2175 Å bump while the silicates did the same for the far uv extinction. Excellent fits were obtained using uncoated grains.

2.7.2 THE FAR ULTRA-VIOLET RISE AND ITS RELATIONSHIP WITH OTHER EXTINCTION FEATURES

Following the slight depression in the curve after the bump, from 5.6 μm^{-1} to 6.2 μm^{-1}, there is rise in extinction into the far uv. Data now being reduced from IUE and ANS satellites are providing much needed information on this part of the spectrum. Recent results have confirmed the long held suspicion that,to quote Massa (1983), 'peculiar ultra-violet extinction is common'.

Meyer and Savage (1981) find that the dust towards many stars exhibits peculiar uv extinctions. They find $E(\lambda^{-1})/E(B-V)$ in samples of normalized extinction curves differing by ± 2 at the extinction bump or at 1500 Å. They also note that the far uv extinctions appear to be totally independent of the 2175 Å bump. Krelowski and Strobel (1983) present extinction curves from Sco OB2 and Per OB1 associations using ANS data. They find the far uv extinctions to be independent of E(B-V) in each

association.

Massa et al., (1983) find that for their sample of stars, the observed variations of the far uv extinction with wavelength, separate out into two classes, which are those where the extinctions arise from clear fields (i.e. extinction is produced by the diffuse cloud medium), and those where the extinction is almost entirely due to localized regions of hot gas and dust.

The present data points towards one thing. There is a need to investigate samples where the extinction is produced by similar environments. This would show whether or not the lack of correlation of the far uv rise with either the 2175 Å bump or the colour excess, E(B-V), is simply an artifact produced by observing the extinction through widely differing environments, where the grains responsible for the extinction may be severely modified by processes such as growth and radiation pressure, and destruction processes such as sputtering etc. The need to avoid complications in such a wealth of data is clearly imperative.

Greenberg and Chlewicki (1983) used early type stars on the verge of emerging totally from their placental cloud (Lada et al., 1978). Having carefully selected their sample so as to minimize local interstellar contributions they used the IUE satellite to aquire extinction data from the diffuse cloud medium to a depth

of 3 kpc. A very high degree of uniformity in the shape of the extinction curve from 1700 Å to 1300 Å was found, the standard deviation from the curvature for 17 stars being only 0.07 magnitudes (which is less than the errors on the data). The data also showed that the far uv rise is totally uncorrelated with the 2175 Å bump, which in turn is correlated with the colour excess in the visual, E(B-V).

On the basis of their results, Greenberg and Chlewicki proposed that the far uv extinction curves all have the same functional form, even though there is a substantial variation by as much as a factor of 3 in the relative strength of the 2175 Å feature and the far uv extinction. Consideration of their findings led them to conclude that totally separate populations of grains must be responsible for these extinction features.

Further to this, Greenberg and Chlewicki proposed that both populations must have extinction cross sections which are size independent and that this is achieved when the particles are such that the extinction is by absorption only i.e. there is no scattering. If graphite based particles are to be held responsible for the bump and silicate based particles for the far uv rise, then on the basis of this theory, they must be limited to sizes which are less than 0.01 μm. The conclusion of this work was that small particles (< 0.01 μm) of some silicate

based and graphite-like substances are required to explain the uv features.

2.8 STRUCTURE AND INTERPRETATION OF THE INFRA-RED REGIME

The study of the interstellar extinction curve was first extended into the ir by Hall, (1937) in his photoelectric investigation of ζ and ε Persei. His observations extended the curve to 1 μm and a relation of the form

$$\Delta m(\lambda) \propto \lambda^{-\alpha} \qquad \ldots.(2.10)$$

was fitted to the observations. Although a coefficient of α=1 fits adequately, a more accurate fit requires α to increase from 1.2 in the visual to 1.6 in the ir. The extension of the curve to wavelengths longer than 1 μm^{-1} was accomplished by Whitford (1948, 1958). The variation of the extinction with wavelength beyond 0.8 μm^{-1} was found to be no longer linear and the curvature corresponded much more to Rayleigh, $1/\lambda^4$ scattering. As with the visual extinction curve, the overall structure in the ir predominantly imparts information concerning the sizes of the grains. However, spectral features of the curve have proved very important. In fact one of the most direct ways to study the chemical nature of the dust in

the interstellar medium is through ir spectroscopy. Such study also affords to us much information concerning the evolution of the dust in differing environments, and has made clear in no uncertain terms that the nature of the grains and their interaction with the interstellar gas is by no means simple. This has led to some workers carrying out laboratory simulations of dust in the interstellar medium in order gain a more detailed understanding of the chemical interactions taking place.

2.8.1 DUSTY ENVIRONMENTS IN THE GALAXY

There are several types of dust environments in which ir observations are important: for example, many stars possess circumstellar dust which when heated radiates thermally in the ir so making investigation of such stars very profitable indeed.

The term 'diffuse cloud medium' refers to dust which is not immediately associated with any particular source. It displays remarkably uniform characteristics throughout the galaxy and has dust temperatures which are very low, typically 10K (Greenberg, 1971). These temperatures are far too low to cause radiation of energy into the ir and the effect of this diffuse dust, as far as ir radiation is concerned, lies in the absorption and

scattering of the incident ir radiation.

In the cores of very dense dust clouds, in regions associated with embedded OB stars and in visible HII regions, both emission and absorption features have been observed at various ir wavelengths. The nature of these features have been found to be strongly dependent on the physical environment where they are formed. The radiation flux is very much reduced by attenuation in these clouds so that the density of photons is often less than that of the atoms and molecules in the cloud. (The converse is true in the diffuse cloud medium.) Temperatures of the dust are typically 50-100 K near very energetic embedded sources. These clouds contain not only dust but many complicated gaseous organic and inorganic molecules, the first of these discovered being formaldehyde (H_2CO) (Snyder et al., 1969). The number now detected is at least 60, the most abundant of these being carbon monoxide. These molecules have largely been detected through radio measurements but their mention in a section on ir data is warranted since, as will be seen, they may have a large part to play in the evolution of a grain.

Discussion will now be concentrated on the spectral features of the ir part of the extinction curve and on the information they have provided.

2.8.2 SPECTRAL FEATURES IN THE INFRA-RED

A summary of the principal spectral features which have been observed in the ir is given in table 2.2. The table indicates the wavelength on which the features are centred, the types of environment where each feature has been observed, and states whether the feature was observed in emission or absorption.

2.8.3 THE 3.1 μm FEATURE

The 3.1 μm absorption band attributable to solid water is, with few exceptions, only seen in spectra of sources associated with dense molecular clouds (Aitken 1981). It was first detected in the Becklin-Neugebauer object (Gillett et al., 1973) whose ir spectrum is shown in figure 2.8. Subsequently it was observed in molecular clouds (Merrill et al., 1976), HII regions (Soifer et al., 1979 ; Willner et al., 1979) and a highly obscured ir source in the Corona Australis dark cloud (Whittet and Blades, 1980). No ice bands of any kind have ever been observed in the diffuse cloud medium.

A number of other minor absorption and emission

Table 2.2

λ(μm)	Emission/ Absorption	Source	First Observers
3.1	absorption	Seen only towards sources associated with dense molecular clouds such as the Becklin-Neugebauer object.	Gillett et al. , 1973
3.3 & 3.4	emission	HII regions in the Orion nebula and M17. Later seen in GL437 which is a cluster of young stars embedded in optical nebulosity	Grasdalen and Joyce, 1976 Kleinmann et al. , 1977
3.4	absorption	Diffuse cloud medium and infra-red sources associated with HII regions.	Willner et al. , 1979
6.2, 7.2 & 11.3	emission	First seen in spectra of infra-red sources HD 44179, NGC7027 and M82.Now observed widely from many sources.	Russell et al. , 1978
9.7	absorption	Becklin-Neugebauer point infra-red source in Orion. This is a very heavily reddened protostar. The feature also was seen in the Kleinmann-Low nebula complex which is situated near the Becklin-Neugebauer object.	Gillett et al. , 1973
9.7	emission	Diffuse, circumstellar envelopes around cool giant oxygen rich stars.	Woolf and Ney, 1969
20.0	emission	As for 9.7 μm emission	Forrest et al. , 1979

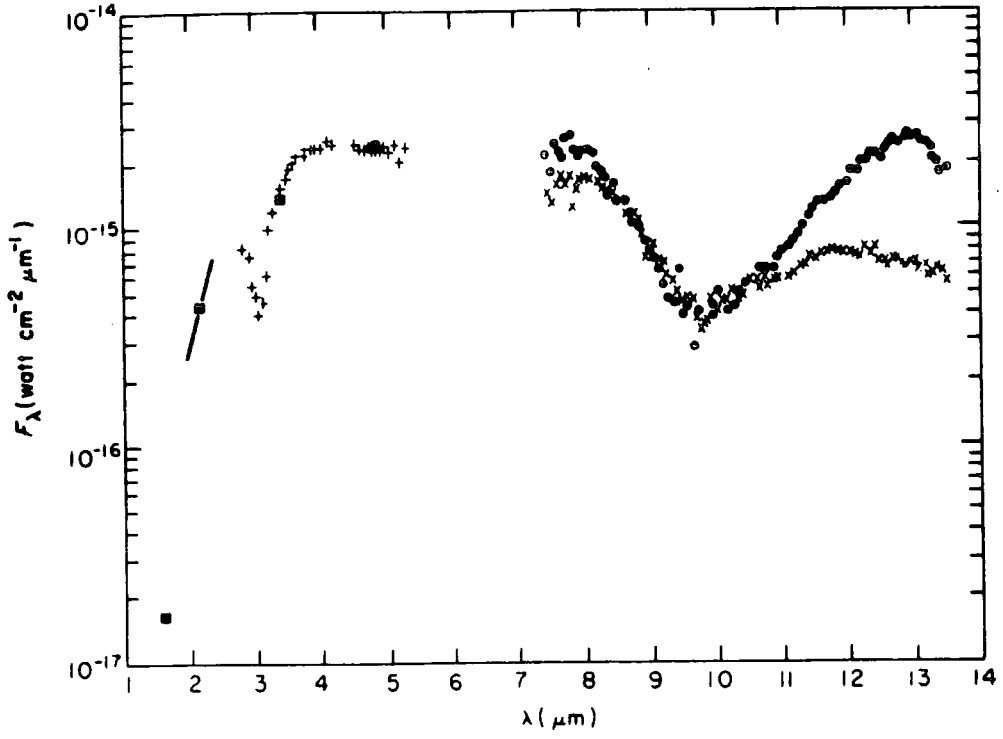

Figure 2.8

Spectrum of the Becklin-Neugebauer star in Orion. The 3.07 μm band is attributed to water-ice and the 9.7 μm feature is attributed to the Si-O stretching mode in silicates.
x's mark the average of 11" beam observations
●'s mark the average of 22" beam observations
+'s mark the average of 11" and 22" beam observations

(Figure taken from Gillet and Forrest, 1973)

features have been seen in some spectra which could be connected to the ice (Willner et al., 1980 : Aitken, 1981) although surface groups as described above have also been proposed as the possible cause.

2.8.4 THE 3.3 μm AND 3.4 μm FEATURES

The 3.3 μm and 3.4 μm features were first observed in emission in HII regions in Orion and M17 by Grasdalen and Joyce, 1976. The 3.4 μm feature was observed in absorption in the spectra of highly reddened stars (Willner et al., 1979 : Wickramasinghe and Allen, 1980). It had been shown earlier that a 3.4 μm feature could be explained by resonances in the C-H bonds of organic material (Duley and Williams, 1979), and the feature in all has provided support for an organic component in the interstellar medium. Both features have since been observed in emission in many other objects such as planetary nebulae, HII regions and galactic nuclei (Dwek et al., 1980 and references therein).

Duley and Williams (1981) propose that both the absorption features seen at 3.4 μm and the emission features seen at 3.3 μm and 3.4 μm arise from small quantities of surface groups bound chemically to active sites on the surface of carbon particles (this proposal is

backed up to some extent by the fact that the emission is particularly strong in C-rich objects (Aitken et al., 1979)). Duley and Williams make the assumption that the carbon particles are not coated with mantles and are free from all other chemical species other than the surface groups. They propose the aromatic CH_3 group to account for the 3.4 μm feature, while aromatic CH groups,which are formed at higher temperatures, account for the 3.3 μm feature. This is consistent with the feature seen being only in emission towards bright ir sources. Duley and Williams also tentatively suggest that other surface groups could be responsible for many other observed ir features, such as aromatic amines (NH_3) which could produce observed emission at 6.2 and 7.2 μm.

2.8.5 THE 9.7 AND 20.0 μm FEATURES

The 9.7 μm feature was first observed in 1973 in absorption towards a new strong ir source found in the Orion nebula and known as the Becklin-Neugebauer object (Gillett et al., 1973). It has subsequently been observed in many ir sources (Merrill, 1976) and is believed to be due to the Si-O stretching mode in silicates. This explanation however predicts that another related feature should be seen at 20 μm. The subsequent observation of

this feature in the spectra of 10 cool, giant oxygen-rich stars by Forrest et al., (1979) seemed to confirm the silicate presence although the exact nature of the material still remains unknown. The best fits to observations have been obtained using amorphous or hydrated silicates (Dorschner et al., 1980). In fact, the observation of both these features in the envelopes of the oxygen-rich stars has caused Dyke and Longsdale, (1981) to argue for the production of silicate grains in the dusty envelopes.

There are however several serious threats to silicate identification. Millar and Duley (1978) show that mixtures of silicon and magnesium oxides display similar characteristics at the same wavelengths as the silicates.

Hoyle and Wickramasinghe (1980) propose that polymers such as polysaccharides and other organic compounds provide better fits to the ir spectrum towards the dusty source OH26.5+0.6 than silicates. The major objection to this theory is that Hoyle and Wickramasinghe are attempting to fit the features of oxygen rich stars where no organic molecules have yet been detected. Also the 9.7 μm feature has not been observed in the spectra of carbon stars which would provide a more favourable site for organic molecule formation. The Hoyle model also has difficulty with the general lack of the 3.1 μm water feature towards highly obscured sources.

2.8.6 THE 11.3 μm FEATURE

This feature was first observed in emission in the circumstellar features of carbon stars and was attributed thermal emission from small carbonate dust grains (Gillett et al., 1973). Gilra (1973) attributed the features directly to silicon carbide. Observations of many ir sources such as CRL437 (Kleinmann et al., 1977), NGC253 (Gillett et al., 1975) and CRL3058 (Gillett et al., 1978) to name but a few have resulted in positive identification of this band. Duley and Williams (1981) again show that the aromatic CH group attached to a carbon core particle as discussed above could provide an alternative origin.

2.8.7 INTERACTIONS OF THE INTERSTELLAR DUST AND GAS

The discovery of formaldehyde in the interstellar gas coupled with the suggestion in 1973 by Greenberg, that the negative ice results towards the highly reddened stars CIT II and VI Cygni 12 could be due to the break up of dirty ice mixtures by ultraviolet photolysis, caused speculation that the two apparently unconnected events may

be related. In fact, Greenberg went so far as to propose that an equilibrium between the molecules observed in the gas phase, and those accreted on the grains could be maintained by the sporadic release of chemical energy stored on the grains in the form of frozen radicals. These are produced in the mantle by photolysis.Previous to this, work had been carried out in laboratories demonstrating the production of complex molecules by the photolysis of low temperature solids (Hallam, 1973 : Miller, 1953). This work provided the motivation to carry out laboratory experiments to investigate the photoprocessing of dirty ice mixtures under interstellar conditions. The laboratory design used by Greenberg and his workers is well described by Hagen et al.,(1979). The overall conclusions of the work will be discussed here.

Consider a dirty ice grain with a size 0.1 μm. Sufficiently energetic uv photons have no difficulty penetrating the grain and breaking the molecular bonds (Greenberg, 1978), as demonstrated in figure 2.9a. An ultraviolet photon with an energy of 4ev or more could cause the production of the hydroxyl (OH^-) radical which may become 'frozen into the grain' due to the low temperatures. Alternatively, with radicals being very reactive, they may combine with other radicals to form new molecules as demonstrated in figure 2.9b. Continued subjection to ultraviolet radiation leads to the

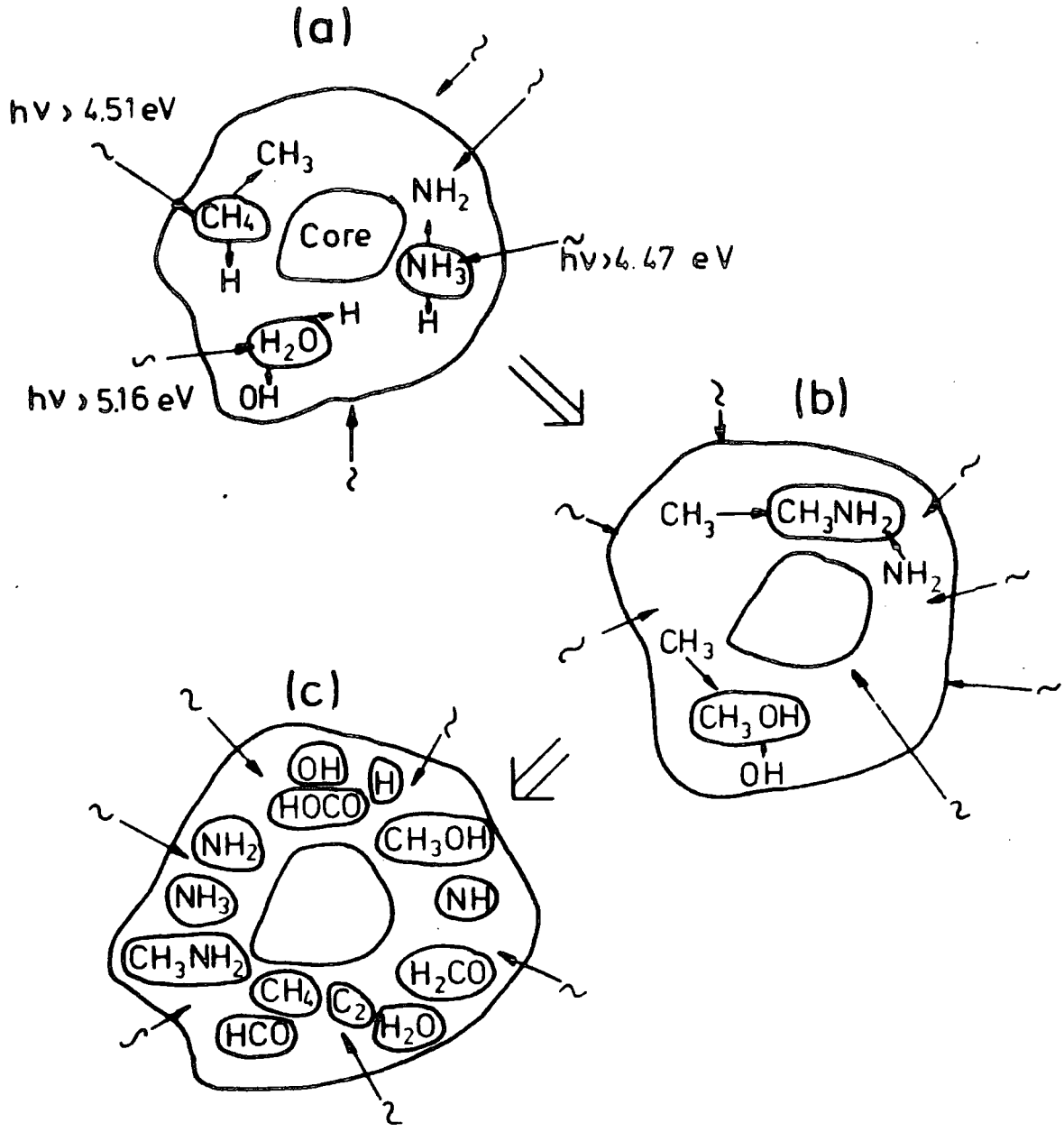

Figure 2.9

Schematic evolution sequence for grain mantles which are subjected to uv photolysis at low temperatures. The processes illustrated are photodissociation, radical-radical combination and production of new molecules and radicals.

(Figure taken from Greenberg, 1983)

production of yet more new molecules and frozen radicals (figure 2.9c).

If enough free radicals are stored on a grain, a triggering event such as a grain collision could lead to a chain reaction, in which the heat generated by radical reactions could free other radicals. This would then enable them to diffuse away from the carrier grains and find other free radicals with which to react. Experiments of such grain explosions have shown that the most likely molecule to form from such recombinations is in fact formaldehyde.

The possibility of the above sequence of events taking place in space has been demonstrated using laboratory techniques. In addition, the experiments have shown that extensive photoprocessing results in a nonvolatile residue being deposited around the original core particle (assumed to be silicates) (Greenberg, 1983). The composition of the mantle was found to be dependent on the initial composition of the dirty ice. The spectra of these laboratory produced grains have been found to contain all the major infrared features which have been observed in emission and absorption (Allamandola et al., 1978 : Allamandola et al., 1979 : Hagen et al., 1980 : Hagen et al., 1983).

Further support for the theory of the photoprocessing of grains in the diffuse cloud medium

comes indirectly from the calculation of the time required for such photoprocessing. For an uv flux of 10^8 $cm^{-2} s^{-1}$ for photons with energies greater than 6ev (typical of the diffuse cloud medium), this time is found to be only about 200 years. This value, when compared to 10^8 years (which is the estimated lifetime of interstellar diffuse clouds) strongly suggests that an ice grain would stand little chance of remaining chemically static in such a harsh environment. Without a doubt one cannot expect to see water absorption features in such a harsh environment. Only the tough nonvolatile mantle could be expected to survive the life in the diffuse cloud medium and one can only expect grains in the diffuse cloud medium to suffer destruction and not growth.

These interstellar clouds can become dense by a variety of processes, perhaps via cloud-cloud collisions or by some external source of pressure (Kwan et al., 1979 : Scoville et al., 1979). Ultimately instabilities cause the initially diffuse cloud to contract, eventually leading to star formation (Woodward et al., 1978 : Bash et al., 1979)). It is only in the dense cloud stage, when the ultraviolet flux is much reduced that atoms and molecules could accrete to the grains. It is known that the grains in molecular clouds are larger than those in diffuse clouds from measurements of the wavelength dependence of the extinction and polarization (Greenberg, 1978). The

diffuse cloud grains contain a lower proportion of the available oxygen than of the carbon and nitrogen (De Boer, 1980 : Greenberg, 1982). It would therefore not be unreasonable to assume that the mantles accreted in the dense clouds would be super-abundant in oxygen and that a very likely form for it to take is water ice on the grain mantle.

Exactly what happens to the grain mantle structures depends very much on how the grains evolve from the molecular cloud, through the prestellar to the early protostellar phase. During the early molecular cloud phase it would seem likely that the grains would tend to maintain a steady state size distribution based on an equilibrium between grain growth and grain explosions. As the cloud approaches the final stages of collapse the ultraviolet radiation is dramatically reduced and the grains would be expected to accrete probably all the remaining condensable constituents from the gas. Those grains far enough away from the protostar to be shielded from destruction by evaporation by the stellar radiation, may be cool enough to maintain their water mantles for some time. The above theory is supported by observations of the Becklin-Neugebauer object where the emitted radiation is heavily reddened and may be attenuated by as much as 70 magnitudes in the visible (Aannestad and Purcell, 1973). The grains observed here are 25% larger

than in the diffuse cloud medium. The molecular cloud has reached the protostellar phase and there is a strong continuum infrared source. The ice band has been clearly identified.

The expected structure of photo-processed grains, formed in the diffuse cloud medium, in dense molecular clouds, and in dense molecular clouds with a protostellar source, are shown in figure 2.10. The evolutionary cycle proposed for the above model is shown in figure 2.11.

2.9 FORMATION OF GRAIN CORES

There is enormous difficulty in processes leading to the direct condensation of core particles from atoms and molecules in the diffuse cloud medium. This is due to the extremely harsh conditions which result from the high uv flux. Alternative sites of formation in much denser environments have been considered. In 1962 Hoyle and Wickramasinghe proposed the formation of nuclei in the atmospheres of cool stars followed by ejection into the interstellar medium by radiation pressure.

In 1970, Hoyle and Wickramasinghe went further to suggest grain formation in supernovae. During the same year, Geisel, Kleinmann and Low observed the decline of Nova Serpentis between 1 μm and 22 μm. At first the visual

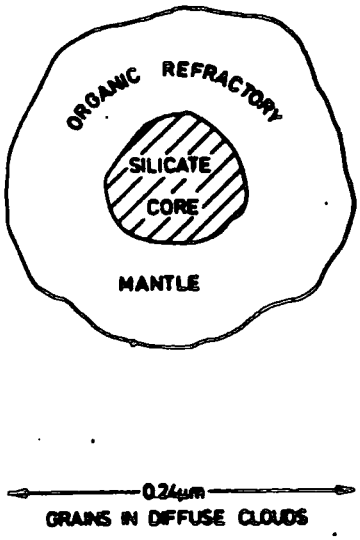

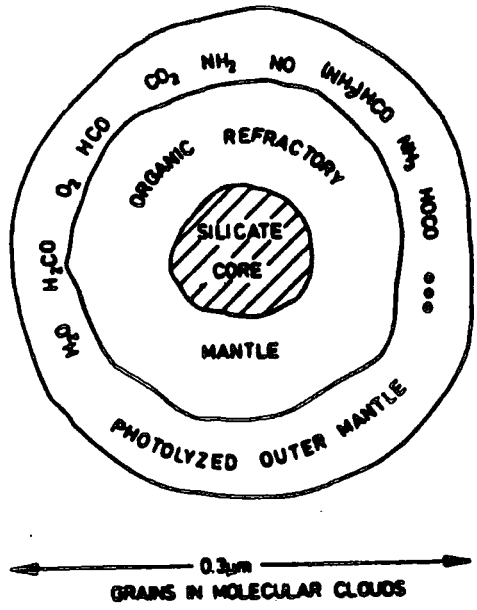

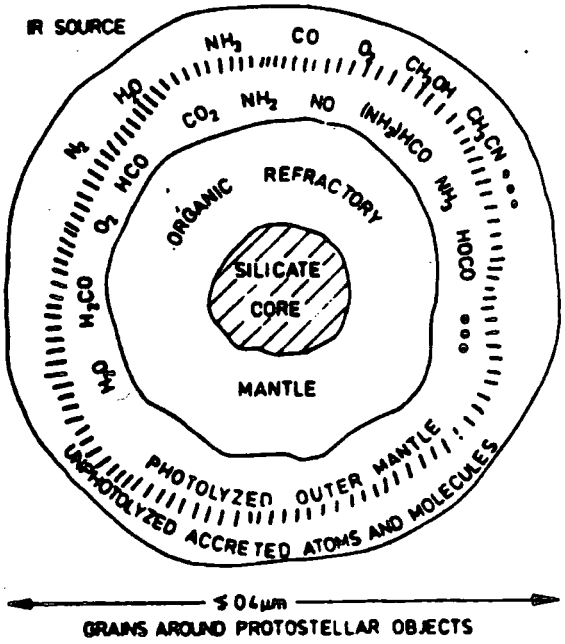

Figure 2.10

Chemical models of interstellar grains expected in different regions of the interstellar medium.

(Figure taken from Greenberg, 1983)

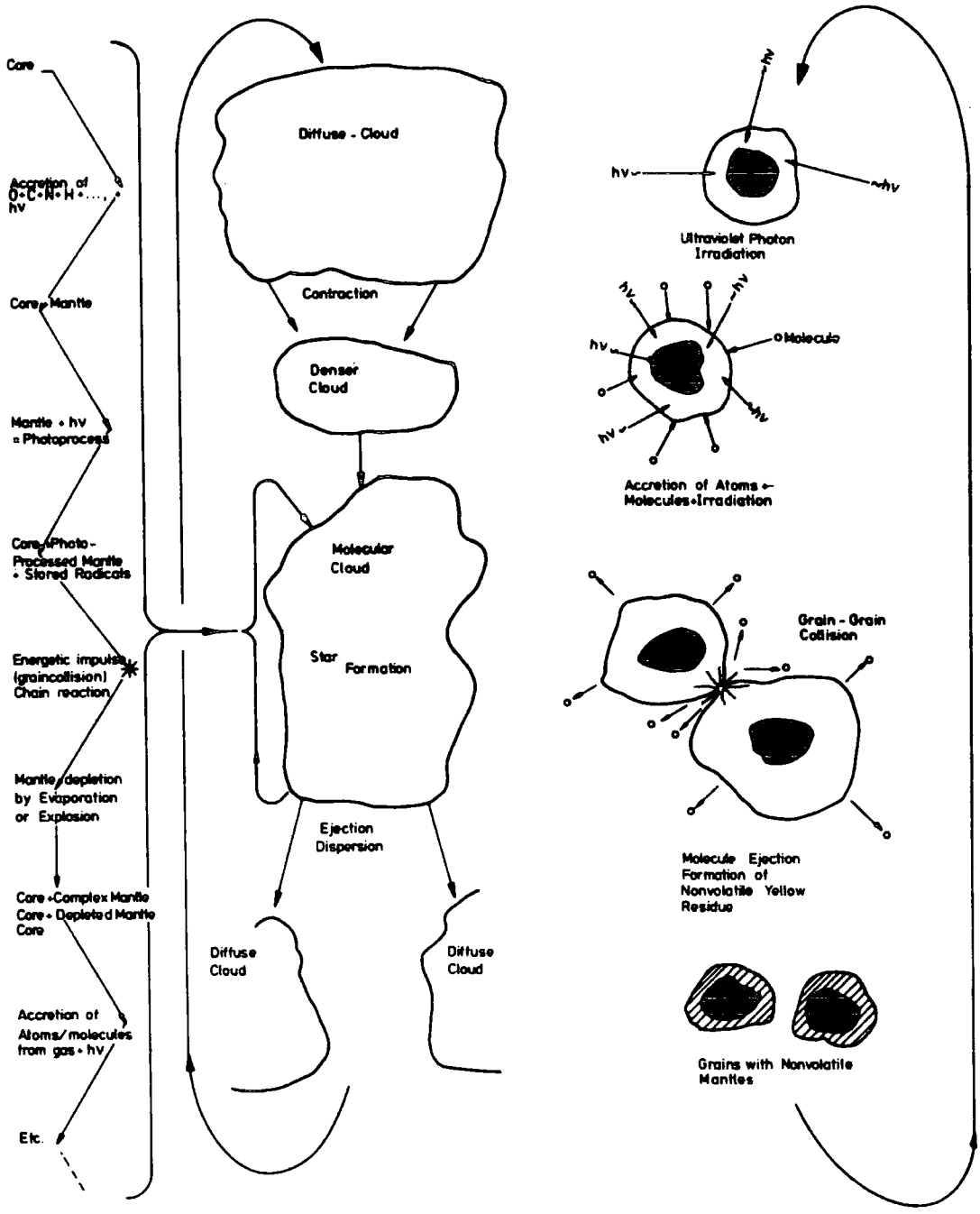

Figure 2.11

Schematic diagram of grain and cloud evolution. The sequence to the left corresponds to the molecular cloud phase, whilst that to the right shows how the grains evolve through the molecular cloud and star formation phase, and then back to the diffuse cloud phase.

(Figure taken from Greenberg, 1983)

decline of the outburst was mirrored in the infrared, until about 50 days later, when the infrared fluxes at all wavelengths began surprisingly to increase. Gradually the infrared began to dominate the energy output from the nova.

The most obvious candidate for the source of the infrared was clearly dust. Due to the lack of 10 μm features, Geisel ruled out silicate grains and proposed that graphite grains had condensed out of the nova ejecta. Clayton and Hoyle (1976) investigated the process in detail and put forward a model whereby the ejecta (which is rich in carbon) expands until a point is reached where the grains can condense. In Nova Serpentis this would only be 11 days after the outburst. The optical depth increases rapidly as the grains grow, cutting off the light of the underlying photosphere. Once formation ceases and the dust shell also begins to thin out, the 'stored' infrared radiation can escape. The main conclusion of this work is that the grains formed can be very large (up to 2 μm) and that up to 0.1% of the interstellar grains could be formed in novae.

2.9.1 DESTRUCTION OF GRAINS AND THE SIZE DISTRIBUTION FUNCTION

Oort and Van de Hulst (1946) proposed that grain growth and destruction should lead to an equilibrium distribution of grain size, this being consistant with the observed general uniformity of the interstellar extinction curve. Their distribution was accepted for many years without much serious challenge from any quarter. As a destruction mechanism, they invoked classical cloud-cloud collisions. This was supposed to result in 'volatilization of solid particles by mutual encounters', for two particles of sufficient velocity. They calculated that the average lifetime of a grain was ~ 10^8 years, which balances with a grain growth of up to 0.1 μm. Given that the age of the galaxy is ~ 10^{10} years, this seemed very favourable towards the concept of an equilibrium size distribution being attained in this manner. The original function was modified by Greenberg (1960) to give a function which was much simpler analytically. The Oort-van de Hulst-Greenberg size distribution is given by

$$n(a) \propto \exp\left[-5 \times (a/0.5)^3\right] \qquad .....(2.11)$$

where n(a)da is the number density of particles with radii

in the range (a, a+da).

The downfall of the distribution was signalled in 1978 when Barlow showed that the classical cloud collision theory on which the above was based, was largely ineffective. Only at the shock interface itself will the relative velocities of the grain be enough for evaporation. Insertion of this fact to the calculations yields a lifetime of $\sim 10^{10}$ years, which is of the same order in time as the age of the galaxy, hence invalidating cloud-cloud collisions as a major destruction process and therefore causing severe problems for the Oort-van de Hulst-Greenberg distribution.

Before considering the distribution function which has since been invoked under many circumstances, it is worth mentioning several other destruction processes which can be important under certain circumstances but which are not universally applicable.

It was once thought that erosion via chemical reactions at bare grain surfaces could be an important destruction mechanism. Bar-Nun (1975) however showed the process to be largely ineffective, although it was still thought that it may be important under certain conditions. This lead Barlow (1978b) to suggest that the weakness of the 2175 Å bump in some objects could be due to chemisorbed hydrogen and oxygen which destroyed the graphite surface and Draine (1979) showed that this

process could well be effective in very compact HII regions. Even so, this kind of erosion has been excluded as an important destruction process.

The process known as sputtering, proceeds via atomic and ionic bombardment of the lattice particles of a solid. The precise effect is strongly dependent on the collisional energies and the chemical constituents of the collision particles and again, was once considered to be of considerable importance as a destruction mechanism. However, Greenberg (1978) proposed that sputtering (principally by He) would only be important where relative speeds of the collision particles are high, such as in shock fronts, and subsequent research into cloud-cloud collisions by Barlow (1978a) supported his proposal.

Shattering mechanisms were not considered at the time of the Oort-van de Hulst-Greenberg function. Since that time however, it has been shown to be of considerable importance. Shattering is in fact found to be an important process in many environments ranging from terrestrial rock fragmentation to asteroid formation and a review by Hartmann (1969) of the large reservior of data available on the size spectra of many fragmentation products has shown up one particularly important point relevant to the present discussion. In every case a power-law distribution for the sizes of the bodies under investigation develops, the index of the distribution being dependent on the

degree of multiple fragmentation.

Hellyer (1970) took Hartmanns work further and showed theoretically, that in any given system where no particles are lost or gained from the system, and shattering mechanisms are in operation, the equilibrium size distribution which results is always power-law in form. So, both theoretically and observationally, it was shown that shattering processes always result in power-law size spectra. Moreover, theoretical work on accretion by Daniels and Hughes (1981) also predicts approximately power-law distributions.

Concerning interstellar grains however, the results of Barlow stand against shattering being important in cloud-cloud collisions in particular. Even so there are other important environments concerning grain modification processes. Burke and Silk (1976) considered processes which might effect grains in clouds undergoing collapse to the formation of a protostar. They showed that in the cloud collapse phase, grains would be expected to couple strongly to the gas and so avoid collisions. However, for 5 solar mass stars or greater, where radiation driven shells are expected to develop (Larson, 1969) the situation becomes much different. Turbulent motions in the expanding shell produce eddies, and grains swept up by these suffer collisions with grains in other eddies on a time scale much shorter than the lifetime of the shell.

Clearly if shattering processes are in operation in this phase, then so are the destruction processes on which the Oort-van de Hulst-Greenberg distribution was based. Burke and Silk went on to show, that if the fraction of the grains which suffered evaporation during the turbulent eddy phase was high, then the final size spectrum would indeed be that described by the Oort vande Hulst-Greenberg distribution, but if this fraction was low, then the shattering mechanism is dominant and a power-law size distribution results.

Clearly, what was needed was an empirical derivation of the grain size distribution. This was carried out in 1977 by Mathis, Rumpl and Nordsieck and their work has already been discussed in section 2.71. Their resultant size distribution was that of the power-law and has gained wide acceptance in recent years. The indices of their power-law distribution took values of 3.3 to 3.6 for spherical grains. It is this distribution that will be used in all subsequent calculations recorded in this text.

2.10 MIE SCATTERING THEORY

It remains to be discussed exactly how the mathematical problem of scattering of light from dust grains in the interstellar medium will be treated. To treat a totally general case of scattering of light, with an initial arbitrary state of polarization, from dust grains of any shape, requires the solution of Maxwell's equations of electomagnetic wave propagation both inside and outside the particle, together with the appropriate boundary conditions at the surface of the grain. Clearly this is a difficult proposition. The shear difficulty of obtaining such a solution has resulted in only several, much simplified cases being treated, for example, that of scattering by infinitely small particles (Rayleigh scattering). The solutions for the case of smooth , homogeneous spheres of arbitrary size were calculated by Mie (1908). Other exact and approximate methods have been applied to other simple geometric shapes,such as cylinders and ellipsoids. A review of the current 'state of the art' is to be found in van de Hulst, 1981.

It is clear from observations of the interstellar polarization that real grains must depart from sphericity to some degree. However, experimental work in the optical

(Chylek et al, 1976) and microwave (Zerull and Giese, 1974) regions show that as long as the degree of ellipticity is small, the scattering behaviour of such non-aligned grains is in good agreement with the overall structure of perfectly spherical grains. Mie calculations as an approximation to light interaction with interstellar grains would therefore seem justified.

2.10.1 THE SCATTERING FORMULAE

Mie scattering is completely defined if the wavelength of the radiation, the radius of the scattering particle and its complex refractive index are known. According to van de Hulst, scattering may be represented by the matrix equation

$$S_S = M(\alpha).S_I \qquad .....(2.12)$$

where S_I and S_S are the incident and scattered Stokes vectors (with components I,Q,U and V). M is the scattering matrix and α is the cosine of the scattering angle. If the normal to the scattering plane is taken as a reference direction for the Stokes parameters, then $M(\alpha)$ has the form

$$M(\alpha) = \begin{bmatrix} C & D & 0 & 0 \\ D & C & 0 & 0 \\ 0 & 0 & E & -F \\ 0 & 0 & -F & E \end{bmatrix} \qquad \ldots.(2.13)$$

where

$$C(\alpha) = 0.5\ (\lambda/2\pi)^2 . [\,|S_1(\theta)|^2 + |S_2(\theta)|^2\,]$$

$$D(\alpha) = 0.5\ (\lambda/2\pi)^2 . [\,|S_1(\theta)|^2 - |S_2(\theta)|^2\,]$$

$$\ldots.(2.14)$$

$$E(\alpha) = 0.5\ (\lambda/2\pi)^2 . [\,S_1(\theta).S_2^*(\theta) + S_2(\theta).S_1^*(\theta)\,]$$

$$F(\alpha) = i/2\ (\lambda/2\pi)^2 . [\,S_1(\theta).S_2^*(\theta) - S_2(\theta).S_1^*(\theta)\,]$$

$S_1(\theta)$ and $S_2(\theta)$ are the complex Mie scattering amplitudes. $S_1(\theta)$ is that perpendicular to the scattering plane and $S_2(\theta)$ is that in the scattering plane and perpendicular to the direction of propogation. These scattering amplitudes are given by

$$S_1(\theta) = \sum_{N=1}^{\infty} ((2n+1)/n(n+1)) . [a_N \pi_N(\cos\theta) + b_N \Gamma_N(\cos\theta)]$$

$$\ldots.(2.15)$$

$$S_2(\theta) = \sum_{N=1}^{\infty} ((2n+1)/n(n+1)) . [b_N \pi_N(\cos\theta) + a_N \Gamma_N(\cos\theta)]$$

π_N and Γ_N are functions derived from the Legendre polynomials. They are given by Wickramasinghe (1973), together with a_N and b_N which are the spherical Riccati-Bessel functions. The percentage polarization of the scattered component for scattering from a single grain is given by

$$P(\theta) = \frac{|S_1(\theta)|^2 - |S_2(\theta)|^2}{|S_1(\theta)|^2 + |S_2(\theta)|^2} .100 \qquad ....(2.16)$$

while the differential cross section (total scattered intensity within a unit solid angle due to a unit incident light flux) is given by

$$I(\theta) = |S_1(\theta)|^2 + |S_2(\theta)|^2 \qquad ....(2.17)$$

In calculations concerning the interstellar medium a power-law size distribution of the grains as given in equation 2.9 will be used. The size distribution is normalized between the minimum and maximum grain sizes such that

$$\int_{AMIN}^{AMAX} n(a)da = 1 \qquad ....(2.18)$$

The average scattering functions then become

$$F_i(\theta) = \int_{AMIN}^{AMAX} |S_i(\theta)|^2 .n(a)da \qquad ....(2.19)$$

for i = 1,2. Incorporation into the scattering matrix results in C taking the form :

$$C(\alpha) = 0.5\ (\lambda/2\pi)^2 \int_{AMIN}^{AMAX} n(a).[\,|S_1(\theta)|^2 + |S_2(\theta)|^2\,]da \qquad \ldots\ldots\ (2.20)$$

and similarly for D,E and F.

A scheme for actually evaluating the Mie functions is given in Wickramasinghe (1973) and has been implemented by Warren-Smith (1979,1983).

2.10.2 THE SCATTERING FUNCTIONS

A selection of scattered intensity and polarization plots are presented in figures 2.12 to 2.17 for a wide range of power indices and refractive indices. Some general characteristics will be outlined here.

1) Figure 2.12 shows the intensity of the scattered light as a function of scattering angle for a normalized size distribution of grains. The general form of these curves is maintained over a wide range of materials and power indices of the size distribution. The grains are very strongly forward scattering with some

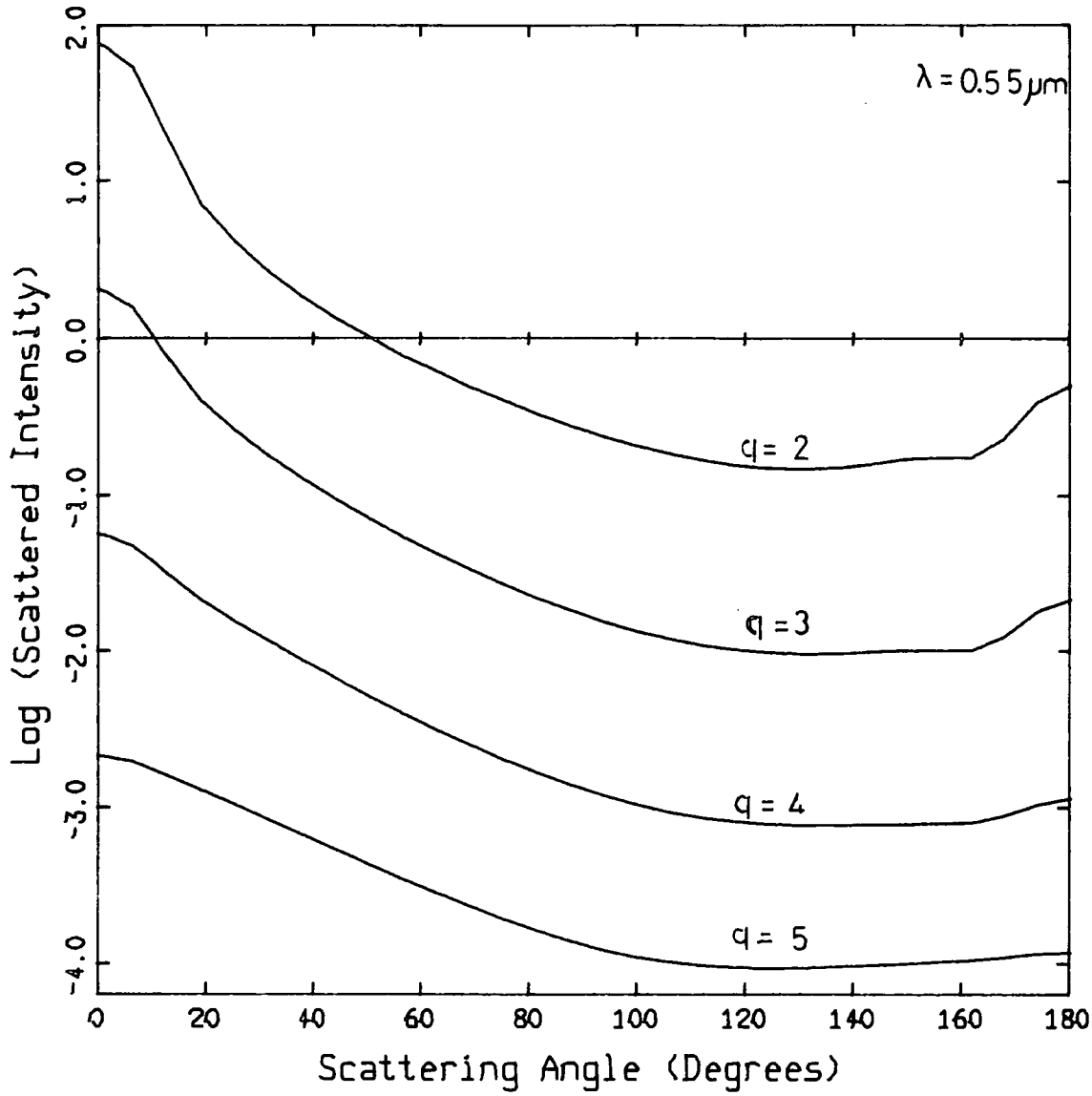

Figure 2.12

Log(Scattered Intensity) as a function of scattering angle for a normalized power-law size distribution of silicate grains. The index of the distribution is marked for each plot.

Refractive index of silicate grains = (1.63,-0.05i)

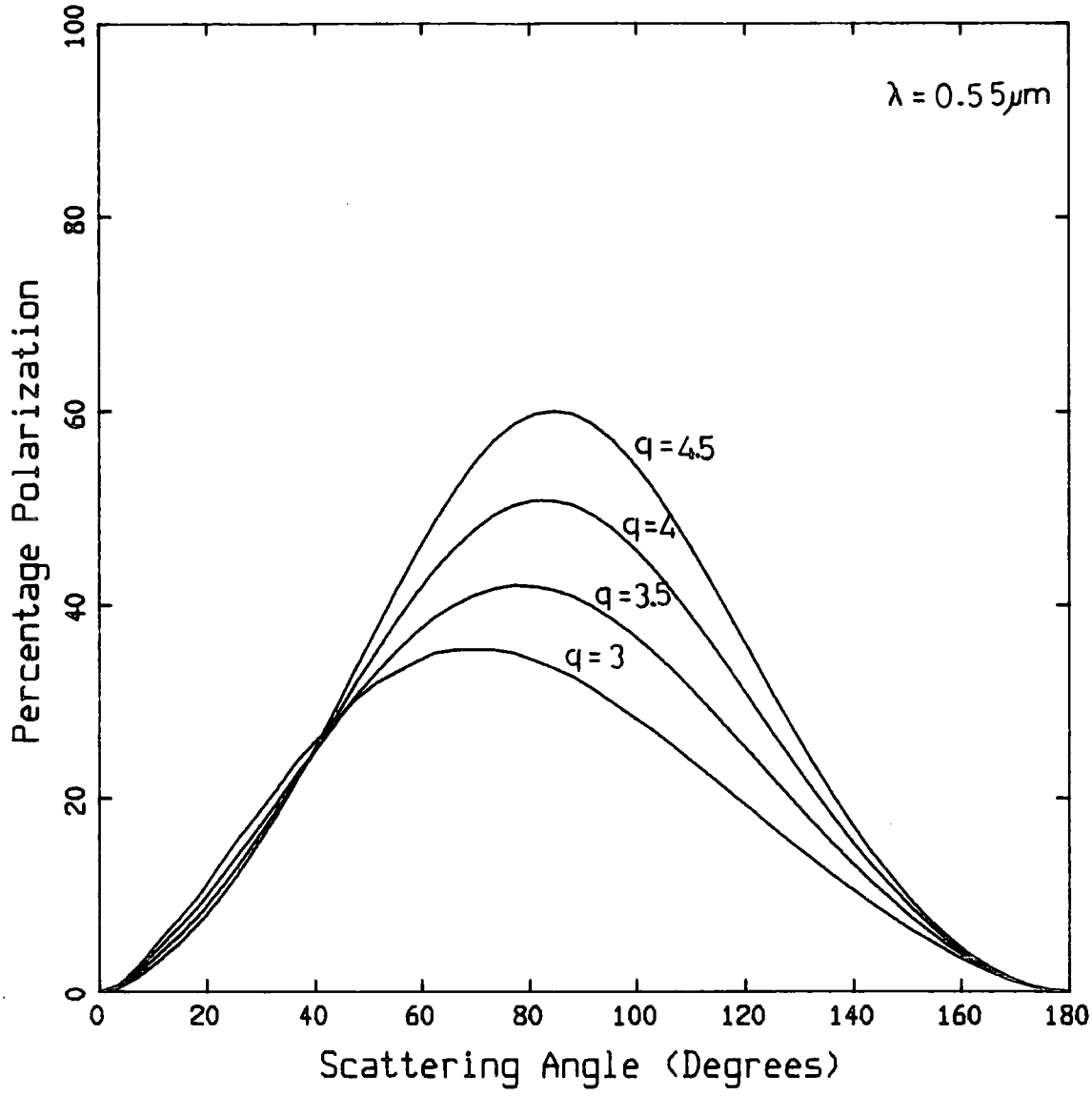

Figure 2.13

Percentage polarization as a function of scattering angle for a normalized power-law size distribution of iron grains. The index of the distribution is marked for each plot.

Refractive index of iron grains = (3.55,-3.0i)

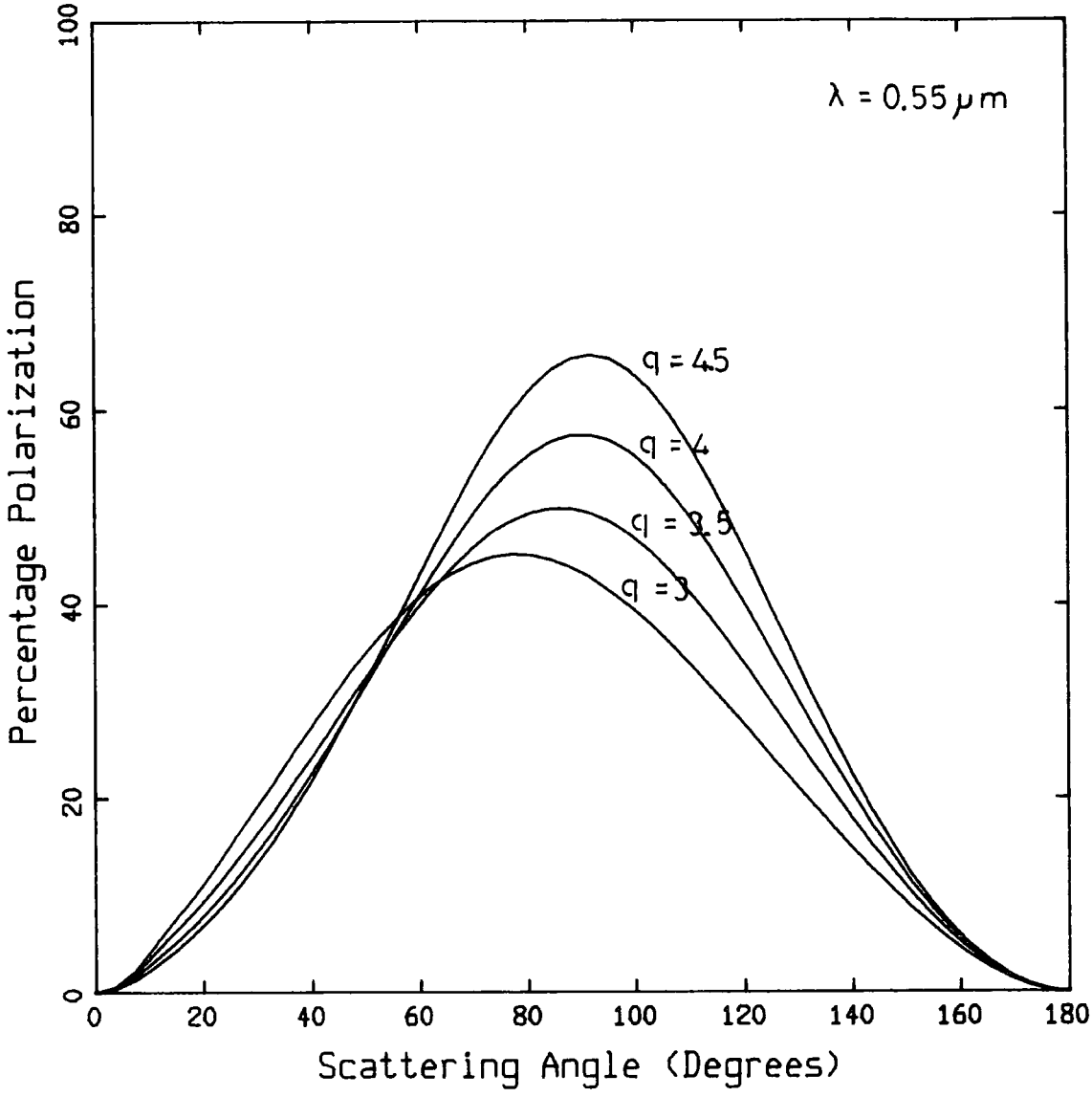

Figure 2.14

Percentage polarization as a function of scattering angle for a normalized power-law size distribution of graphite grains. The index of the distribution is marked for each plot.

Refractive index of graphite grains = (2.5,-1.3i)

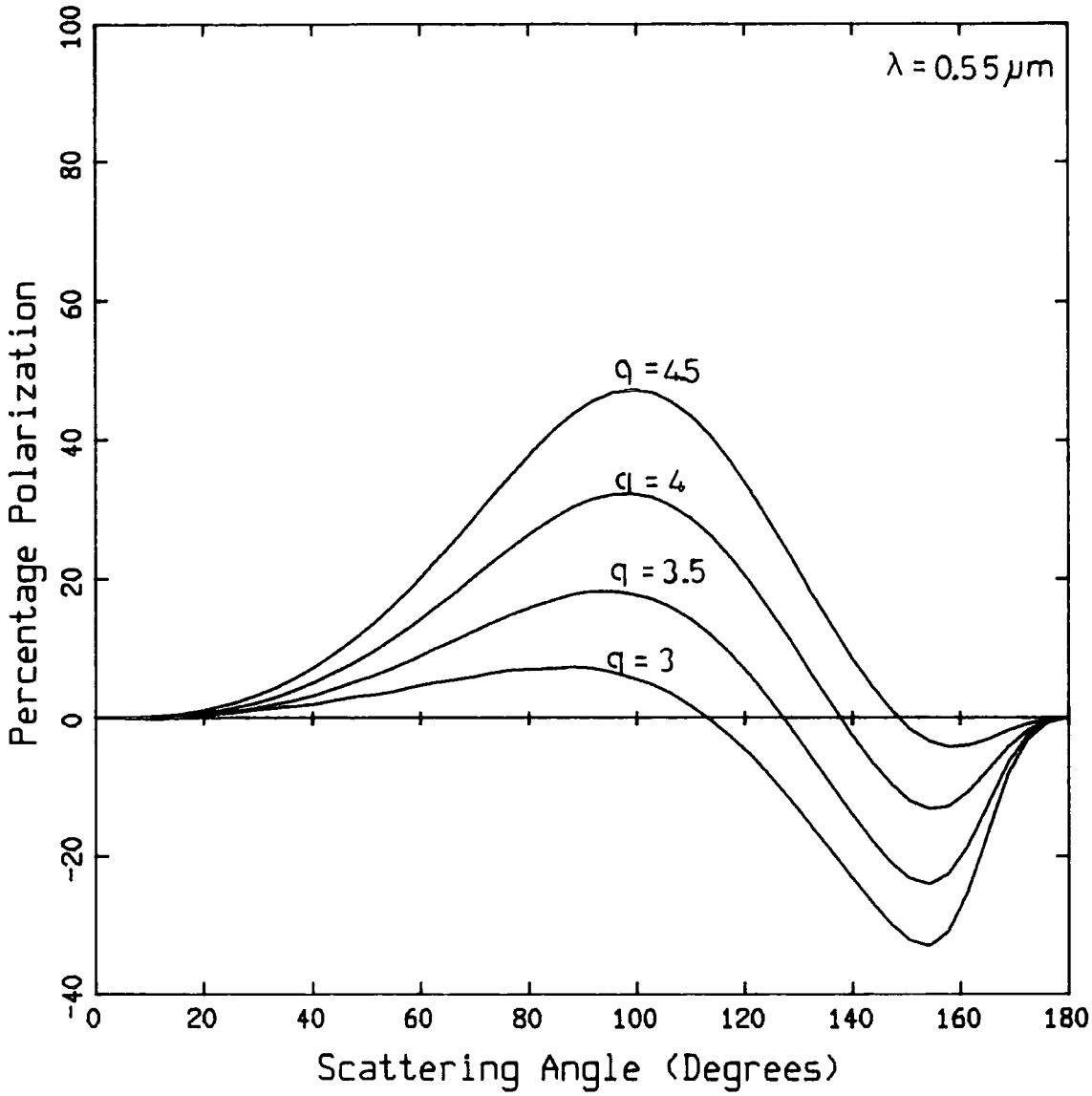

Figure 2.15

Percentage polarization as a function of scattering angle for a normalized power-law size distribution of silicate grains. The index of the distribution is marked for each plot.

Refractive index of silicate grains = (1.63,-0.05i)

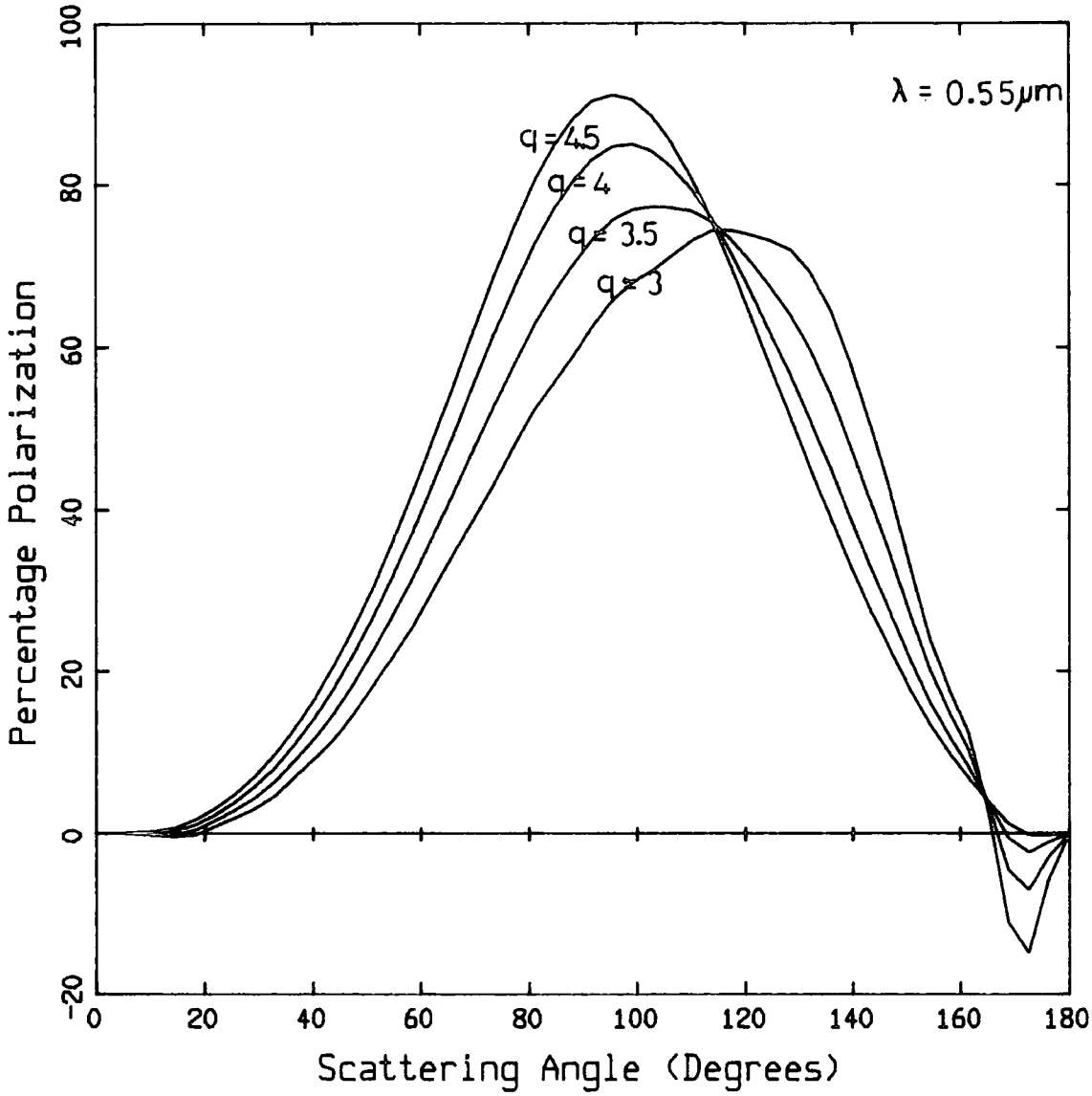

Figure 2.16

Percentage polarization as a function of scattering angle for a normalized power-law size distribution of organic grains. The index of the distribution is marked for each plot.

Refractive index of organic grains = (1.16,0.0i)

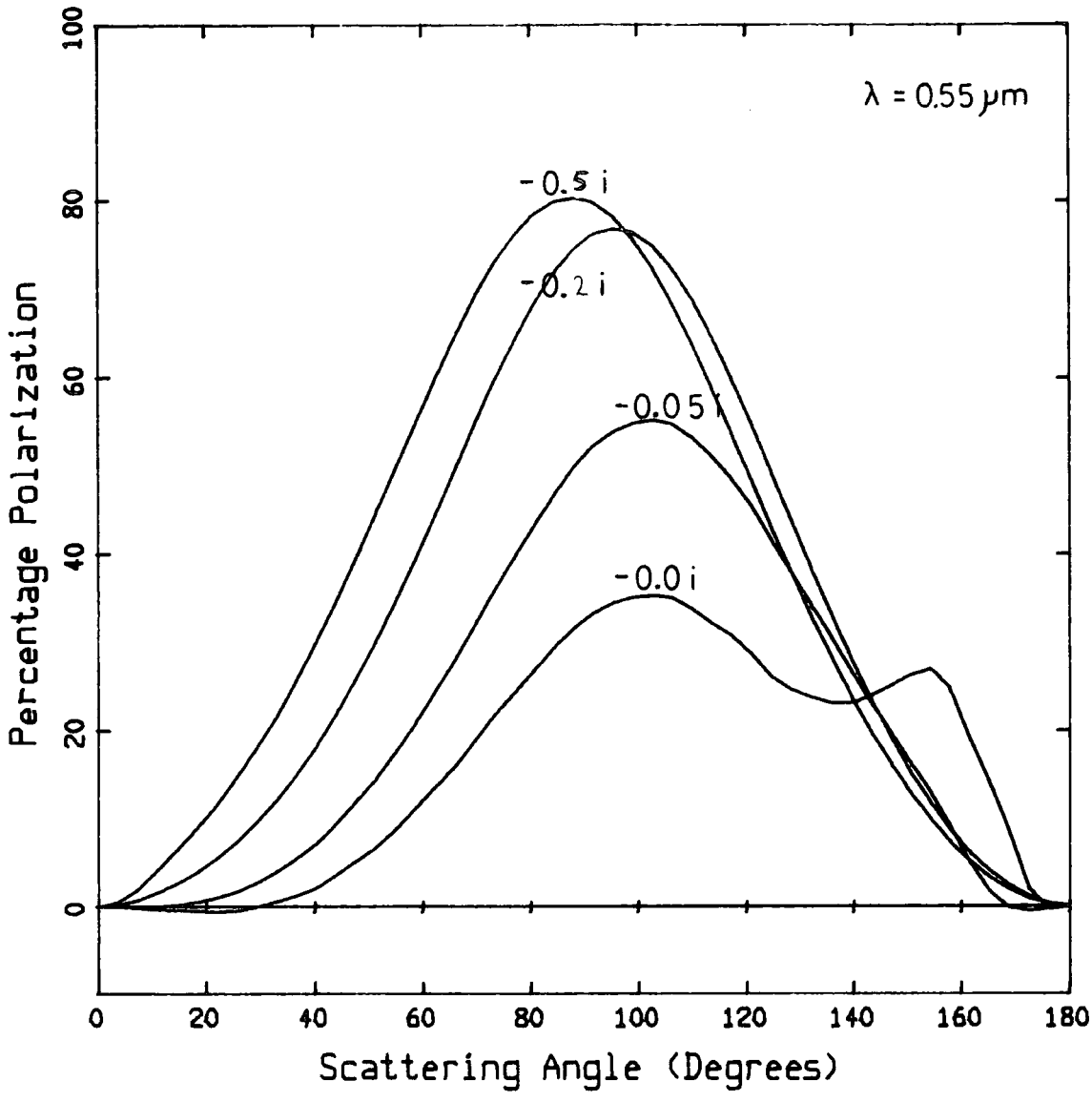

Figure 2.17

Percentage polarization as a function of scattering angle for a normalized power-law size distribution of ice grains. The index of the size distribution was 3.5. The imaginary part of refractive index was altered for each curve as marked above.

Refractive index of ice grains = (1.33,-0.0i)

materials showing a slight rise around 180 degrees backward scattering.

2) Figures 2.13 to 2.17 show that the polarization behaviour of grains is certainly complex. All materials show a peak in polarization around 90 degrees. For materials of low refractive index, the peaks tend to be around 100 degrees, whereas for high refractive index they are around 80 degrees.

Increasing the real and/or imaginary parts of the refractive index causes an increase in the peak polarization.

Increasing the power index of the size distribution causes an increase in polarization in all cases. Typically, with q = 7, the peak polarizations are around 100%. This is caused by the dominance of small particles for high q, since small particles are typically highly polarizing.

Clearly then, measurements of polarization over extended objects such as reflection nebulae, where the polarization is being viewed at different scattering angles depending on the geometry of the nebula, could provide valuable information on both the power index of the size distribution and the refractive index of the grains.

Negative polarizations are observed when $|S_1(\theta)| < |S_2(\theta)|$, and corresponds to the polarization being

parallel to the scattering plane. Negative polarization usually results from backward scattering.

CHAPTER 3

REFLECTION NEBULAE

3.1 INTRODUCTION

A reflection nebula, as implied by its name, owes its diffuse brightness to the scattering of incident light by the constituent nebular medium. The difference between reflection nebulae and other diffuse galactic nebulae, such as HII regions and dark clouds, lies in differences in the nature of the source of illumination. Two principal mechanisms are responsible for the illumination and excitation of nebulae which may be observed visually.

1) Stars of spectral type BO or earlier are able to cause photoionization of the local gas (Kaplan and

Pikelner, 1970), which causes it to become a luminous 'emission' nebula. Such nebulae are commonly known as HII regions and their spectra are dominated by emission lines. They have been found to be associated with regions of star formation.

2) Clouds of gas and dust may be illuminated by the radiation from stars of spectral type B2 and later which is unable to cause ionization of the nebulosity and principally just scatters from the dust. The spectra simply reproduce that of the illuminating star. Stars of type B0 and B1 produce nebulae which have both a scattered and an emission component.

There are three distinct groups which together make up the set of objects known as reflection nebulae. These are:

1) Nebulosities found at high galactic latitudes, which appear to be illuminated by the integrated light from the galactic plane (Innanen, 1969).

2) Nebulosities, illuminated by one or more stars, which are almost certainly part of a more extensive molecular cloud and are often referred to as 'interstellar reflection nebulae'.

3) Compact nebulae, where the gas and dust is definitely connected in some way to the illuminating stars. Of the above, the last two groups are the most important to the study in hand and will be discussed in

more detail.

3.2 INTERSTELLAR REFLECTION NEBULAE

Hundreds of these nebulae have been found on sky survey plates and have been catalogued by Cederbland (1946) and Dorschner and Gurtler (1966). Typically, they have surface brightnesses in the range of 20 - 22 magnitudes per square arc second although the detection limit is determined by the sensitivity of the instrumentation. The objects are intensity bounded rather than density limited. Hubble (1922), derived a theoretical relationship, based on the inverse square law of illumination, between the apparent magnitude of an illuminating star, m, and the angular extent of the associated reflection nebula in minutes of arc, a, (taken from the star to the most distant patch of nebulosity which could be detected). The relationship derived is given below.

$$m = -5\log_{10}(a) + k \qquad .....(3.1)$$

The constant term, k, is found empirically.

Over the last 20 years, evidence has built up demonstrating that there is a strong connection between early type stars and interstellar clouds. Roberts (1957)

and Ebert (1968) found that nearly all early type stars are found in clusters. Often, so are reflection nebulae (van de Bergh, 1966). Furthermore, these reflection nebulae clusters lie within the boundaries of recognized OB associations (Racine, 1966). The picture of a star forming at the centre of a protostellar cloud, which has undergone gravitational collapse due to some initial instability (Larson, 1969), has gained overall acceptance, enormous effort has been put into trying to understand the nature of reflection nebulae with respect to their geometries, illuminating stars, and dust and gas content, in order to further our understanding of early star formation.

It is from this basis that the compact nebulae, in particular those associated with pre-main sequence objects, must be examined, since they are intimately connected to the physical processes which concern the illuminating stars, and one would therefore expect that they could afford to us much valuable information.

3.3 COMPACT REFLECTION NEBULAE

Often these reflection nebulae have very striking geometric configurations, and in recent years a great deal of attention has been directed towards the study of a

class of peculiar objects known, on purely morphological grounds, as 'bipolar nebulae'. Their distinctive appearance is reflected in their names. Examples are the 'Cygnus Egg Nebula' (CRL 2688) (Ney et al., 1975; Crampton et al., 1975), 'Minkowski's footprint' (M1-92) (Herbig, 1975), the 'Red Rectangle' (HD44179) (Cohen et al., 1975), the 'Boomerang Nebula' (ESO-172?07) (Taylor and Scarrott, 1980), Eta Carinae (Warren-Smith et al., 1979), S106 (Sharpless, 1959) and the classical 'hourglass' of LkHα208 (Hubble, 1922).

Each of these objects is characterized by a pair of apparently circular or fan shaped nebular lobes, symmetrically placed about a compact stellar-like source which may be seen in the visual and/or infra-red. Circumstellar rings are frequently associated with the objects and may cause the central star to be heavily obscured, depending on the tilt of the major axis of the lobes with respect to our line of sight.

Another group of objects falling into the class of compact nebulae are the cometary nebulae. They are similar to the bipolars but have only a single nebular lobe. Examples are the nebulosities associated with ZCMa, (Herbig, 1960) and R Mon (Slipher, 1912). R Mon illuminates the classical cometary, NGC 2261. Also there are the FU Ori stars which now comprise FU Ori itself, V1057 Cyg (Welin, 1971) and V1515 Cyg (Wenzel et al.,

1975). Each of the FU Ori stars had large ir excesses and after brightening considerably in the optical region, (in 1970 and 1974 respectively for the latter two), now illuminate small reflection nebulae. Herbig proposed in 1977, that these nebulae were pre-existing structures that were simply illuminated when their respective stars brightened, and that they were not ejected from the stars at the time of the outbursts.

It is commonly believed that cometaries and bipolar nebulae may well be very closely related. This relationship will be discussed further in a later section concerning formation mechanisms.

3.4 GENERAL BRIGHTNESS CHARACTERISTICS OF REFLECTION NEBULAE

Due to the surface brightness of these objects being comparable to the sky brightness or fainter, early photographic studies of their colour and polarization were notoriously subject to systematic error. The inherent accuracy of the equipment now used is much improved compared to that used over the last century, and has increased the reliability of faint object measurements. Even so, there are certain problems that may always be with us, such as the sky brightness estimation.

Nowadays, it is clear that reflection nebulae are bluer than their illuminating stars, but become progressively reddened with offset distance from the star (early observations indicated the contrary). Martel (1958), Hall (1965) and Zellner (1970, 1973) for instance, have demonstrated these trends conclusively in various nebulae.

The above work also showed that many reflection nebulae have surface brightnesses that are greater than expected, even though there is an overall general agreement with Hubble's relationship. As understanding of the complex scattering processes at work inside the

nebulae grew, so this problem was resolved. The dust grains comprising the nebulae are predominantly forward scattering and not isotropic, as was implicitly assumed by Hubble in 1922 (see section 2.5), and multiple scattering within an optically dense nebula has been found to provide an important contribution to the observed brightness

3.5 POLARIZATION STUDIES OF NEBULAE

An important characteristic of all these objects is the generally high degree of linear polarization observed in the lobes. Polarizations of up to 60% are not uncommon.

Warren-Smith et al., (1980) report polarizations of up to 40% for NGC1999 which is illuminated by the star V380 Orionis. A linear polarization map of the nebulosity shows a circular pattern of electric vectors centred on V380 Ori (figure 3.1). Such a pattern is typical of polarized light resulting from the scattering of radiation from a central object, by dust in the surrounding medium.

In a later work, Warren-Smith (1983) uses sophisticated modelling techniques to simulate the nebular brightness and polarization. Such modelling enables him to place constraints on possible nebular geometries, on the grain size distribution function, the grain material and

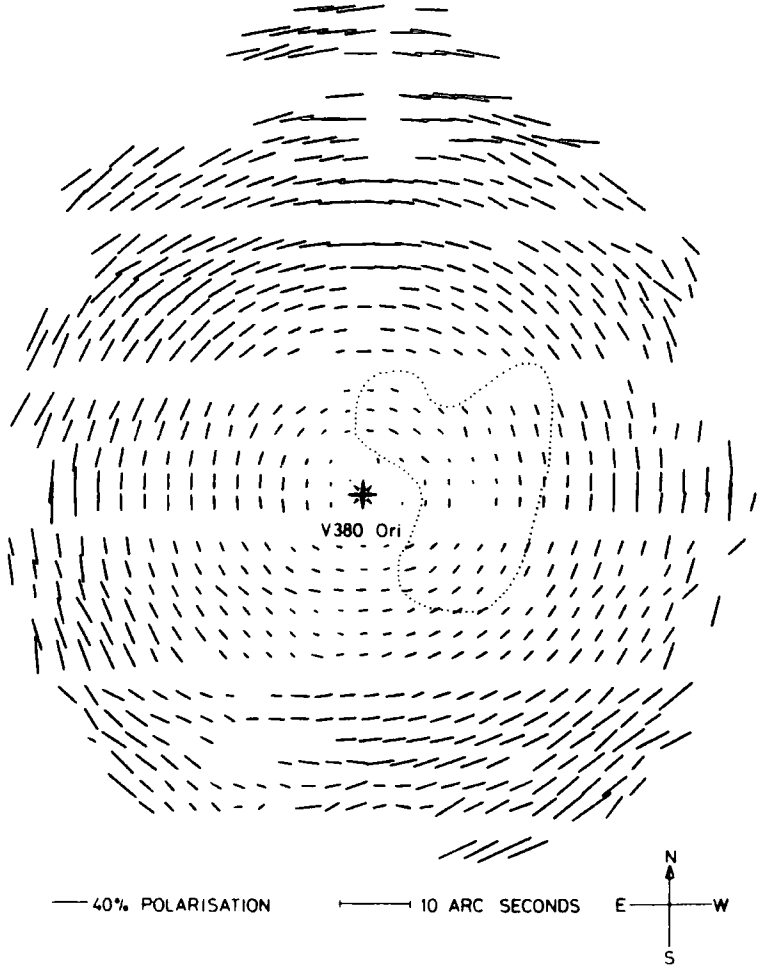

Figure 3.1

The linear polarization map of NGC 1999. Integration bins of 5 x 5 arcseconds have been used. The measurement at each point is represented by a line, the length of which is proportional to the degree of polarization and orientation of which is parallel to the E vector.

(Figure taken from Warren-Smith et al., 1980)

on optical depths within the nebula. Warren-Smith finds his data to be best accounted for if the grains are high in albedo (>0.7) with a real part to the refractive index of 1.19 ± 0.09. The distribution of grain sizes is required to be approximately power-law, with an index of -4.25 ± 0.18.

These results lead to the suggestion that the size distribution function varies slowly with grain size, the index of the distribution becoming more negative with increasing grain size. This would account for the discrepancy between Warren-Smith's calculation of -4.25 for the size index and -3.5 found by Mathis et al. (1977). The nebular model under investigation by Warren-Smith is sensitive to grain sizes from 0.2 to 0.5 μm, while the higher index derived from the mean interstellar extinction curve (Mathis et al.), is sensitive to sizes around 0.03 μm. Such a variation of the power index with grain size is also required physically, since it is known that power-law, size distributions cannot exist over a large range of grain sizes without requiring more condensable material in the grains than is cosmically available (Greenberg, 1978).

Polarizations of up to 60% are reported for the northern lobe of the Boomerang Nebula (Taylor and Scarrott, 1980). The polarization map of the object again shows a centro-symmetry typical of nebulae illuminated by

a central star. Near the star, along the minor axis of the nebula, the polarization is reduced and a band of vectors are seen to lie parallel to this axis. Taylor and Scarrott propose that this band is due to multiple scattering of the radiation in a dense, optically thick disc of dust around the star. On the basis of the observed polarizations and colours of the nebula, they propose that the lobes are tilted with respect to our line of sight and that the star is seen obliquely through the disk. Their work supports classification of the object as a proto-planetary nebula.

Low, but revealing polarizations of up to 5% have been observed for S106 (Perkins, King and Scarrott, 1981). S106 is a compact HII region with a central source which is obscured by 20 magnitudes in the visual (Eiroa et al., 1979). The low polarization is explained as being the result of extensive dilution of the scattered light by intrinsic emission from the excited gas in the nebula. The polarization vectors again form the centro-symmetric pattern typical of this type of object and Perkins et al. find the centre of the pattern, hence identifying the most likely region in which to find the hidden illuminating source. Their conclusions support advocates of a central, early type star for the object, surrounded by a dense dust disc which allows light to escape along the optically thinner axes perpendicular to the plane of the disc.

Clearly, there is enormous power in mapping the polarization and colours of reflection nebulae and it would seem important then, to outline clearly the information that one could expect to gain from these observable quantities, since they will be used later in proposing a model for the bipolar nebulosity centred on the star LkHα208.

3.6 NEBULAR PROPERTIES WHICH RELATE TO THE NEBULAR POLARIZATION AND BRIGHTNESS

In any discussion such as this, it is important to bear in mind that the grains responsible for scattering in the visual waveband are those which have sizes ~ the wavelength of visible light. They are strongly forward scattering but exhibit peak polarizations around the 90 degree scattering angles (see section 2.10.1). The nebular properties important to polarization and colour measurements are the nebular geometry, the grain type and albedo, the grain size distribution, any dust density variations within the nebular structure and the photon mean free path (which in turn determines the degree of multiple scattering of the light).

The mean level of polarization is principally determined by the grain type and size distribution. The

range of polarization, whilst being also dependent on the grain parameters, is strongly influenced by the nebular geometry and to a lesser extent, by any dust density gradients. These determine the range of angles through which the light may be scattered.

The surface brightness is strongly affected by the grain albedo and dust density variations. Since the grains are forward scattering, the geometry of the front face of the nebula plays an important part in any brightness variations. Multiple scattering within an optically thick nebula generally serves to increase the surface brightness at the same time as leading to an overall depolarization of the scattered light, which lowers the general levels of observed polarization.

It is seen then, that while polarization and colour mapping can potentially provide us with much information concerning a given nebulosity, extracting it is no simple task due to the complex interplay of so many parameters, all of which have an effect to a greater or lesser extent on the observations. This has resulted in workers turning to numerical simulation models to make fuller use of the available data.

An attempt to actually predict some of the properties of bipolar nebulae has been carried out recently by Yusef-Zadeh et al., (1984). They consider the multiple scattering of light within a dusty, anisotropic

medium, and allow radiation from a central source to be scattered once or more in an optically thick circumstellar disk, before scattering from dust which lies above and below the plane of the disk. The proposed nebular structure is depicted in figure 3.2. Dust densities above and below the plane of the circumstellar dust are assumed to decrease with radius as r^{-2}, where r is the distance from the illuminating star.

While attempting to simulate the optical appearance of the Red Rectangle (HD44179), CRL 2688 and Minkowski's Footprint (M1-92) (references concerning these objects are given in section 3.3), no attempt is made to actually fit the observational data and consideration of the polarization is deferred. In principle this model seems feasible, but sections 5.3 and 5.3.1 will demonstrate that the model as it stands, will probably fail when attempting to reproduce the polarizations observed for these objects

Having now discussed some observational features of bipolar reflection nebulae and the parameters which give rise to these observations, it is important to discuss also their evolutionary status and present as far as possible, a coherent picture of their part in stellar evolution.

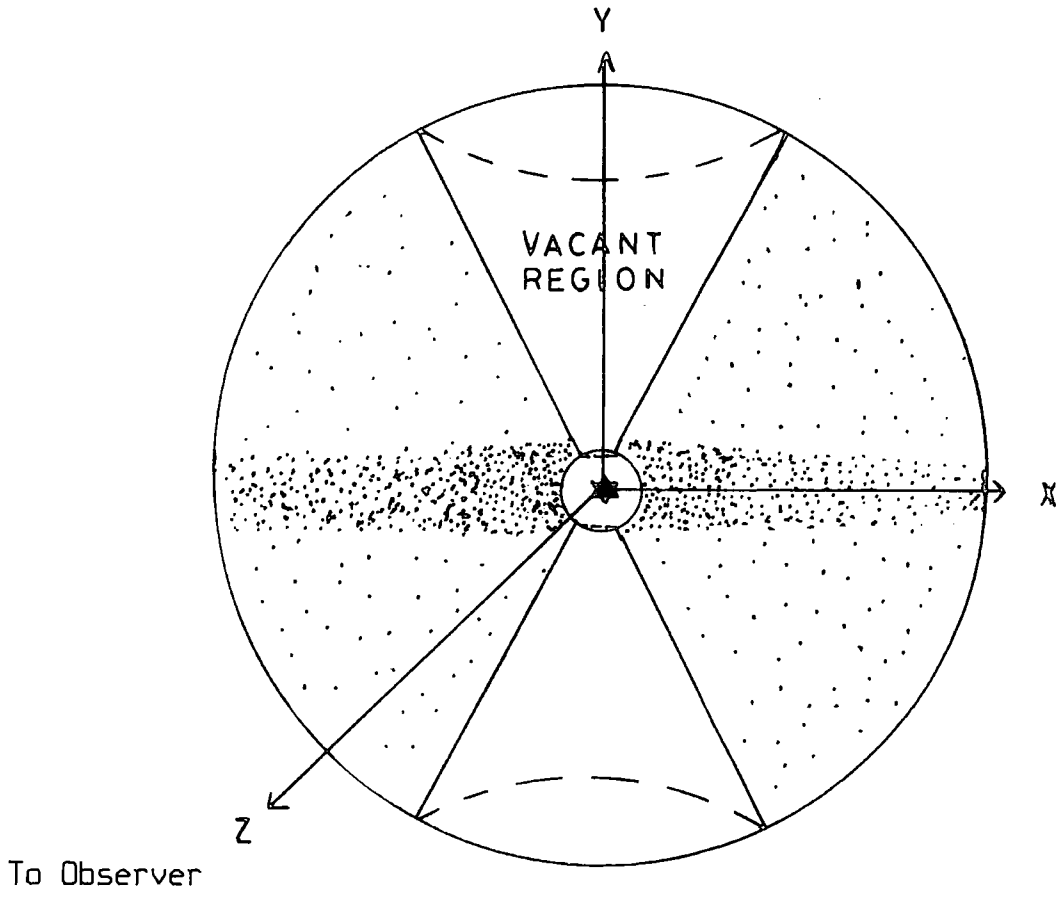

Figure 3.2

Structure of a bipolar nebula, as envisaged by Yusef-Zadeh et al., 1984. The central source is seen through a thick circumstellar disk. Perpendicular to the plane of the disk there is a biconical cavity which is devoid of dust.

3.7 THE EVOLUTIONARY STATUS OF BIPOLAR NEBULAE

Since the discovery of the first bipolar, HD44197 (the Red Rectangle), in the CRL Infra Red survey (Ney et al., 1975) followed closely by many others, the question that needed to be answered was: do these objects all represent the same phenomenon or is it possible for stars of different masses to establish a bipolar nebula at very different evolutionary phases? Attention was directed towards establishing the most likely evolutionary state of the central illuminating sources of these objects. From the very beginning, results hinted towards the phenomenon being exhibited in the pre- or post main sequence phases of stars. Cohen and Kuhi (1977), on investigation of the Cygnus Egg Nebula (CRL 2688) and Minkowski's footprint (M1-92), proposed a post-main sequence evolutionary state for CRL 2688 and a pre-main sequence state for M1-92. Calvet and Cohen (1978) investigated 10 bipolar nebulae using optical spectrophotometry, ir photometry and radio continuum observations of the central stars (and in a few cases the nebular lobes as well). They also included already published data on 3 other objects. Six of their objects, they classified as being protoplanetary nebulae and two, as evolved planetary nebulae. The remaining

three, LkHα233, LkHα208 and Parsamyan 22, they classified as pre-main sequence objects.

Of particular interest to the present work are the nebulosities associated with early stellar evolution. It is important to realize that at the same time as the above work was being carried out, much new information was being gathered concerning early stellar environments and data was becoming available concerning the nature of T Tauri and Herbig Ae and Be stars, which are believed to be among the earliest stellar objects known. Molecular clouds were being discovered and also Herbig-Haro objects were under investigation, both phenomena having possibly important connections with early stellar evolution. As momentum in these fields has gathered, it has become increasingly clear that observations of bipolar nebulae are but a single stage of a complex evolutionary process. In order to gain an overall picture, some of the work in these other fields will be reviewed, and finally evolutionary models will be presented which attempt to explain the observed bipolar phenomenon.

3.8 T TAURI AND HERBIG Ae/Be STARS

Discussion of the nature of young stellar objects really divides into two sections, that of the low mass and that of the high mass objects. The former are a fairly well defined group which have been well studied whilst the latter are much less well defined and studied. Work has had to concentrate on establishing criteria by which the high mass objects can be identified and on confirming that they are not ordinary stars of the same spectral type.

T Tauri stars are low mass stars ($M < 2.5M_{\odot}$) and have been recognized as a distinct class of emission line variables associated with nebulosity since the 1940's (Joy, 1942,1945,1949). Ambartsumian suggested in 1947 that they represented a group of very young pre-main sequence stars of intermediate mass. Since this time, a wealth of observational data has confirmed their pre-main sequence nature. They are found in regions of nebulosity, which are both bright (eg. in Orion) and dark (eg. in Taurus-Auriga), and form groups called 'T associations'. Commonly found in dark clouds with regions of active star formation (Kuhi, 1983), they are typically 12 magnitudes or fainter in brightness and show irregular variations in their light output. Timescales for these variations vary

from minutes (Worden et al., 1981) to decades (Bellingham and Rossano, 1980). Many T Tauris show ir excesses of the order of 0.5 - 1 magnitudes brighter than normal stars of the same spectral type (Haro and Herbig, 1955). The excess is believed to be due to thermal emission of hot circumstellar dust or bound-free and free-free emission from ionized hydrogen.

An interesting point about T Tauris, is that since they are very young stars, one might expect that they would still have considerable angular momentum and therefore be rapid rotators, having only recently condensed from their protostellar clouds. However, Vogel and Kuhi (1981), on investigation of T Tauri stars in Taurus-Auriga and NGC2264, conclude that the angular momentum problem has basically been solved before the stars become visible.

Herbig (1960) was the first to look at the possibility of the existence of higher mass analogues of the T Tauris. He made rough estimates of the numbers of high mass stars, which could be expected to be still in their contracting phase and lie within 1 kpc of the sun. On finding their numbers to be small, but not negligible, he proceeded to look for some characteristic quantity that would define such a group. Herbig chose 26 stars (including LkHα208) which he felt were the strongest candidates. They are now known as the Herbig Ae/Be stars

(HBeS). In an attempt to exclude any interlopers from his sample, (in particular, normal Ae and Be type stars) he chose only stars which fulfilled the following requirements:-

1) They should have spectral type A or earlier with emission lines.
2) They should lie in an obscured region.
3) They should illuminate dust in the region to produce a fairly bright nebula.

At the end of his study, it was clear that the stars did not form a spectroscopically unique group and Herbig was unable to draw any other conclusion than at the outset, ie. the stars in his sample were still the strongest candidates for high mass counterparts of the T Tauris.

Since Herbig's initial work, many others have collected information on these stars in attempts to identify them unambiguously as members of the proposed group. Gillet and Stein (1971) were able to place lower limits on the visual absorption optical depth of an assumed shell of solid particles expected to exist around such stars. They found that they required optical depths of the order of unity to explain their visual and ir data, and so argued strongly for hot dust to be present close to the stars. Cohen (1973) found that the presence of circumstellar dust close to the stellar surface is a

common trait of the HBeS and argued that the existence of grains in such a distructive environment must be regarded as standing in favour of their youth.

Strom et al., (1972) provided further evidence of their youth by calculating their surface gravities relative to ZAMS (zero age main sequence stars). He found many of the stars to have gravities less than ZAMS and further, argued against their being ordinary Be stars on the basis of their ir dust shell emission, which is too great to arise from free-free emission only (as is typical for normal Be stars (Woolf et al., 1970)). Strom also concluded that only 2 out of 14 HBeS used in his set showed any evidence of their being rapid rotators, which is a characteristic of normal Be stars. As with T Tauri stars, the angular momentum problem seems to have been solved before the stars appear visibly. Davies et al., (1983) confirmed Strom's results showing that HBeS of spectral type B6 to B9 rotate significantly slower than ordinary Be stars.

Even so, it still remains for some characteristic group property to be found which conclusively defines the HBeS stars to be high mass pre-main sequence stars. It is clear that spectroscopic characteristics do not provide the required answer.

Finkenzeller and Mundt (1984) have recently compiled all the published optical and ir magnitudes of

the now 57 HBeS and possible candidates with the aim of using photometric data to unambiguously define the group. For 43 of the stars they also collected H_α and NaD profiles. Using this data, they have been able to clearly demonstrate the difference between normal Be stars and HBeS. The location of the two groups is quite different on a H-K, K-L two colour diagram as shown in figure 3.3. Hertzsprung Russell diagrams have also been drawn which show clearly that most of the Herbig Ae/Be stars lie above the main sequence.

3.9 HERBIG-HARO OBJECTS AND MOLECULAR CLOUDS

The prototypes of the Herbig-Haro object class were discovered independently by Herbig (1951) and Haro (1952) near NGC1999 in Orion. Their location in a dark cloud region in the vicinity of the young Orion population stars was immediately taken to infer association of these objects with stellar formation processes (Ambartsumian, 1954).

Extensive work in the optical (Schwartz, 1978 ; Dopita, 1978), near ir (Cohen and Schwartz, 1979) and radio (Rodriguez et al., 1980) have provided much needed observational data concerning these objects. They can be described as being small (typically 1000 AU) optical

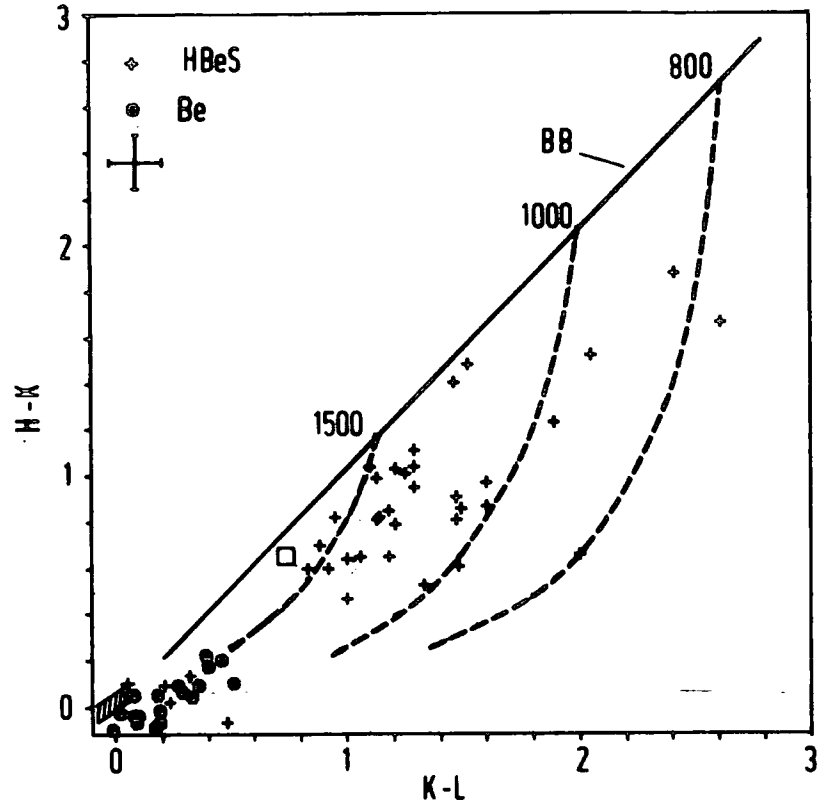

Figure 3.3

H-K, K-L two colour diagram of all Herbig Ae/Be stars for which colours are available. The + signs mark the Herbig Ae/Be stars, while the ●'s mark a number of classical Be stars which have been given for comparison purposes. The typical error on the ir colours is indicated in the upper left hand corner. The main sequence from B0 to F0 is indicated as a hatched bar at the lower left hand corner.

(Figure taken from Finkenzeller and Mundt, 1984)

nebulosities found in small groups near the surfaces of molecular clouds. Their spectra are low excitation emission spectra and are not stellar in origin (Herbig, 1962). The most widely accepted explanation for the observed spectra is that they arise in shocked gas (Dopita, 1978 and Raymond, 1979). A number of models have been put forward explaining the Herbig-Haro nebulae in terms of supersonic mass outflows from young stars which shock against ambient dense cloudlets resulting in the observed Herbig-Haro object (Schwartz, 1978 and references therein).

The exact nature of the energy source is still the basic problem in the study of these objects, as it has been since they were first discovered. The idea of shocked gas being the source, the gas flows emanating presumably from some young star in the vicinity of the Herbig-Haro object, has caused researchers to look for any obvious physical involvement of T Tauris and Herbig-Haro nebulosities. Many such connections have been found, although the proposed exciting stars are rarely directly visible. An exception was the discovery of HH55 in the immediate vicinity of the T Tauri star RU Lupi (Schwartz, 1977). Near ir searches of the surroundings of AS353A (Cohen and Schwartz, 1983) show this star to be responsible for HH32A and HH32B. In all, at least 5 cases of Herbig-Haro association with T Tauris have been found

and many cases are known of Herbig-Haro association with embedded sources having energy distributions consistant with those of T Tauri stars.

Observations of substantial proper motions for some Herbig-Haro objects, and also of the linear alignment of these nebulae with their exciting ir sources, together with the discovery of high velocity, anisotropic molecular flows centred on young objects in dense molecular clouds, have provided the basis for the most recent steps forward.

Cohen and Schwartz (1979) first noticed the alignment of a faint star having weak T Tauri characteristics with HH1 and HH2. Herbig and Jones (1981) published results showing these Herbig-Haros to be moving in opposite directions away from the star. Several other Herbig-Haros have also been found in significant positions with respect to their exciting stars. Examples are HH31A, B and D which are well aligned with IRS2 (Cohen and Schwartz, 1983). HH32A, B and C are aligned with their candidate star AS353A (Mundt et al., 1983). HH39 has been observed to be moving away from R Mon (Jones and Herbig, 1982) and HH28 and 29, from L1551 (Cudworth and Herbig, 1979). All these alignments indicate anisotropic mass loss from the candidate stars, which is probably well collimated (Cohen and Schwartz, 1983).

The phenomenon of CO bipolar flows in deeply embedded sources seemingly provides further information on

the subject. High velocity gaseous outflow in regions of star formation have been under scrutiny since the first source of such a flow was detected in Orion (Zuckerman et al., 1976). Recently, high resolution studies of the flow have shown it to be bipolar (Erikson et al., 1982). In 1980 spatially extended outflows associated with L1551 (Snell et al., 1980) and Cepheus A (Rodriguez et al., 1980) were reported. In both of these sources blue and red shifted CO emissions were observed and found to arise from two separate regions which extended in opposite directions. The number of such known high velocity ($V > 30$ kms^{-1}) flows, has increased to about 20 and these are centred on ir sources buried deeply in molecular clouds (Rodriguez et al., 1982 ; Bally and Lada, 1983). At least half of these are bipolar with a strong possibility that the others appear isotropic only due to projection effects or to the lack of angular resolution. Bally and Lada (1983) find that the linear dimensions of the high velocity flows fall within the narrow range 0.1-0.3 pc. They also note that these flows decrease as the objects evolve, since they find only low velocity flows ($V < 10$ kms^{-1}) with no specific morphology for most of the cometary and bipolar nebulae in their sample (which included the bipolar nebula centred on LkHα208). No clearly defined bipolar molecular flows have yet been recognized around any visible T Tauri.

REFLECTION NEBULAE

The association of high velocity molecular gas, Herbig-Haro objects and low luminosity ir sources embedded in dark clouds, suggests that the interaction of winds from young stars with the ambient molecular cloud, may give rise to these phenomena. The picture that is emerging is one where oppositely directed flows develop from deeply embedded sources in dense molecular clouds. The flows can be detected by mapping of the CO emission. Only when the flows break free of the dark cloud material do we see evidence of this ejection in the form of shocked gas, appearing to us as Herbig-Haro objects (and also water masers although these will not be discussed here). The lack of observed bipolar flows around visible T Tauris, or HBe stars for that matter, together with the lack of high velocity flows around visual compact nebulae could be evidence that the well collimated mass loss/outflow stage occurs only at the earliest periods of development of the stars. An interesting point to note is that in a recent search in the UBVRI wavebands for previously unknown bipolar nebulae, covering nearly the whole Milky Way north of $\delta=-30^{0}$, the twenty new objects found all had similar dimensions to the sizes of the known high velocity molecular flows (Neckel and Staude, 1984).

Various theoretical models have been developed to explain the environmental observations concerned with young star forming regions. Most attention has been

directed at explaining the bipolar flows and Herbig-Haro objects and to a lesser extent bipolar and cometary nebulae. Canto and Rodriguez (1980), Canto at al. (1981), Barral and Canto (1981) and Konigel (1982) have produced fairly comprehensive models based on the collimation of stellar winds which could occur when an originally isotropic stellar wind interacts with a surrounding cloud. A basic outline of several of the models will be presented here.

3.10 THEORETICAL MODELS

The need for anisotropic flows emanating from the central object is becoming more and more clear from observational data and theoretical calculations. Isotropic unfocused stellar winds would require much higher velocities than could be reasonably expected if they were to produce the shock processes believed in many quarters to be necessary to explain the Herbig-Haro phenomenon.

Among early work which explored possible wind focusing mechanizms was the work by Canto and Rodriguez (1980). They considered the interaction of an isotropic stellar wind with a nebular environment having a pressure gradient - a situation that could well apply for recently formed stars located at the edge of a dark cloud. The

result is the formation of an ovoid shaped cavity (figure 3.4). The stellar wind suffers a shock at the cavity walls and is refracted to the tip of the ovoid, towards the lower density medium. Another shock occurs here and on cooling, the shocked gas radiates as a Herbig-Haro object. Canto and Rodriguez applied their model to HH1 and found it to be satisfactory in accounting for the observations.

Canto et al., (1981) soon applied their ideas on focusing to the more particular case of the nebulosity NGC2261, illuminated by R Mon. Seven arc minites (1.4pc) north of R Mon and on the axis of symmetry of the nebula is the Herbig Haro object, HH39. CO observations of the region show an elongated (0.8 × 0.4 pc) molecular cloud centred on the star. There is also evidence of two antiparallel, low velocity molecular flows, with speeds of a few kms^{-1} perpendicular to the direction of elongation of the cloud. Canto et al., propose that R Mon has recently formed out of the disk shaped molecular cloud and that an initially isotropic stellar wind was focused by the pressure distribution in the disk, into two antiparallel streams along the poles. These created a bipolar cavity in the disk and the northern cavity shines by reflected light from R Mon and is seen as NGC2261. The southern cavity is obscured by the cloud, due to the tilt of the nebula with respect to our line of sight. Thus Canto et al., propose that the cometary nebula is in fact

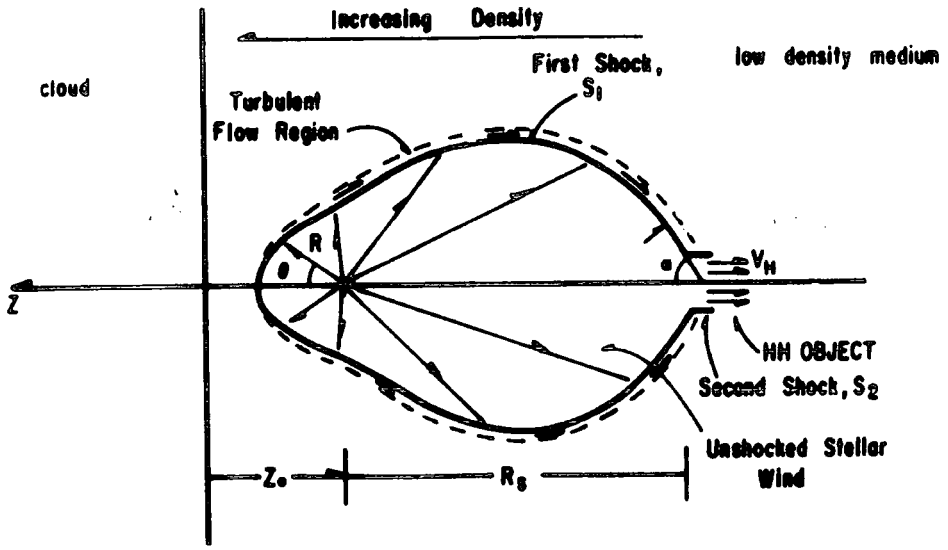

Figure 3.4

A scheme showing the main characteristics of the stellar-wind focusing mechanism. The stellar wind suffers a first shock, S_1 at the walls of the ovoid configuration and is refracted towards the distant tip. A second shock, S_2 occurs here. Upon cooling the shocked gas radiates as a Herbig Haro object.

(Figure taken from Canto and Rodriguez, 1980)

bipolar, but one lobe is obscured. The bipolar streams are finally injected into the low density surrounding medium. Canto et al. then propose that on emerging from the cloud, the streams narrow and HH39 is the result of the northern stream shocking against another cloud. The above scenario is named the interstellar nozzle effect and is depicted in figure 3.5.

Among the most recent and complete models is that proposed by Konigel (1982). The scenario envisioned by Konigel is one where a spherically symmetric stellar wind expands into the surrounding molecular cloud which has an anisotropic and inhomogeneous density distribution. The wind evacuates an interstellar bubble which elongates along the direction of the steepest external density gradient. Under conditions which may characterize the protostellar environment, Konigel shows that this bubble can become unstable, leading to the formation of nozzles which then channel the flow into two oppositely directed supersonic jets.

The jets will accelerate any dense clumps of matter lying in their path and these may then be identified as Herbig-Haro objects. In this way Konigel is able to explain the observed proper motions of the Herbig-Haro objects. While the jets are confined to the molecular cloud, they push ahead of them dense layers of shocked and swept up ambient material. These layers move

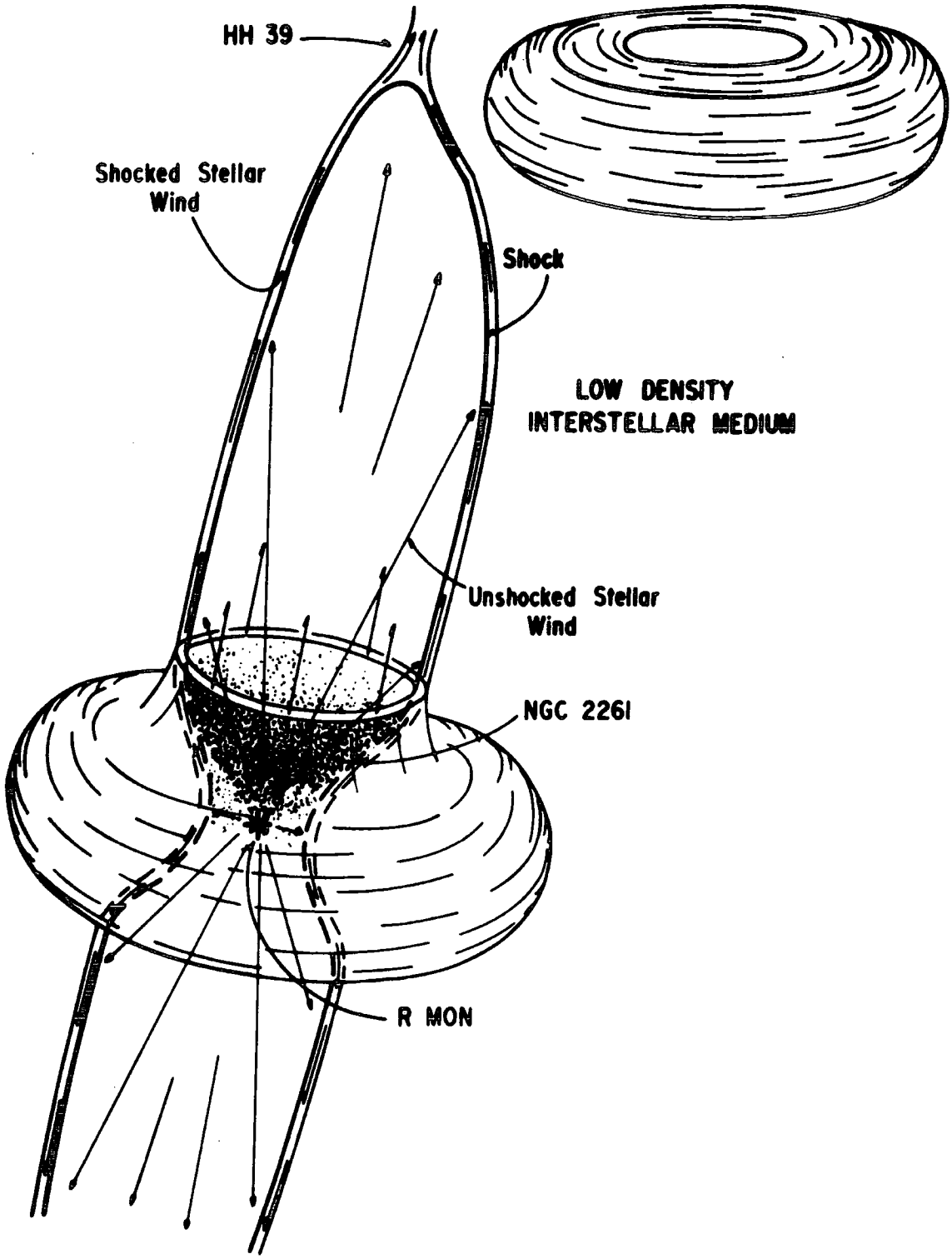

Figure 3.5

The interstellar nozzel.

(Figure taken from Canto et al., 1981)

more slowly than the jets and are proposed to be responsible for the observed molecular flows. On emerging through the cloud, the ends of the jets will be seen as cometary or bipolar nebulae, depending on the orientation of the structure with respect to our line of sight. The object will finally be observed through a thick disk or torus centred on the star, with one or two nebular lobes.

As more observational data becomes available the above evolutionary models will be changed and refined. In view of this, observational data already published on the bipolar nebulosity centred on LkHα208 will be presented, followed by chapters presenting new data on the nebulosity together with interpretations. These may help to shed more light on the latter stage of the above scenarios, namely that of the bipolar nebular phenomenon.

3.11 LkHα208 AND ITS NEBULOSITY

Herbig (1960) included LkHα208 ($\alpha=6^{H}2.1^{M}$, $\delta=+18^{0}42'$, epoch = 1900) in his sample of 26 stars which he examined with the aim of identifying a class of objects that would be higher mass analogues of the T Tauris. He found it to be a thirteenth magnitude star, and described the spectrum as being that of an extended envelope superimposed on a rather late type B star. Herbig and Rao

(1972) designated the spectrum of the star as B5-B9e. It is located near the edge of a dark cloud which extends about 1 degree to the north and south, and lies precisely between two nebular lobes which give the object the appearance of an hourglass. The lobes are about 1 arc minute in diameter, and the spectrum of the northern nebulosity shows strong absorption lines of hydrogen and appears to be purely a reflection of the star (Herbig, 1960)

1.8 degrees north of LkHα208 is a large HII region, NGC2175, which is excited by HD42088, an O6 star with a distance modulus of 11.5 magnitudes (Walker, 1956). If the two nebulae are associated in space then this gives a distance of 2 kpc to the object. Calvet and Cohen (1978) however, place a lower limit of 0.44 kpc to the object, assuming association with a bright A0 star (HD41787) which lies 3 arc minutes east of LkHα208. They also classify the spectral type of LkHα208 as F0V, proposing a possible change in spectral type over the last 50 years, although they note that there is cause for caution, since they examined different spectral regions to Herbig for their classification. On the basis of continuum measurements, they calculate an intrinsic extinction to the star as $A_V \simeq 3.5$.

Alan (1973) measured the near ir magnitudes of 248 early type emission stars. For LkHα208, he found colour

indices of H-K>0.7 magnitudes and K-L>1 magnitude. Of the two possible mechanisms which could account for such ir excesses, namely thermal radiation from hot circumstellar dust and/or electron bremsstrahlung originating in a shell of ionized gas, Alan concluded that the colour indices in this case were too high to be accounted for by the latter alternative. This work has further been confirmed and discussed by Strom et al., (1972), Cohen (1973), Calvet and Cohen (1978), and Finkenzeller and Mundt (1984). All argue for the presence of hot (1600 K) circumstellar dust, possibly in the form of a disk perpendicular to the major axis of the lobes and close to the stellar surface. Vrba (1979) to some extent confirmed the above deductions by observing the intrinsic polarization of the star through a 10 arc second aperture from 1 to 3 μm^{-1}. However, it seems very likely that this aperture would contain not only circumstellar dust but also material contained in the nebular lobes. He found polarizations in the range of 1% to 3% with vector position angles perpendicular to the major axis of the disk and argued that the low levels of polarization are consistant with the production method being that of scattering from the circumstellar dust, which is inefficient.

Cohen (1980) investigates the nature of the dust by looking for spectral features in the 10 μm region. He finds that for LkHα208, the emission spectrum matches the

features of silicate grains identified in the Trapezium region of Orion. Finkenzeller and Mundt (1984) have compiled all available data concerning LkHα208 and 56 other Herbig Ae/Be candidates, and together with new data, clearly demonstrate that LkHα208 belongs to the Herbig class of pre-main sequence, high mass counterparts of the T Tauris.

Observational information concerning LkHα208 is listed in table 3.1. Note that the visual extinction has been calculated with R=3.1 and the ir excess at 3.5 μm is defined by $(V-L)-(V-L)_0$ where $(V-L)$ is the dereddened measured colour and $(V-L)_0$ is the intrinsic colour of a main sequence star with the same spectral type.

Observations of molecular flows around the object have revealed evidence for only low velocity flows (6.5 kms^{-1}) with no specific morphology (Bally and Lada, 1983). Bally and Lada find it difficult to decide if the flows reflect localized energetic activity centred in the star or turbulent, gravitationally bound motions in the ambient molecular cloud.

The only investigation so far to have been carried out concerning the nebular lobes was by Khachikyan and Parsamyan (1965), who photographed the nebulosity in three colours in a system similar to the UBV system and reported the northern lobe as being brighter than the southern lobe by one magnitude in U and half a magnitude in B and V.

Table 3.1

Observations		Reference
Photographic magnitude	13	Herbig (1960)
Spectral type	B5 - B9e	Herbig and Rao (1972)
H_α equivalent width	5 Å	Finkenzeller and Mundt (1984)
H_α FWHM	210 kms^{-1}	
H_α profile type	double peak emission	
Visual magnitude	12.74	Dibai (1969)
U-B	0.31	
B-V	0.47	
Visual Extinction, Av	1.9	
Infra-red magnitudes		
H	9.85	Alan (1973)
K	8.88	
L	7.28	
Infra-red excess at 3.5 μm	4.0	

They propose that the luminosity of the nebula cannot be solely attributed to reflection of the light by the central star, since they calculate the brightness of the nebula to exceed by three stellar magnitudes that predicted by the Hubble relationship.

New data of the nebular lobes will now be presented with the aim of further investigating the role of bipolar reflection nebulae in the pre-main sequence evolution of stars.

CHAPTER 4

NEW OBSERVATIONAL RESULTS

4.1 OBSERVATIONAL DETAILS

Polarimetric observations were made of the nebulosity illuminated by the star LKHα208, on January 1st, 1979. The observers were Drs. S.M.Scarrott, K.J.Watts and R.F.Warren-Smith. The instrumentation consisted of the Durham imaging polarimeter and a McMullan electronographic camera. These were used in conjunction with the 1 metre telescope at the Wise Observatory, Israel, at the f/13.5 focus. The operation of the polarimeter system and the subsequent data reduction procedures has already been well documented by Warren-Smith (1979) and Scarrott et al.,

(1983). Four one hour exposures were taken using a broad band V filter (GG455 + BG38), and Ilford L4 emulsion. The grids were aligned north to south, and the nebula lay along the centre of one of the polarimeter grids. Reduction of the data was carried out on a Vax11/750 computer using the suite of programmes developed by Warren-Smith.

The nebulosity was later observed in the standard UBVR wavebands using only the electronographic camera. The observations were again made at the Wise Observatory, this time at the f/7 focus, on the nights of the 17th to 23rd November 1982. The observers were D.S.Berry and the author. Flat field exposures were made for each waveband, a screen on the inside of the observatory dome being uniformly illuminated for this purpose. Kodak electronographic emulsion was used and altogether, exposures totalling 230 minutes were aquired of the object in U, 150 minutes in B, 160 minutes in V and 180 minutes in R. In between each exposure the image was moved by several millimetres on the photocathode of the electronographic camera. This ensured that in the event of any part of the photocathode being insensitive (due, for example, to photocathode defects), all parts of the object could still be measured.

4.2 REDUCTION OF THE DIRECT ELECTRONOGRAPHIC DATA

The electronographs were digitized using the P.D.S. microdensitometer at the Royal Greenwich Observatory. The reduction procedure was then standard, apart from some alignment problems which necessitated using defects on the photocathode to line up the flat fields and the object electronographs. Procedures from the Electronographic Data Reduction System (EDRS) developed for Starlink (a network of Vax11/780 and Vax11/750 computers comprise the S.E.R.C Starlink project) by Warren-Smith, were applied to the raw data. These enabled removal of the unexposed film density from each exposure. Slight nonlinearities in the response of the emulsion and microdensitometer, and drifts in the zero level which occur during scanning, were also accounted for. Flat fields were 'cleaned' by locating localized blemishes, such as scratches and dirt, and were then checked for consistancy between different images to locate any smooth blemishes. The flat field exposures were then aligned and averaged to produce a map of the photocathode. The map acts as a sensitivity calibration, enabling correction of the object electronographs for the point to point variations in the sensitivity of the photocathode. After

subtraction of the background night sky signal from each of the object plates, the object images were aligned using appropriate stars in the field. The images were then stacked to produce a final, corrected image.

Both the polarimetry images and the direct images were calibrated for scale using the coordinates of six stars in the field of the object. These coordinates were taken from the Palomar Sky Survey plates and are listed below in table 4.1. The stars concerned are marked on plate 1. The scales of the final images are listed in table 4.2, as are the seeing disk sizes for each waveband. The seeing disk size was estimated for each colour by fitting gaussian profiles to star images in the field.

Table 4.2 also lists the mean effective wavelength, and the bandwidths for each filter. These were calculated by determining the resultant spectral energy distribution of the star when observed through the various optical components. The spectral characteristics of the individual filters, the telescope mirrors, the atmosphere and the electronographic camera were taken into account. The source, LKHα208 was represented by a black body radiating at 7000 K (Calvet and Cohen, 1973).

It has not been possible to calibrate the zero point in the magnitude scale for any of the images, since the central star LKHα208 was burnt out on both long and short exposures. All of the other stars in the digitized

Table 4.1

Number of star on plate 1	Right Ascension (1950)	Declination (1950)
1	$6^H\ 4^M\ 58.169^S$	$18^\circ\ 40'\ 53.13"$
2	$6^H\ 4^M\ 53.419^S$	$18^\circ\ 41'\ 30.84"$
3	$6^H\ 4^M\ 53.197^S$	$18^\circ\ 42'\ 03.66"$
4	$6^H\ 4^M\ 48.896^S$	$18^\circ\ 41'\ 38.67"$
5	$6^H\ 4^M\ 52.725^S$	$18^\circ\ 38'\ 28.10"$
6	$6^H\ 4^M\ 47.195^S$	$18^\circ\ 38'\ 55.25"$

Table 4.2

Waveband	Scale in arcseconds per pixel	Seeing disc (arcseconds)	Mean Wavelength	Bandwidth of Transmitted Spectrum
U	1.8	3.0	3805Å	325Å
B	1.8	2.8	4473Å	941Å
V	1.8	2.4	5402Å	713Å
R	1.8	2.3	6479Å	1488Å
V(GG455 + BG38)	1.4	3.5	5198Å	1133Å

field, for which the magnitudes were known, were also burnt out. Attempts were made to calibrate the data by comparison with that of Khachikyan and Parsamyan (1965) who recorded their data in 9.7 arcsecond bins. Unfortunately, it was difficult to compare their data points with the new data, since the presentation of their data with respect to north was found to be in error. At best the new data in B and V could only be calibrated roughly to within 0.5 magnitudes.

Plate 1 shows a print of the object in the visual using an electronograph as the negative. The presence of the dark cloud to the ~~right~~ left hand side of the print may be inferred by the low number of stars in this region. Plates 2, 3, and 4 are photographs of the nebula in the visual waveband. They have been taken from an image display unit. The upper and lower data values displayed are changed for each plate, so highlighting the different features of the nebulosity. Contour maps of all the colours are presented in figures 4.1 to 4.4. A polarization map of the object is presented in figure 4.5. The polarization at each point is represented by a line, the length of which is proportional to the degree of polarization and the orientation of which is parallel to the E vector. The polarization is shown superimposed on a contour map of the object in figure 4.6. Traces of polarization and brightness along the major axis of the nebula (running north to south through the star

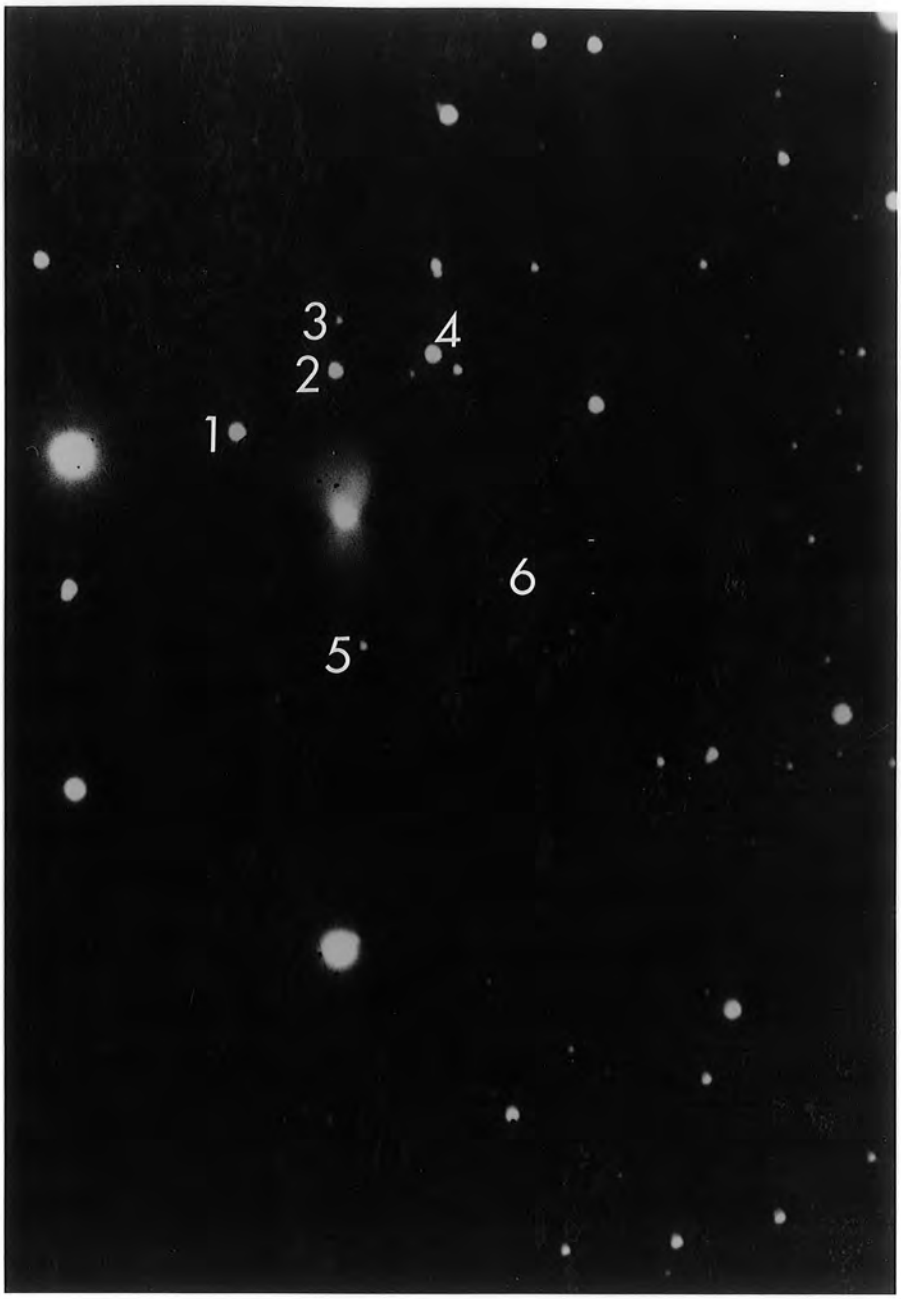

PLATE 1

A print of the nebulosity illuminated by LKHα208 in the visual waveband. An electronograph was used as the negative. The polarimetry images and the direct images were calibrated for scale using the coordinates of the six marked stars.

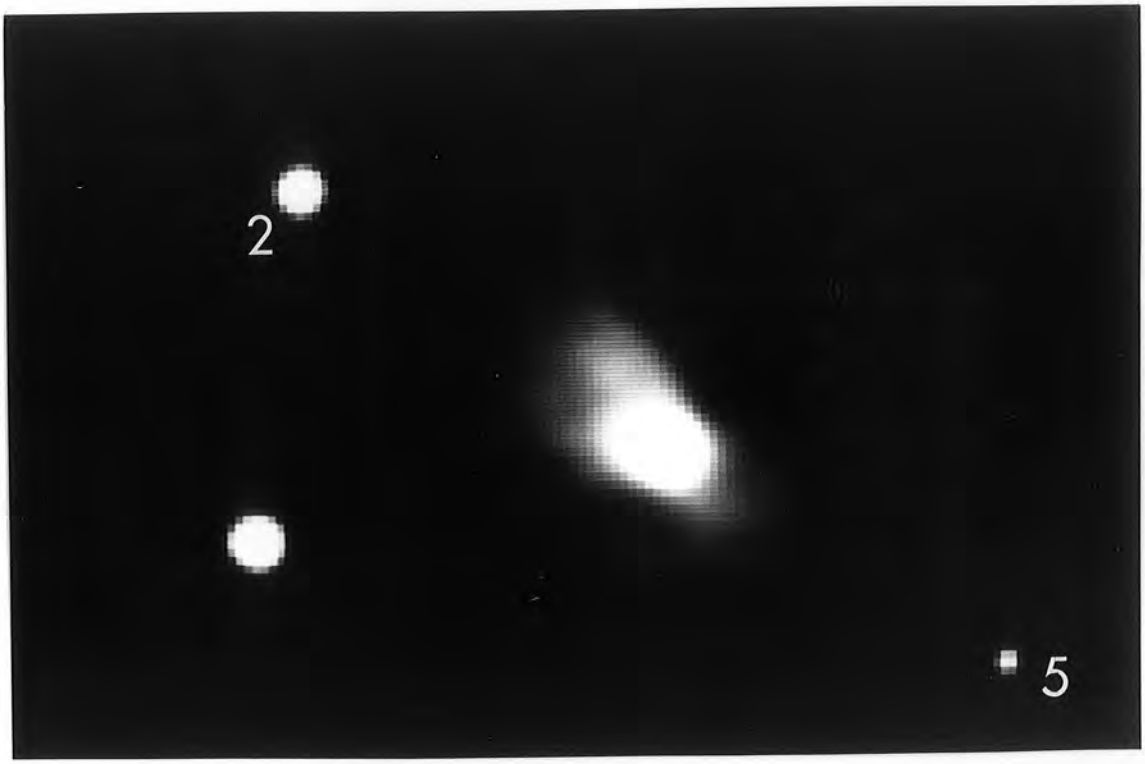

PLATE 2

Plates 2, 3, and 4 are photographs of the nebula in the visual waveband. They have been taken from an image display unit. The upper and lower data values displayed are changed for each plate, so highlighting the different features of the nebulosity. Plate 2 displays the highest intensity regions and plate 4 displays the lowest. The stars marked 2 and 5 on plate 1 are also shown.

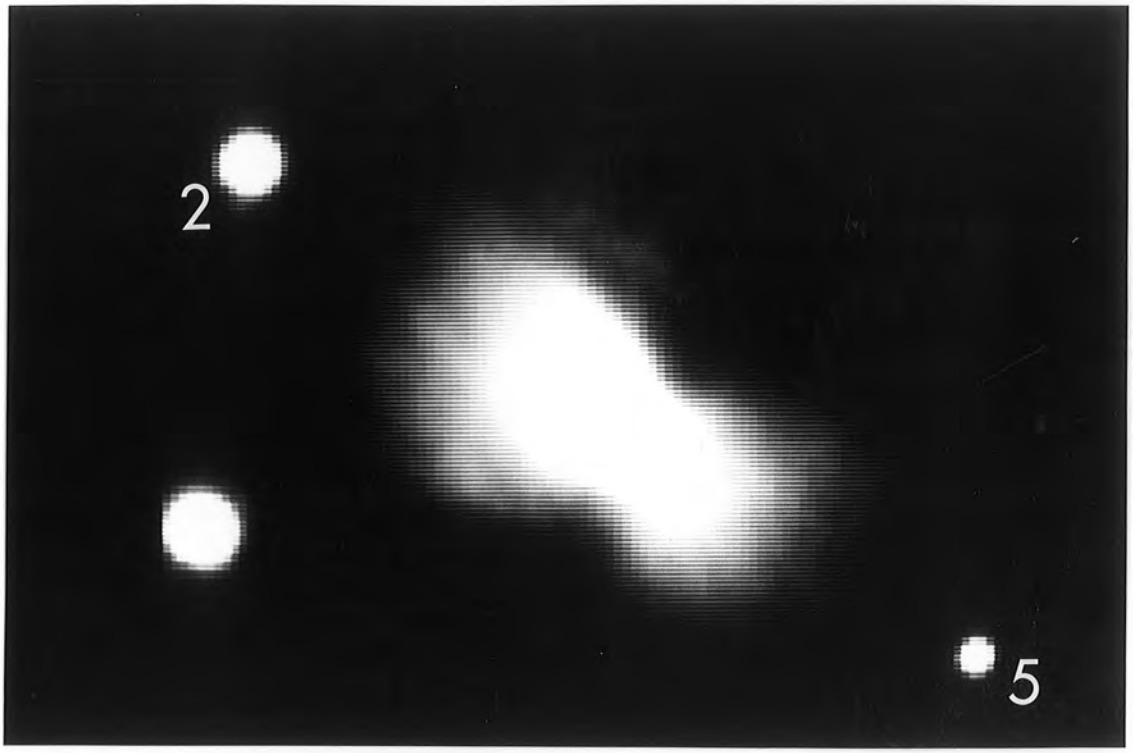

PLATE 3

The nebulosity illuminated by LKHα208
in the visual waveband.

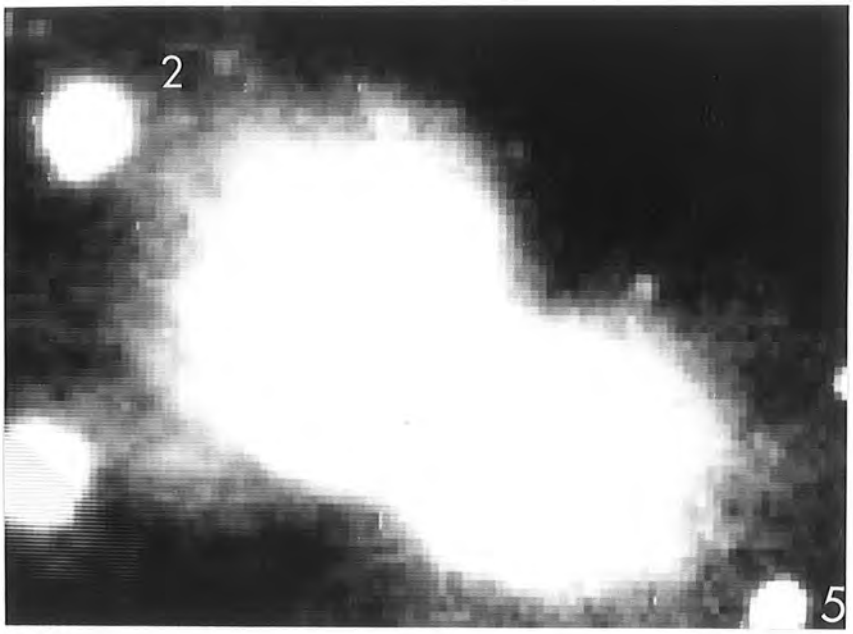

PLATE 4

The nebulosity illuminated by LKHα208
in the visual waveband.

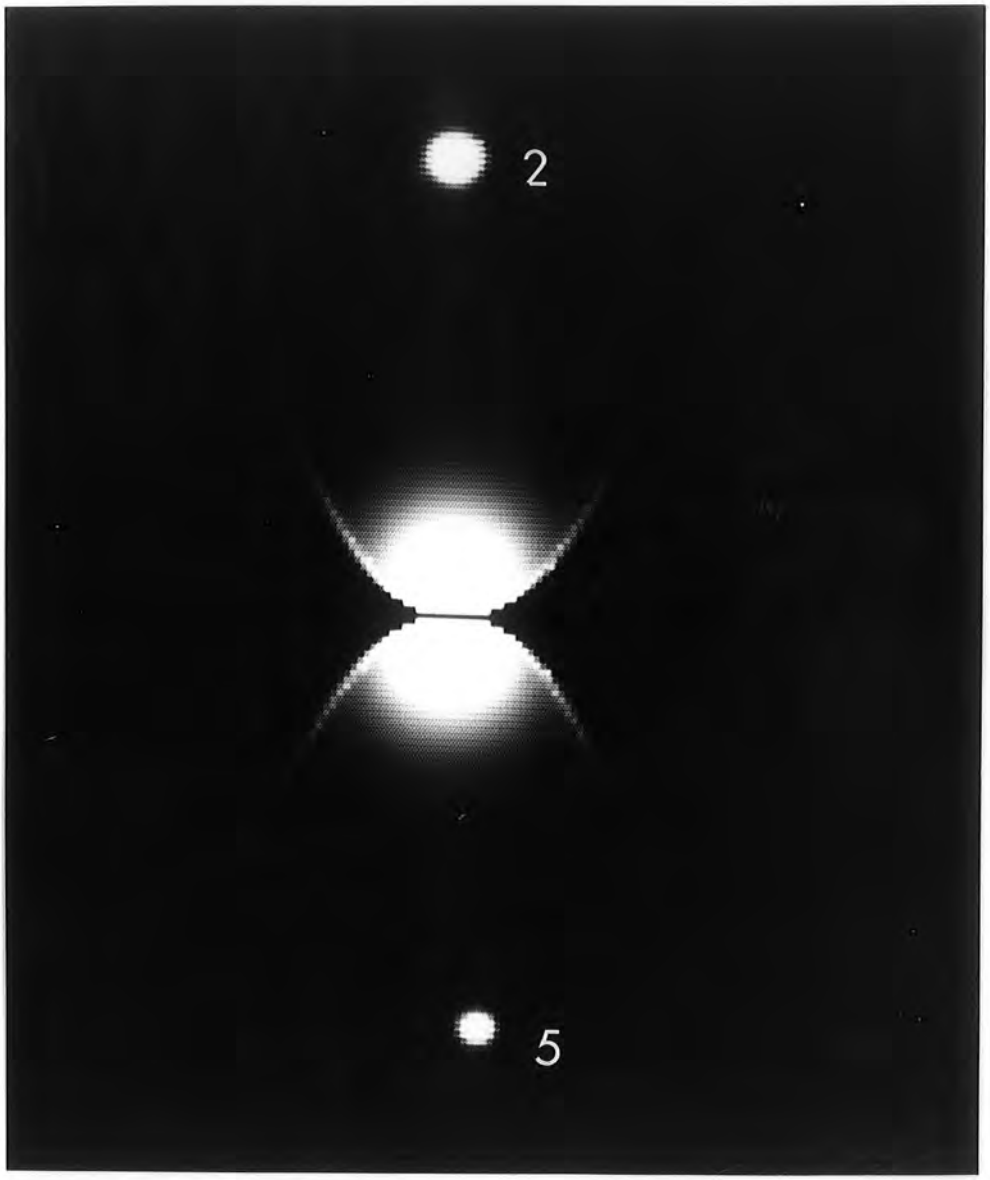

PLATE 5

A simulated model image of the nebulosity in the visual waveband. The dust responsible for the scattering of radiation from LKHα208 is concentrated at the parabolic surfaces of the cavity model nebula. The optimized nebula parameters, recorded in the text, were used to generate this image. The photograph has been taken from an image display unit and the stars marked 2 and 5 on plate 1 are also shown.

Focus of inner paraboloid = 10.97 arcseconds
Focus of outer paraboloid = 8 arcseconds

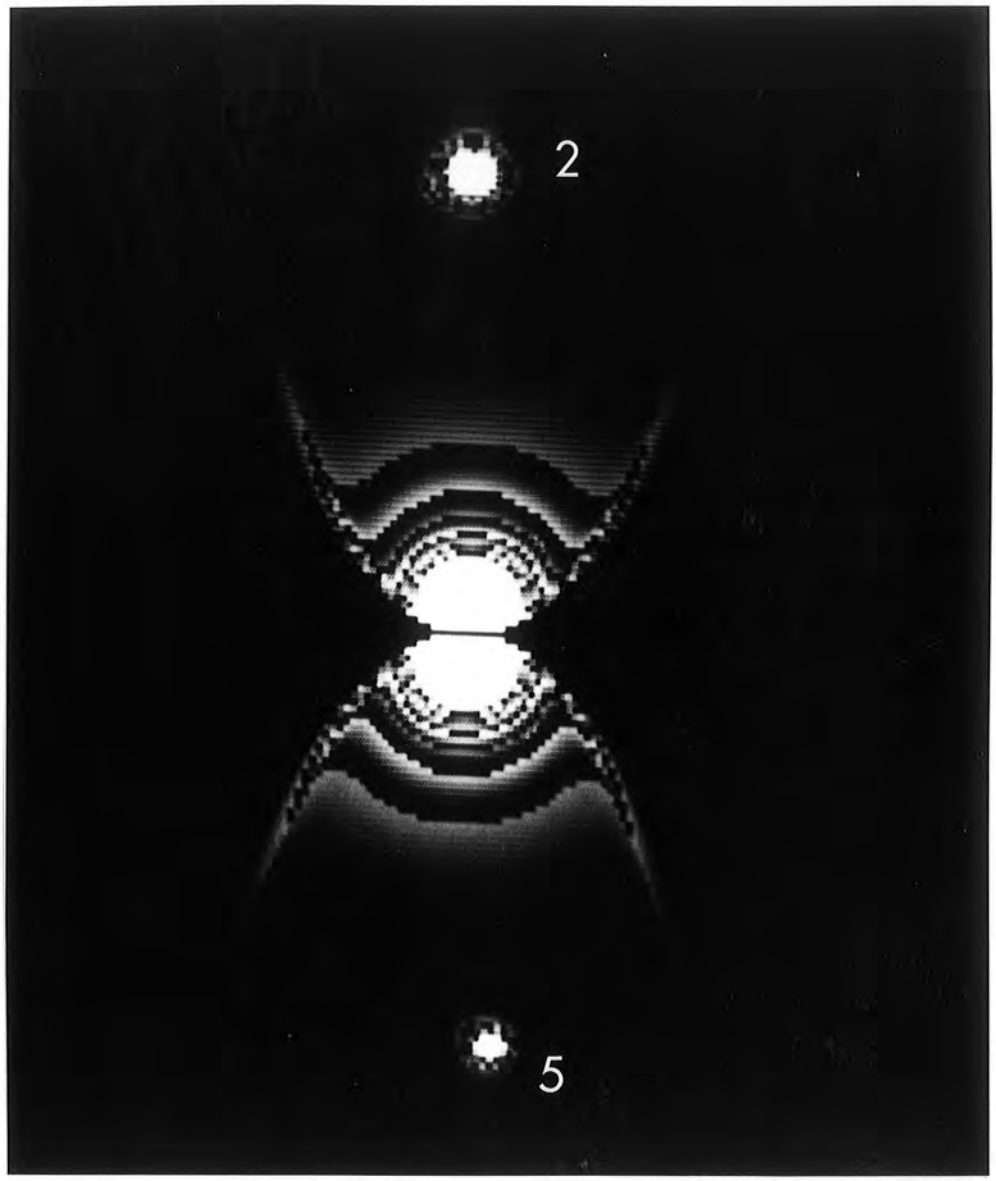

PLATE 6

A simulated model image of the nebulosity in the visual waveband shown contoured, to give an impression of the form of the intensity fall-off with increasing distance from the star. Again, the photograph was taken from an image display unit and stars 2 and 5 are marked.

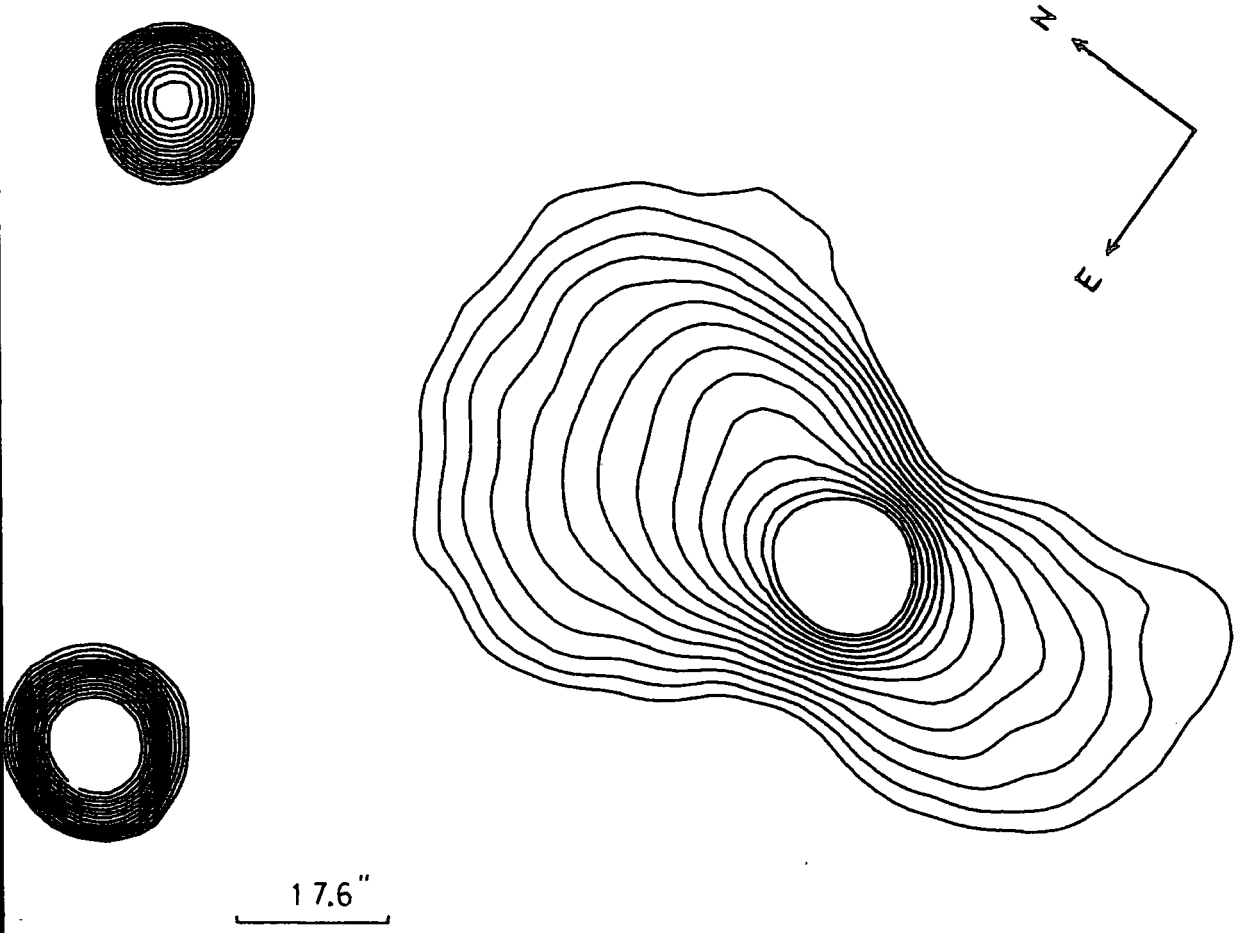

Figure 4.1

A contour map in the ultra-violet waveband, of the bipolar nebulosity illuminated by the star LkHα208. The contour spacing is 0.2 magnitudes. The data presented here has been smoothed by averaging in bins of 2x2 pixels.

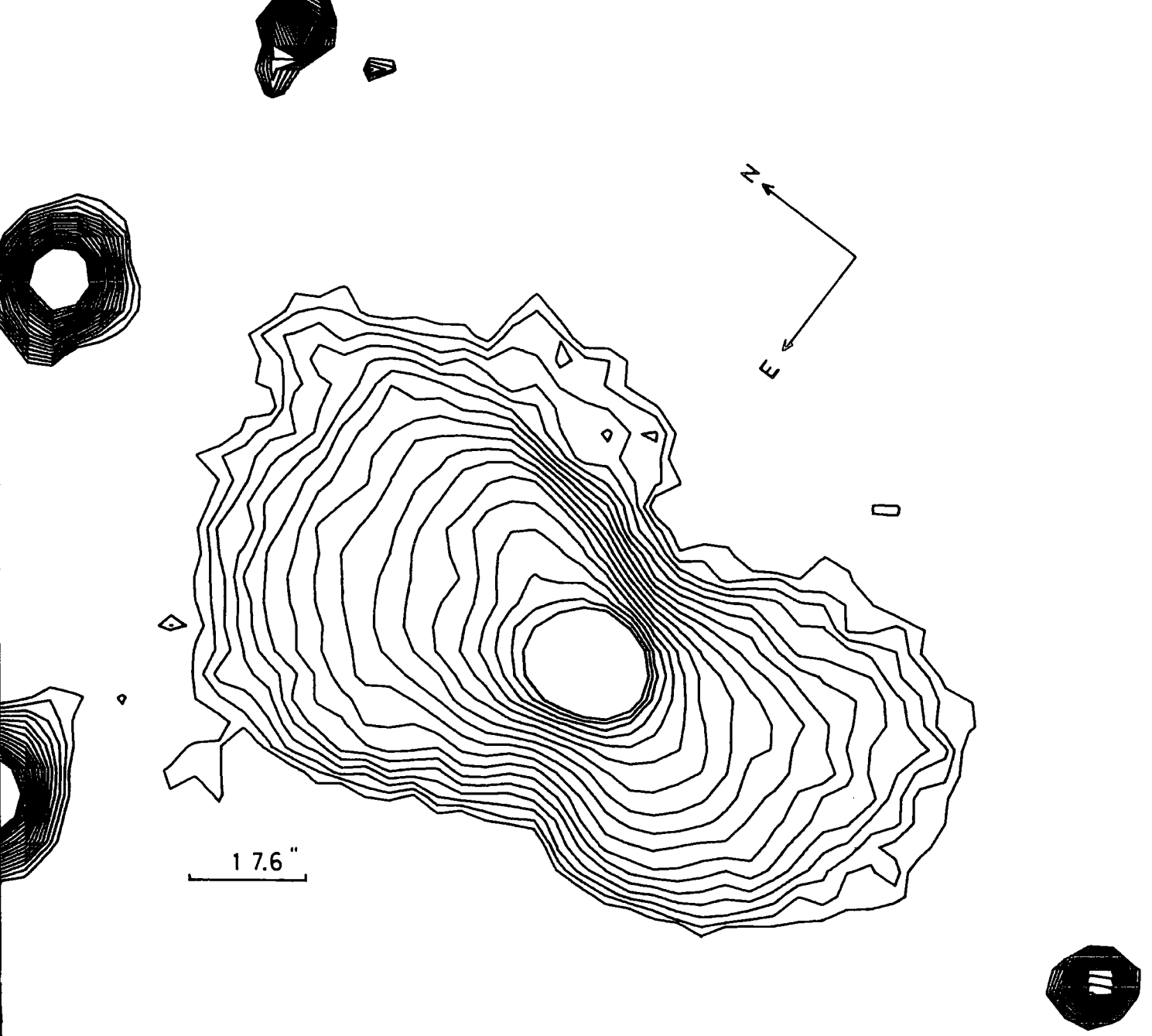

Figure 4.2

A contour map in the blue waveband, of the bipolar nebulosity illuminated by the star LkHα208. The contour spacing is 0.2 magnitudes.

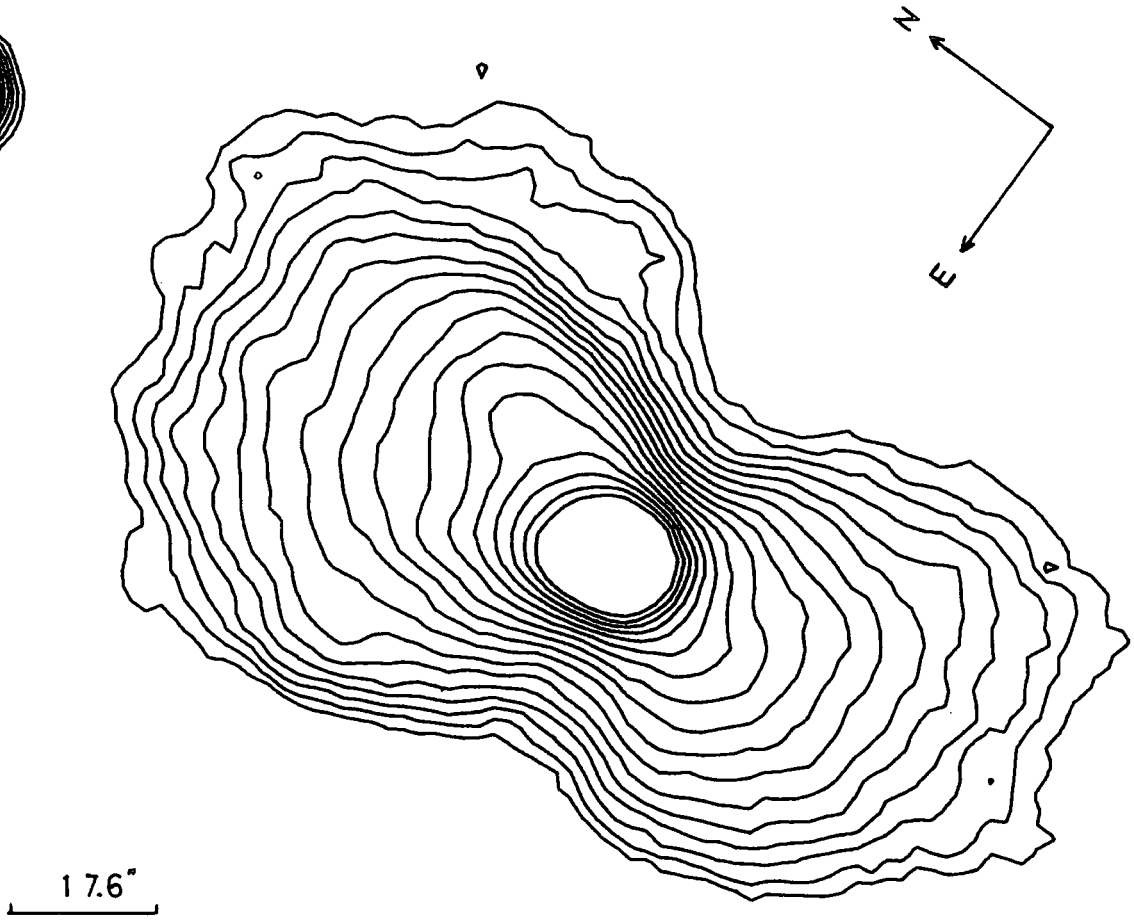

Figure 4.3

A contour map in the visual waveband, of the bipolar nebulosity illuminated by the star LkHα208. The contour spacing is 0.2 magnitudes.

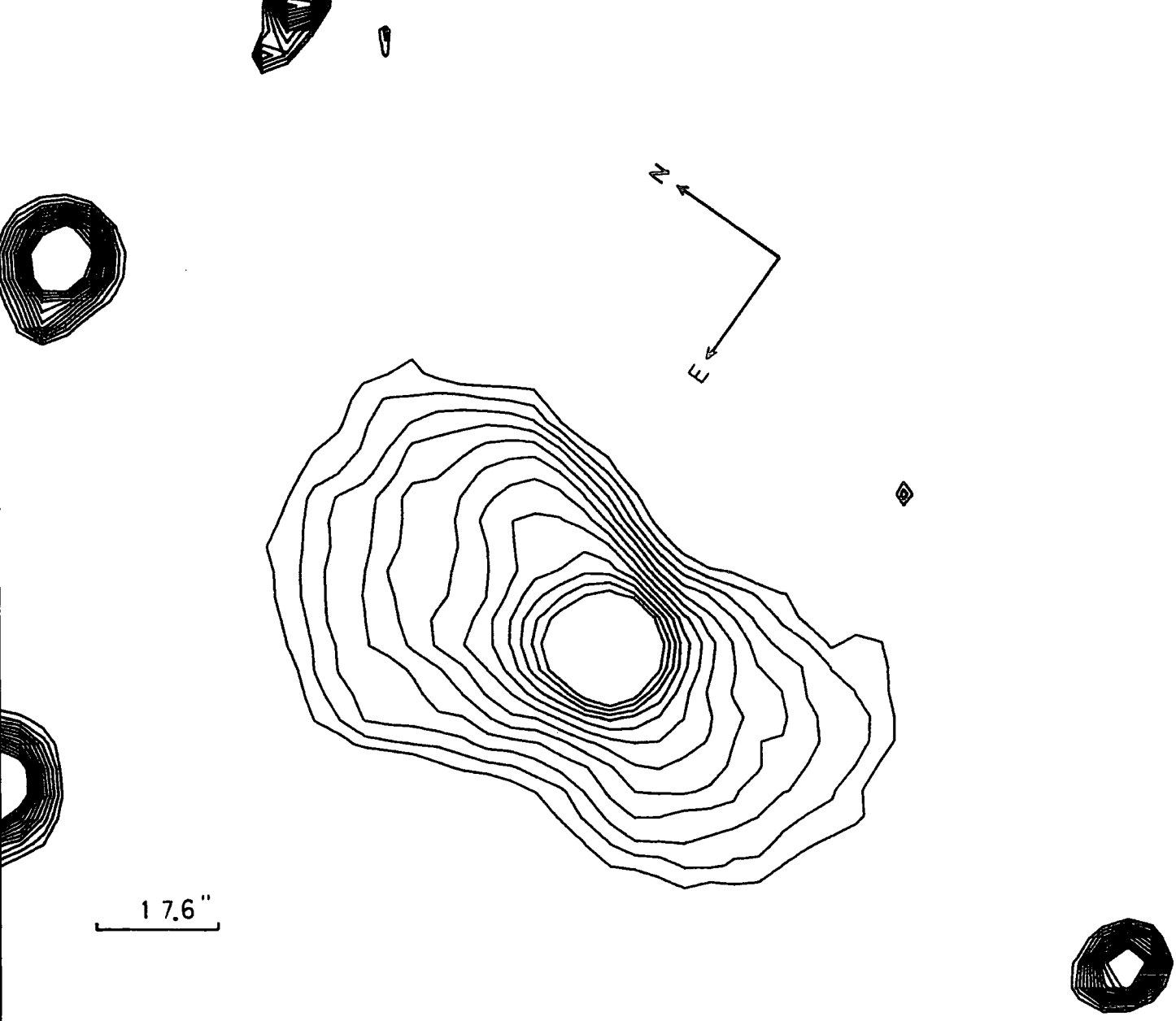

Figure 4.4

A contour map in the red waveband, of the bipolar nebulosity illuminated by the star LkHα208. The contour spacing is 0.2 magnitudes. The data presented here has been smoothed by averaging in bins of 2x2 pixels.

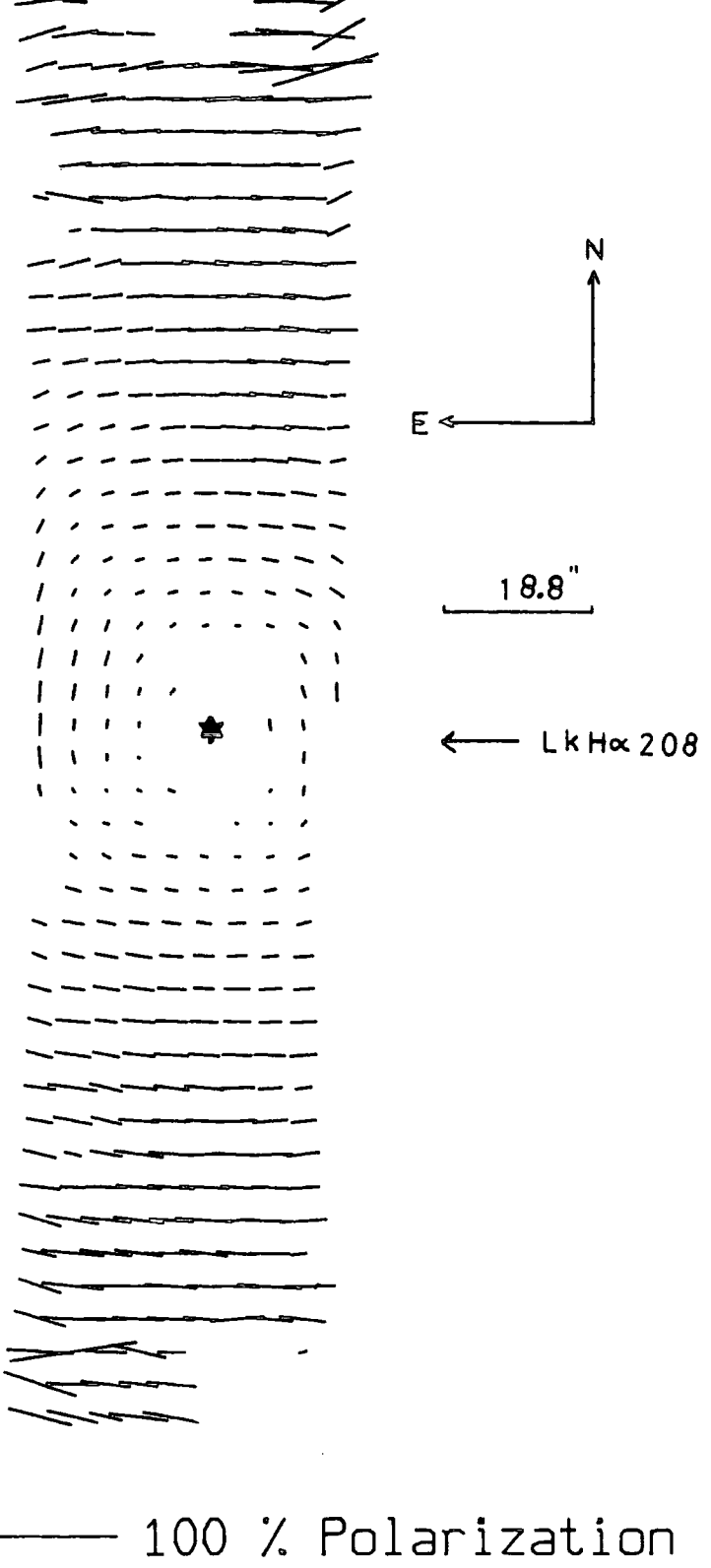

Figure 4.5

The linear polarization map of the bipolar nebulosity associated with LKHα208. The integration bins used are 3 × 3 pixels, at 3 pixel intervals. The observations were made using a broad band V filter.

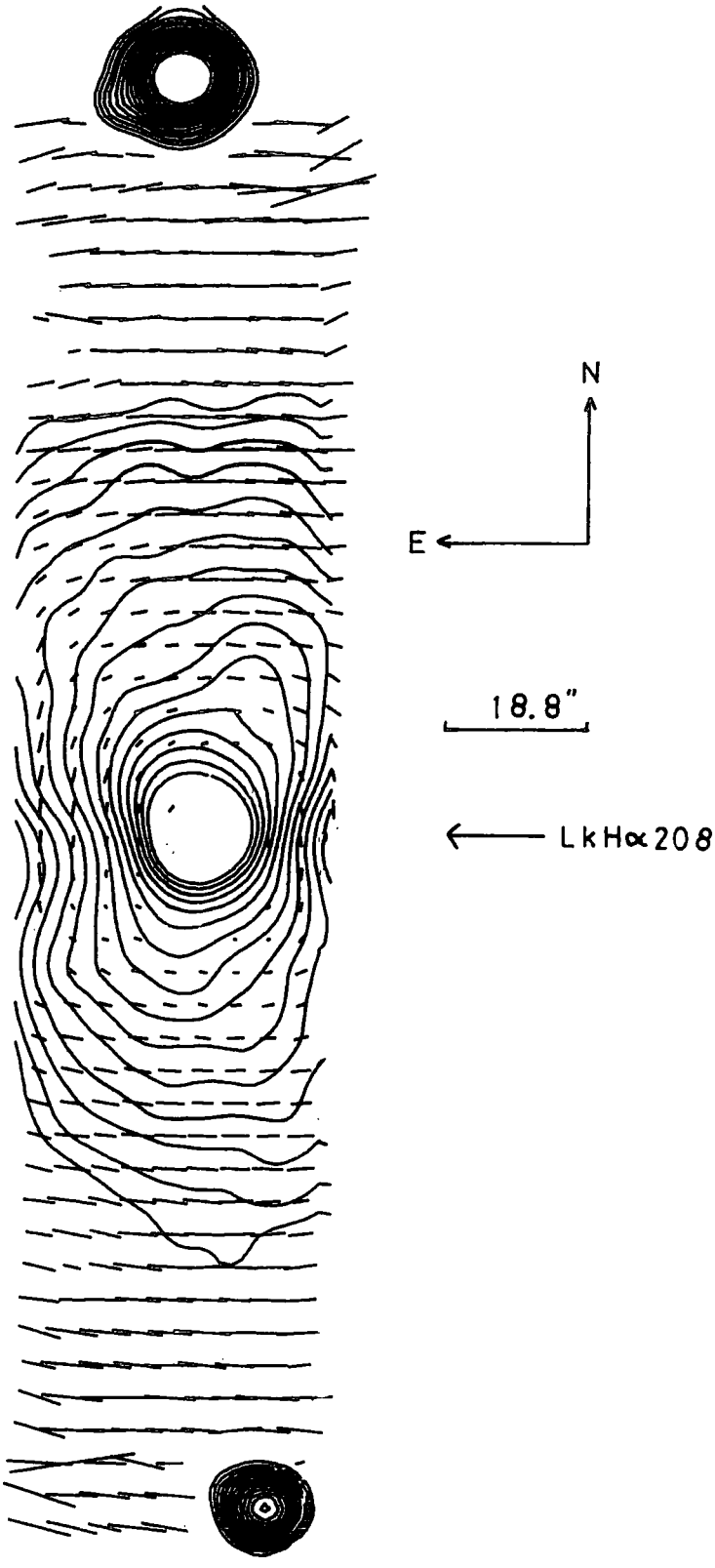

Figure 4.6

A contour map of the bipolar nebula, shown superimposed on the linear polarization map. The contour spacing is 0.2 magnitudes.

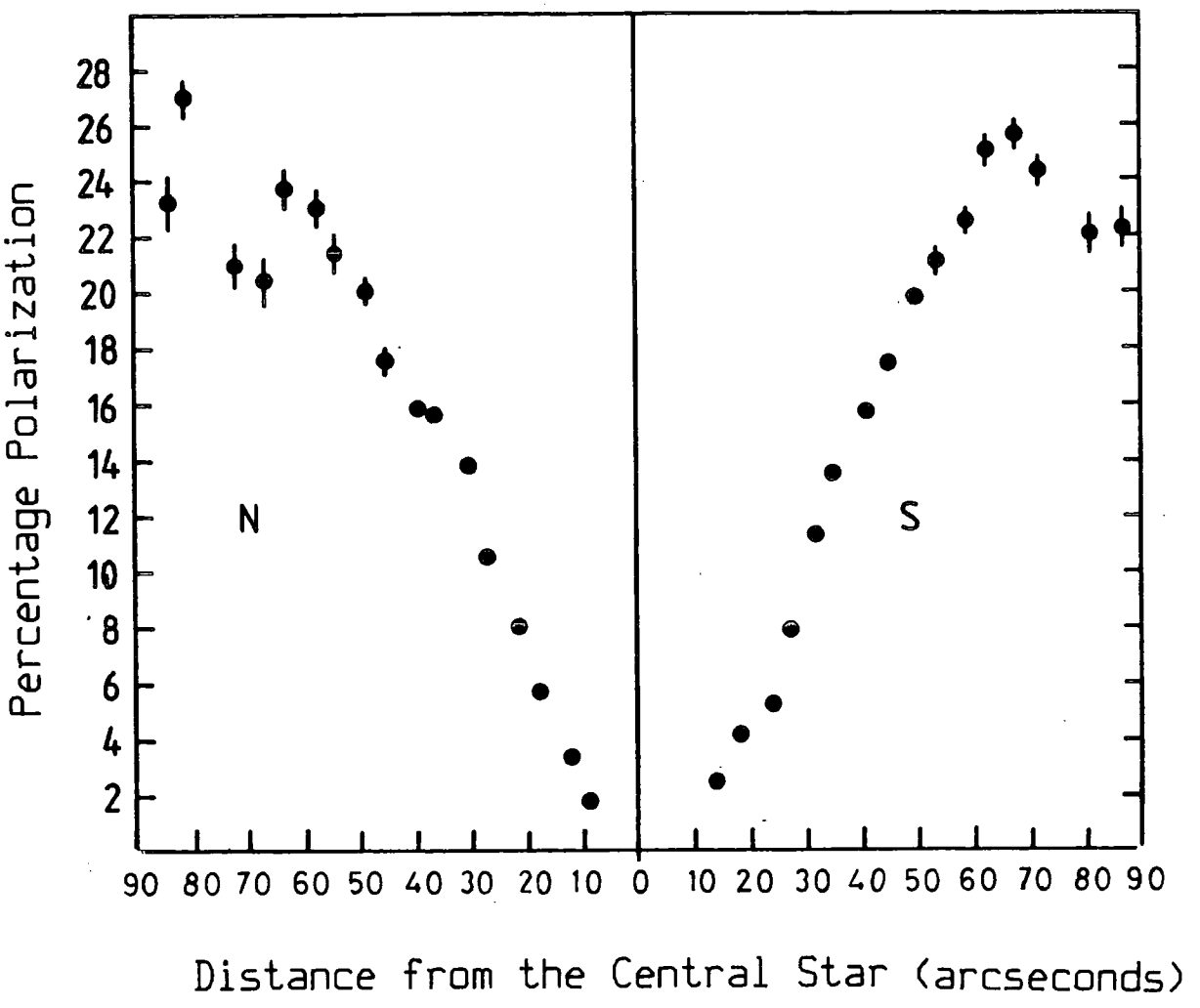

Figure 4.7

A trace, taken along the major axis of the nebula, of the degree of polarization as a function of the distance from the central star. The integration bins used here are the same as in figure 4.5.

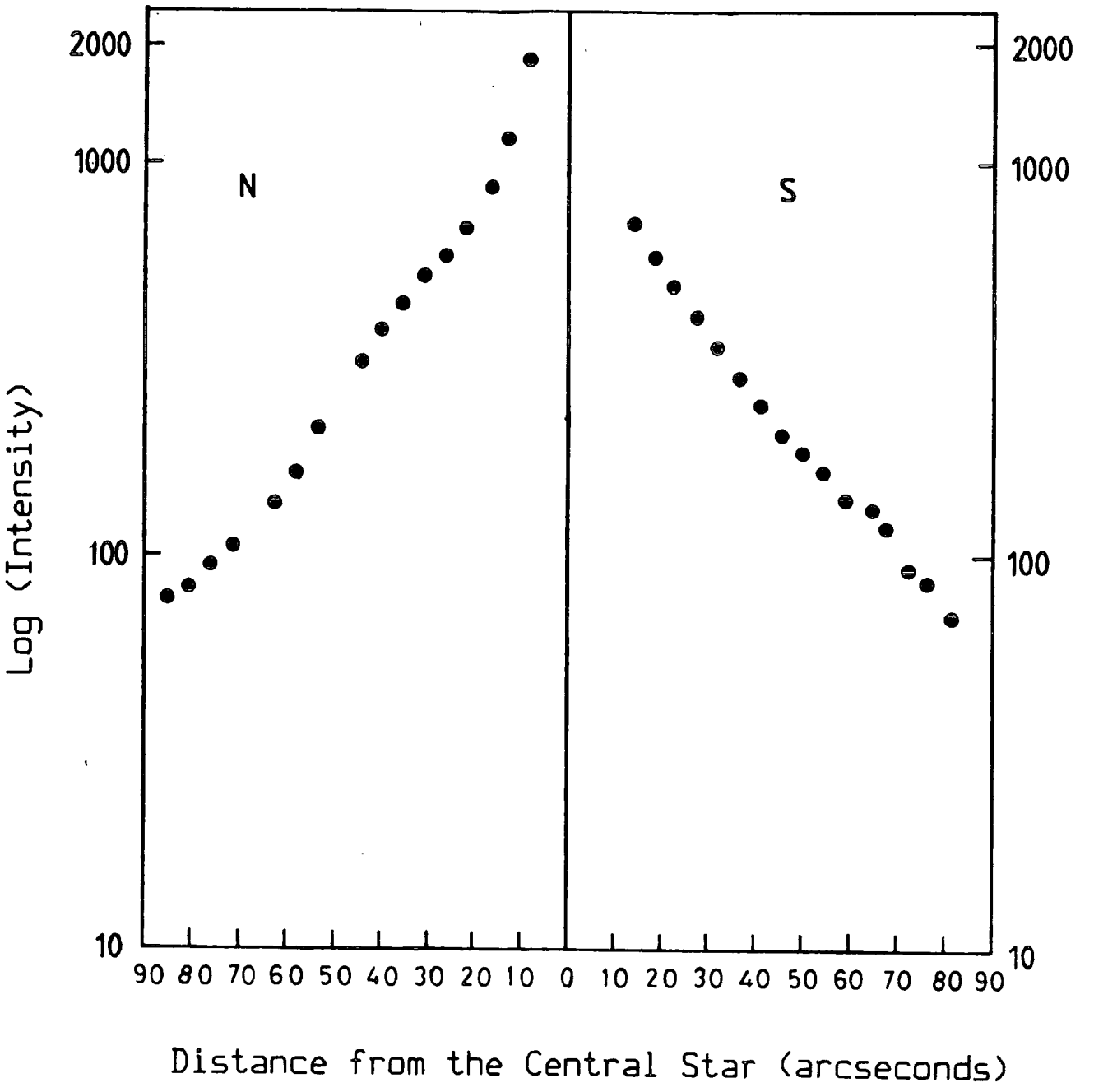

Figure 4.8

A trace, taken along the major axis of the nebula, of log (intensity) as a function of the distance from the central star. The integration bins used here are the same as in figure 4.5.

centre) are given in figures 4.7 and 4.8.

4.3 DISCUSSION OF THE PHOTOMETRIC FEATURES

At first glance one of the striking features of the photometric data, as already commented upon by Hubble (1922), is the classical hourglass appearance of the nebulosity, with the northern lobe being clearly brighter than the southern in all colours. A closer investigation of figures 4.1 to 4.4, however, soon reveals asymmetries in the object about the major axis.

All four colours show an intensity enhancement in the north-western part of the northern lobe, which gives the impression of a jet emanating from the central object. The percentage polarization appears to be well correlated with the feature, the polarization rising significantly, by as much as 10% above the corresponding area in the north-eastern lobe. The jet extends over 22 arcseconds. It could be due to a higher concentration of dust in this vicinity as compared to the corresponding area in the north-eastern part of the lobe. Excessive dust would cause more light to be scattered out of the nebula and towards the observer, so enhancing the observed brightness of this region. If the jet is oriented such that light scattering from the dust in the jet is scattered through angles close

to ninety degrees, then an increase in the percentage polarization would also be expected. The rapid brightness fall off, seen by the strong gradients to the west of the bump, could be evidence of a fall off in the dust density away from the jet, causing the brightness to also fall rapidly (by a maximum of 0.2 magnitudes per square arc second).

The enhancement may be purely an illumination effect, in the form of a shaft of light penetrating the dust at an appropriate angle, so causing both the polarization and the brightness in the region to increase. If this feature is indeed an illumination effect, but is caused by some source other than the star, then there should be some deviation in the centro-symmetry of the polarization pattern. This is not observed, and there is therefore no evidence indicating any source of illumination other than LKHα208 for the nebulosity contained in the region of the enhancement.

All of the maps hint at the possibility of a second jet-like feature in the south-eastern part of the southern lobe. The percentage polarization measurements, however, give no such indication, and show a high degree of symmetry about the major axis.

The other obvious feature of the photometric data is the pinched 'waist' of the hourglass, perpendicular to the major axis of the lobes. As discussed in previous

chapters, there is ample evidence to suggest and support arguments for the existance of circumstellar rings around Herbig Ae/Be stars, and indeed around LKHα208 itself. The present data adds further support to this work. The brightness gradients throughout the 'waist' increase from the red through to the ultra-violet and so indicate increased extinction of the stellar radiation with decreasing wavelength, as would be expected for radiation which is extinguished by dust.

The nebulosity is known to lie at the edge of a dark cloud to the east. Inspection of the photometric data implies that in general, the brightness falls off faster in all colours in the eastern parts of the nebular lobes than in the western parts. This has the effect of giving the object a slight boomerang shape, the lobes appearing swept towards the west.

As already noted above, the northern lobe is brighter than the southern lobe. The brightness difference between the two lobes was examined by comparing data points in the northern lobe with their corresponding, diametrically opposite points in the southern lobe. These differences were found to vary widely (by ~~at least~~ up to 1 magnitude) over the nebulosity in each colour. However, the values reported by Khachikyan and Parsamyan, of differences of one magnitude in U and half a magnitude in B and V, are certainly representative of the average

brightness differences of the two lobes.

Figure 4.9 presents curves showing the brightness differences (in magnitudes), between the north-eastern and south-western parts of the lobes, as a function of radial distance from the central star. For all colours, there is a maximum brightness difference around 24 arcseconds from the central star which then decreases as the distance from the centre increases. The differences were plotted against $1/\lambda$, and were found to show a roughly linear increase with inverse wavelength, as is observed for interstellar extinction. The light from the southern lobe is likely to be extinguished by dust, since there are few other processes that could account for the above data.

If it is assumed that the southern lobe is intrinsically as bright as the northern lobe, but appears fainter only due to obscuration by dust lying between the observer and the lobe, as proposed above, then it is possible to calculate from each pair of data points, $E(\lambda-V)/E(B-V)$ for the obscuring dust in all four colours. ($E(\lambda_1-\lambda_2)=A(\lambda_1)-A(\lambda_2)$, and the extinction, $A(\lambda)$, for a given colour, is simply the brightness difference in that colour, between the two lobes.) The data were smoothed by averaging in bins of 4 pixels before the calculations were made.

On averaging the results for all the pairs of points, it is found that the standard deviations from the

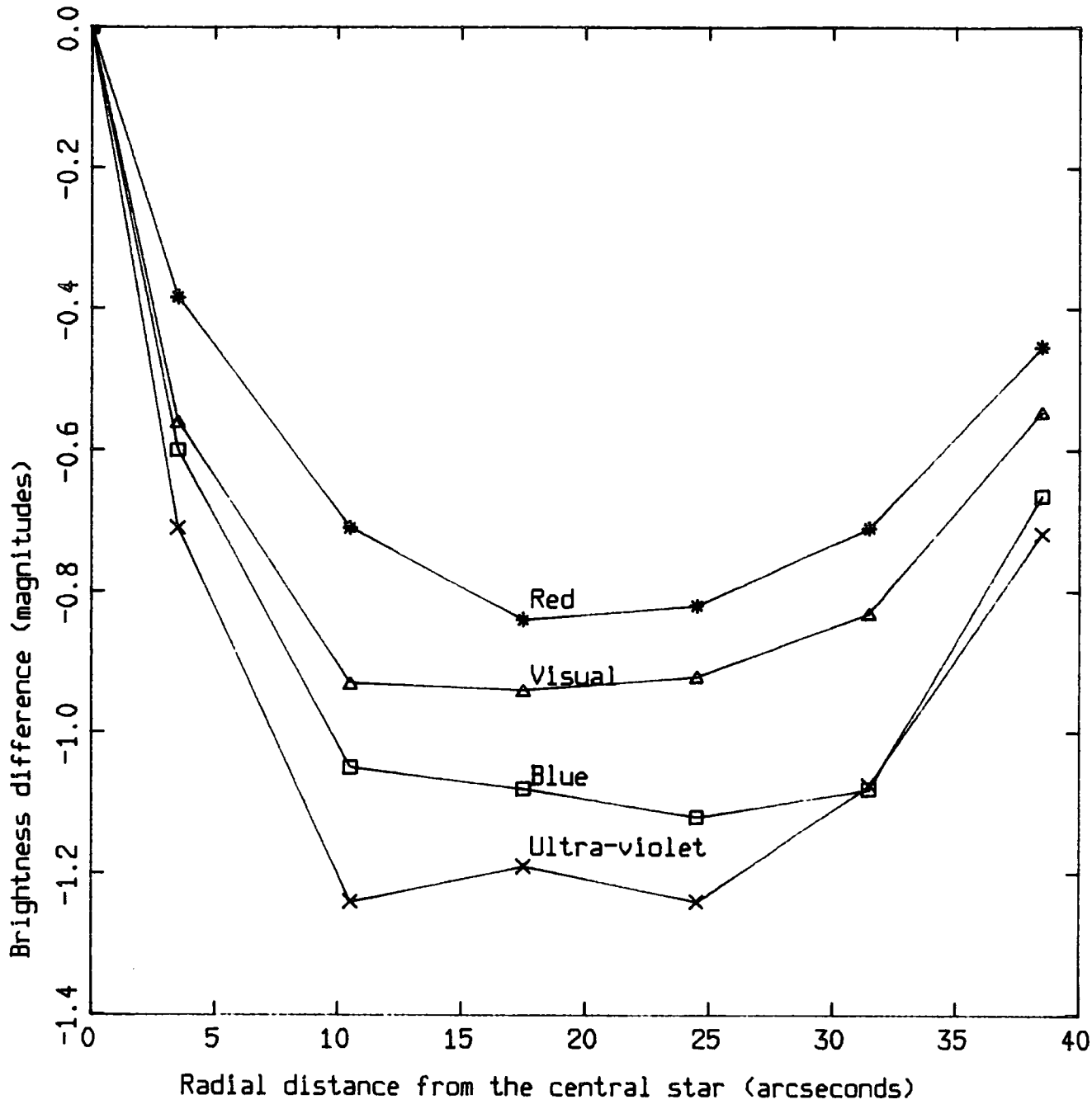

Figure 4.9

The brightness difference (in magnitudes) between the north-eastern and south-western nebular lobes as a function of distance from the star centre. The images in each colour were first smoothed, by averaging in bins of 4 x 4 pixels, and the differences were then calculated from data lying on the SE/NW nebular axis.

mean for the normalized extinctions in each colour are very large. If the assumption that the two lobes are intrinsically of the same brightness is valid, then the normalized extinctions should be the same for all of the points. Clearly then, the two lobes are not reflections of each other in every detail (as exemplified by the presence of the jet-like feature in the NW part of the northern lobe). This, combined with the fact that there is clearly asymmetric obscuration of the object, such as that due to the dark cloud (which gives the object its slight boomerang shape), accounts for the large variations in the normalized extinctions when calculated over the whole nebula. However, on the basis of the polarization observations (discussed in detail below) and the data shown in figure 4.9, the two lobes must basically be very similar in structure and the southern lobe must be seen extinguished by dust since there is no other explanation for the observed increase in extinction with increasing $1/\lambda$.

It has been demonstrated clearly that the observed brightness distributions are not symmetric either about the major axis of the nebula or about the plane of the dust ring. Further implications and discussion of this work will now be reserved until chapter 5, where the information gained from the numerical modelling of the nebulosity will be presented.

4.4 DISCUSSION OF THE POLARIZATION FEATURES

The polarization map of the nebulosity shows the typical, centrosymmetric pattern expected of a nebula which is illuminated by a single point like source (as discussed in section 3.5). The electric vectors close to the star form an elliptical arrangement, suggesting a source which is slightly extended along the minor axis of the nebula, parallel to the ring.

The trace of the percentage polarization along the major axis of the lobes as given in figure 4.7, shows that the degree of polarization is very symmetric about the star position. This is remarkable considering the asymmetry of the brightness distribution between the two lobes. It is worth noting, however, that a close investigation of the curve reveals that for several points, the polarization in the southern lobe is marginally (~ 1%) lower than the corresponding point in the northern lobe.) The level of polarization rises rapidly with offset distance from the star, from typically 3% close to the star up to 24% at 55 arcseconds along the major axis.

There are several possible nebular structures which may prove suitable in accounting for the

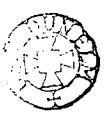

observations. They fall into two groups. One consists of nebular lobes which are filled with scattering material and the other consists of cavity lobes in which the scattering material is concentrated on the walls of the structure.

Any nebular model must attempt to explain the observed levels and gradients in the percentage polarization plots together with the brightness differences between the lobes. In earlier work (Shirt et al, 1982) the high degree of symmetry in the polarization at equivalent positions in the lobes was taken to indicate that the scattering geometry in each lobe is very similar, which implies that there is little or no tilt of the major axis of the nebula with respect to our line of sight. An upper limit of 10 degrees was placed on the tilt. The different brightness distributions of the two lobes could be accounted for by a circumstellar ring which is very extensive in the radial direction. Such an interpretation seemed confirmed from plots of the intensity ratios of the two lobes along the major axis. At large distances (60 arc seconds) from the central star, the ratio was found to be unity and the lobes were of equal brightness. Taking these measurements to indicate extinction of the southern lobe by the ring material, the mass of the ring, assuming it to be in the form of a thin disc with a circularly symmetric radial density fall-off, was estimated as 0.3 $M_{\odot}$.

Further investigation requires numerical modelling of the data in order to assess precisely how large a tilt of the nebular lobes is acceptable and to determine the geometric parameters of the nebulosity. Modelling is also expected to provide information concerning the nature of the grains, their size distribution and any dust density gradients in the nebulosity.

CHAPTER 5

NUMERICAL MODELLING OF REFLECTION NEBULOSITY

5.1 FORMULATION A SINGLE SCATTERING MODEL

The polarization and intensity of the radiation which scatters from dust contained in the nebular medium, is determined by the composition and size distribution of the grains, dust density variations within the nebular medium, the nebular geometry, and the relative position of the illuminating source. These quantities have been discussed in a qualitative manner in section 3.6. The theoretical calculations necessary to predict actual polarizations and brightnesses for model reflection nebulae will now be presented.

NUMERICAL MODELLING OF REFLECTION NEBULOSITY

Consider an arbitrary shaped nebula illuminated by a single point like source as depicted in figure 5.1. For any line of sight column through the nebulosity, the observed intensities and polarizations are the combined result of scatterings taking place at each element along the given column.

According to van de Hulst (1957), the scattering of a beam of light from a smooth, homogeneous sphere may be represented by the matrix equation

$$S_s = M(\alpha).S_I \qquad .....(5.1)$$

where S_I and S_s are the Stokes vectors describing the incident and scattered beams (discussed in section 2.10.1). $M(\alpha)$ is the scattering matrix and α is the cosine of the scattering angle. According to this formulation, the incident Stokes vector has units of Watts per unit area (ie. units of flux), the scattered Stokes vector has units of Watts per steradian (ie. units of power), and the scattering matrix has units of area. If the normal to the scattering plane is taken as a reference direction for the Stokes parameters (figure 5.2), then $M(\alpha)$ has the form

$$M(\alpha) = \begin{bmatrix} C & D & 0 & 0 \\ D & C & 0 & 0 \\ 0 & 0 & E & -F \\ 0 & 0 & -F & E \end{bmatrix} \qquad .....(5.2)$$

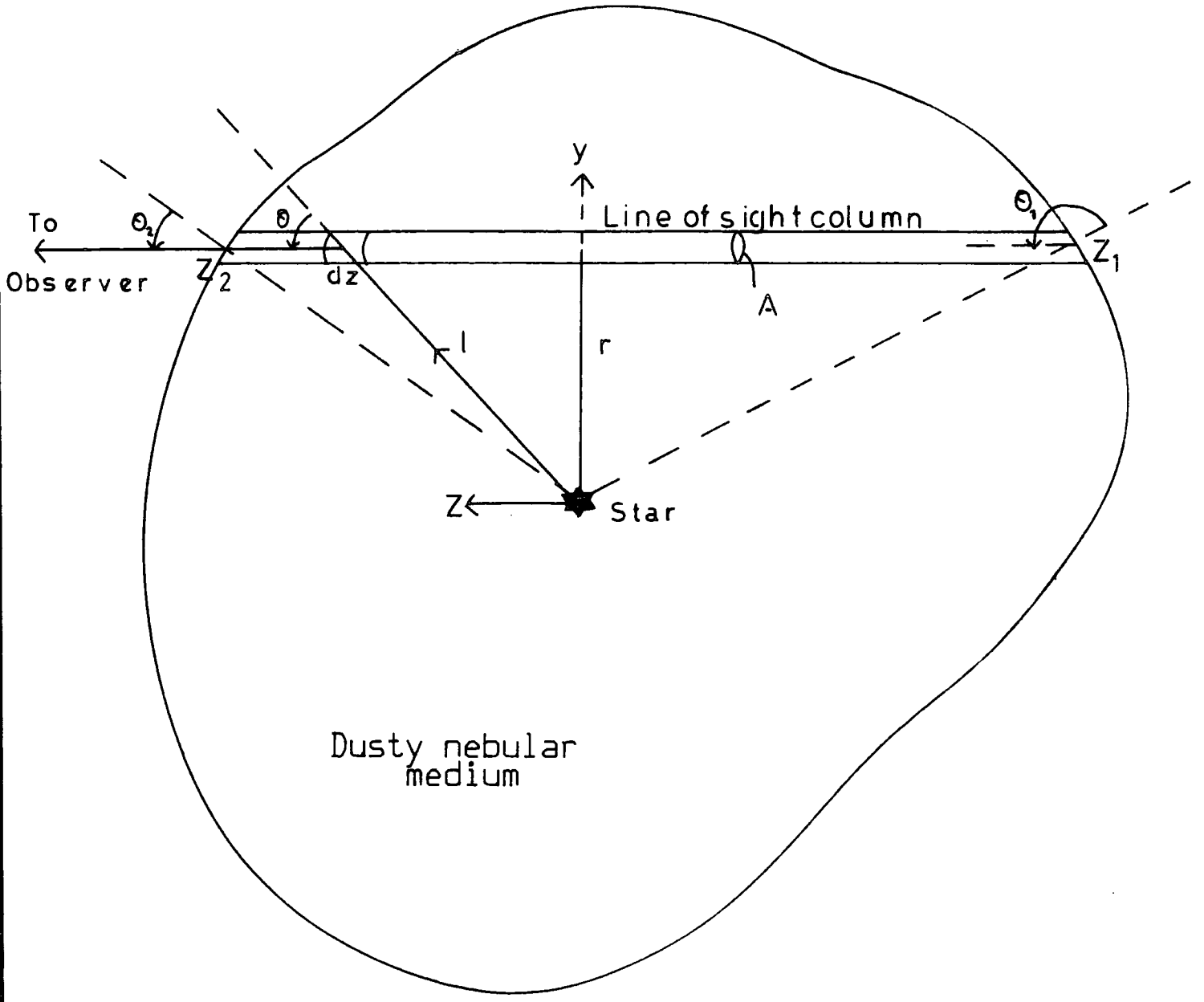

Figure 5.1

Single scattering in an arbitrary shaped nebula illuminated by a single source. The x axis is directed perpendicularly out of plane of the page.

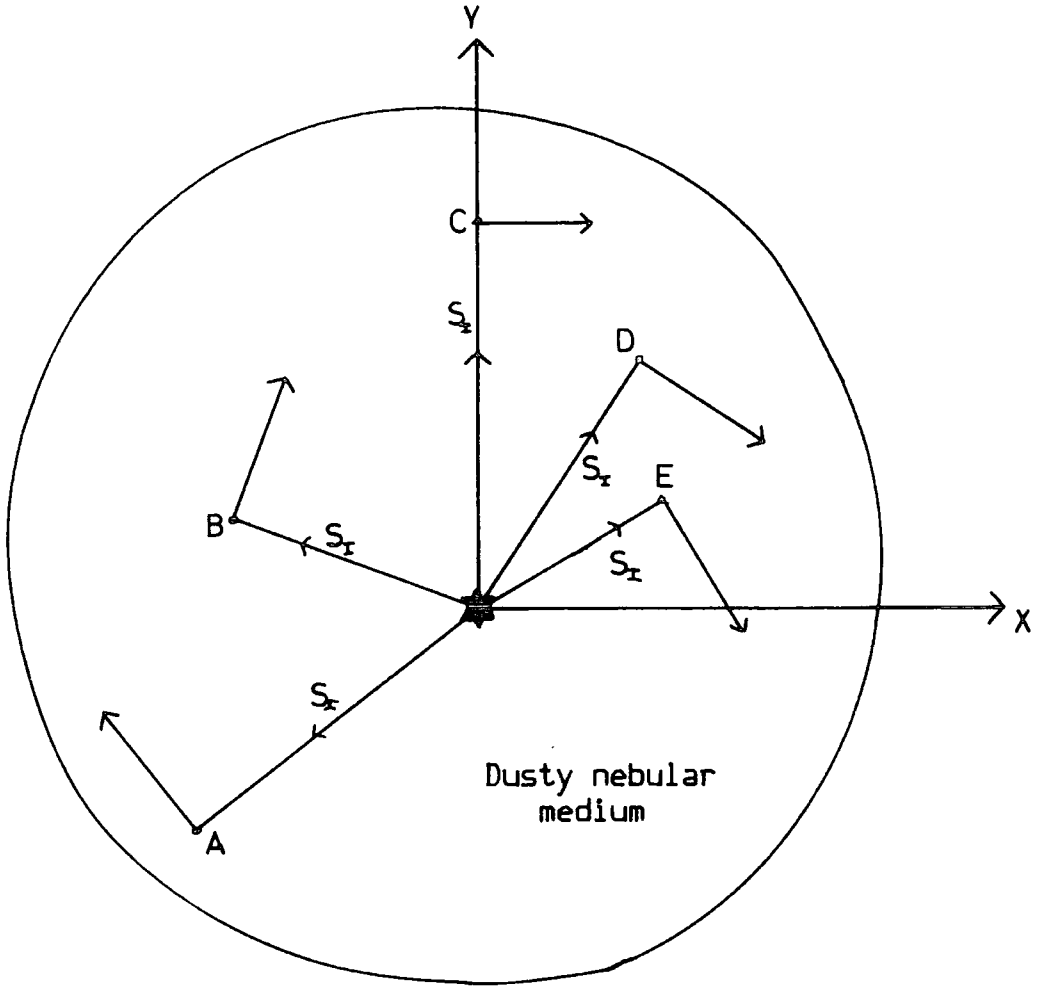

Figure 5.2

Single scattering from an arbitrary shaped nebula. The XY plane contains the plane of the sky, and the scattered light propogates perpendicularly out of the plane of the paper. Several lines of sight, A to E, are shown, and the direction of the normals to each scattering plane are indicated. When the Stokes vectors of the scattered light have been calculated, they may simply be transformed to refer to the x axis as their reference direction.

where C, D, E and F are combinations of the complex Mie scattering amplitudes, described in section 2.10.1

Light from the star is unpolarized and may be represented by the Stokes vector

$$S_I = \begin{bmatrix} 1 \\ 0 \\ 0 \\ 0 \end{bmatrix} \qquad .....(5.3)$$

The scattered light then, is described by the Stokes vector

$$S_s = \begin{bmatrix} C \\ D \\ 0 \\ 0 \end{bmatrix} \qquad .....(5.4)$$

taking the normal to the scattering plane as the reference direction. The scattered intensity is given by the first component of S_s and the scattered polarized intensity, by the second component (this is seen from equations 1.11 and 1.14). In order to calculate the brightness and polarized intensity of the light from each square arcsecond of the nebulosity the following procedure was adopted.

Consider an element of the nebular medium of length dz at a distance l from the source, on the line of sight column of cross sectional area A, shown in figure

5.1. If w is the total power scattered into unit solid angle by a single dust grain in the element, and the number density of scattering particles per unit volume of the nebular medium is N, then the total power W scattered by this column is given by

$$W = \int_{z_1}^{z_2} w.N.A.dz \qquad .....(5.5)$$

w, the power scattered by a single grain may be calculated from

$$w = \frac{1}{2}.(\lambda/2\pi)^2.(F_1(\theta)+F_2(\theta)).I \qquad .....(5.6)$$

(equations 5.1, 5.2, 2.14 and 2.19 lead to this result), where $F_1(\theta)$ is proportional to the power scattered perpendicular to the scattering plane, and $F_2(\theta)$ is proportional to the power scattered in this plane and perpendicular to the direction of propagation. I, the light flux at each element, is simply

$$I = \frac{L}{4.\pi.l^2} \qquad .....(5.7)$$

where L is the stellar luminosity. Combination of equations 5.5, 5.6 and 5.7, enable the total scattered power to be written as

$$W = \frac{\lambda^2 . A . L .}{32 . \pi^3} \int_{z_1}^{z_2} N . \frac{(F_1(\theta)+F_2(\theta))}{l^2} . dz \qquad .....(5.8)$$

Changing variables from z to θ leads to

$$W = \frac{\lambda^2 . A . L .}{32 . \pi^3 r} \int_{\theta_2}^{\theta_1} N(\theta) . (F_1(\theta)+F_2(\theta)) . d\theta \qquad ....(5.9)$$

where $N(\theta)$ is the dust density evaluated on the line of sight column at the position where the scattering angle is θ.

The line of sight column subtends a solid angle A/D^2 to the observer, where D is the distance to the nebula. The energy flux from an element of nebulosity subtending a solid angle of one square arcsecond is therefore

$$I_0 = W/A\alpha^2 \qquad ....(5.10)$$

(α = (206265) is the number of arcseconds in a radian), or more completely,

$$I_0 = \frac{\lambda^2 . L .}{32 . \pi^3 r \alpha^2} \int_{\theta_2}^{\theta_1} N(\theta) . (F_1(\theta)+F_2(\theta)) . d\theta \qquad ....(5.11)$$

Since the flux from the star at the observer is

$$I_{STAR} = L/4\pi D^2 \qquad ....(5.12)$$

the brightness of the nebulosity (measured in magnitudes) may be given in terms of the stellar brightness.

$$m_{NEB} = -2.5 \log_{10} \frac{I_{STAR} . D^2 . \lambda^2}{8 . \pi^2 r \alpha^2} \int_{\theta_2}^{\theta_1} N(\theta) . (F_1(\theta)+F_2(\theta)) . d\theta \quad ....(5.13)$$

so

$$m_{NEB} = m_{STAR} - 2.5 \log_{10} \frac{D^2 . \lambda^2}{8 . \pi^2 r \alpha^2} \int_{\theta_2}^{\theta_1} N(\theta) . (F_1(\theta)+F_2(\theta)) . d\theta \quad ....(5.14)$$

where m_{NEB} and m_{STAR} are the brightnesses of the nebula and star in magnitudes per square arcsecond. As is clear from equations 5.1, 5.2, 2.14, and 2.19, calculation of the polarized intensity simply requires changing the term $F_1(\theta)+F_2(\theta)$ to $F_1(\theta)-F_2(\theta)$.

Internal extinction of the light by the nebular medium has not been considered so far. It is negligible for very optically thin nebulae, but must otherwise be taken into account. Two principle mechanisms contribute to the removal of light from an incident beam, namely absorption and scattering of the radiation at the grain surfaces. The extinction length along a path, t_0, is given by the average extinction cross section (due to both scattering and absorption of radiation) of the grains, C_{EXT} and the number of scatterers along the path, N, such that

$$t_0 = 1/(N . C_{EXT}) \quad ....(5.15)$$

A beam of light traversing a path of length a, will be

reduced in intensity by a factor of $\exp(a/t_0)$ at the end of the path. If t_0 becomes comparable to or less than the dimensions typical of the nebula under consideration, then the amount of light which undergoes several scatterings before escaping from the nebula is no longer negligible, particularly if the albedo of the grains is high. Under such conditions, this multiply scattered light must then be taken into account. In this text however, only optically thin model nebulae will be considered and simply taking account of internal extinction as described above is sufficient.

For finite optical depths, the light will be extinguished in its passage from the star to the scatterer and from there to the surface of the nebula. Following figure 5.1 and considering the scattering element shown, the path lengths to the scattering centre and then to the nebular surface are given by

$$(r.\mathrm{cosec}\theta) \quad \text{and} \quad (r.\cot\theta_2 - r.\cot\theta) \qquad ....(5.16)$$

respectively. So an extinction factor, $\gamma(\theta)$, given by

$$\gamma(\theta) = \exp\left(-r(\mathrm{cosec}\theta + \cot\theta_2 - \cot\theta)/t_0\right) \qquad ....(5.17)$$

should be in the line of sight integral in equation 5.14. Also, the term $-1.086.(r_0/t_0)$ should to be added to expression, to account for the extinction of the star within the nebula. r_0 is taken to be the distance of the star from

the front surface of the nebula.

During the course of the work to be presented, investigations were carried out concerning the effect of a non-uniform dust density distribution on the calculated polarizations and brightnesses of various model nebulae. The distribution investigated was assumed to consist of a power-law fall-off in the dust density with increasing radial distance from the star. It took the form

$$N \propto 1/l^{Q} \qquad \ldots.(5.18)$$

(where Q is the power-index of the distribution) and when included in the integral of equation 5.11, causes it to take the form

$$\frac{1}{r^{Q+1}} \int_{\theta_2}^{\theta_1} (F_1(\theta)+F_2(\theta)).\sin^{Q}(\theta).d\theta \qquad \ldots.(5.19)$$

(note $l=r/\sin\theta$).

Evaluation of equation 5.14 and the similar equation which leads to the calculation of polarized intensity, required using Simpsons rule to carry out the necessary integrations over the scattering functions. Simpsons rule was applied successively to increasing numbers of points until the required accuracy in the integration was obtained. The scattering functions were calculated under the exact conditions required, using linear interpolation of functions which were previously evaluated at 200 scattering angles and stored in a look-up

table.

In order to find the nebular model which best reproduces the observational data, a modification of Peckhams (1970) algorithm, as implemented by Warren-Smith, (1983) was used. For a given set of model parameters, the procedure calculates the residuals between the model data and the observational data. These are then weighted according to the errors on the observational data. Next, the algorithm adjusts the parameters of the model and approximates the gradients of each residual with respect to each model parameter using a local linear function, from which it then estimates the position of the least squares minimum. A weighted set of the previous results of the function evaluations are used in forming the estimates. Warren-Smith also uses the method to perform error analysis for each of the parameters obtained at the best fit position.

5.2 SELECTION OF THE OBSERVATIONAL DATA POINTS TO BE USED IN FITTING PROCEDURES

The observational data values which have been used in the model-data fitting procedures all lie along the major axis of the nebular lobes, and due to their position, are believed to be characteristic of the general

nebulosity. No other data were involved, since it was evident from early calculations that it would not be realistic to try to reproduce the observations throughout the nebulosity. Modelling asymmetries such as the jet-like feature in the north-western part of the nebula (whilst in theory possible), would require the introduction of so many parameters, in order to define all possible structures of the jet, that a unique solution could not exist. Simulation of the east to west variations of the data, caused by the dark cloud to the east, is similarly unrealistic due to the lack of information regarding the cloud optical depth, its exact location and its extent with respect to the nebulosity.

The observational data were prepared by calculating polarizations and brightnesses (in magnitudes) that would be measured from a 10 arcsecond circular aperture centred on selected pixels lying on the major axis. The data used during modelling procedures are presented in figures 5.3 and 5.4.

5.3 CONSTRAINTS ON THE NEBULAR PARAMETERS

Typical optical depths within the nebulosity (which determines the dust density) are unknown. It seems likely, however, that they will be low (ie. less than

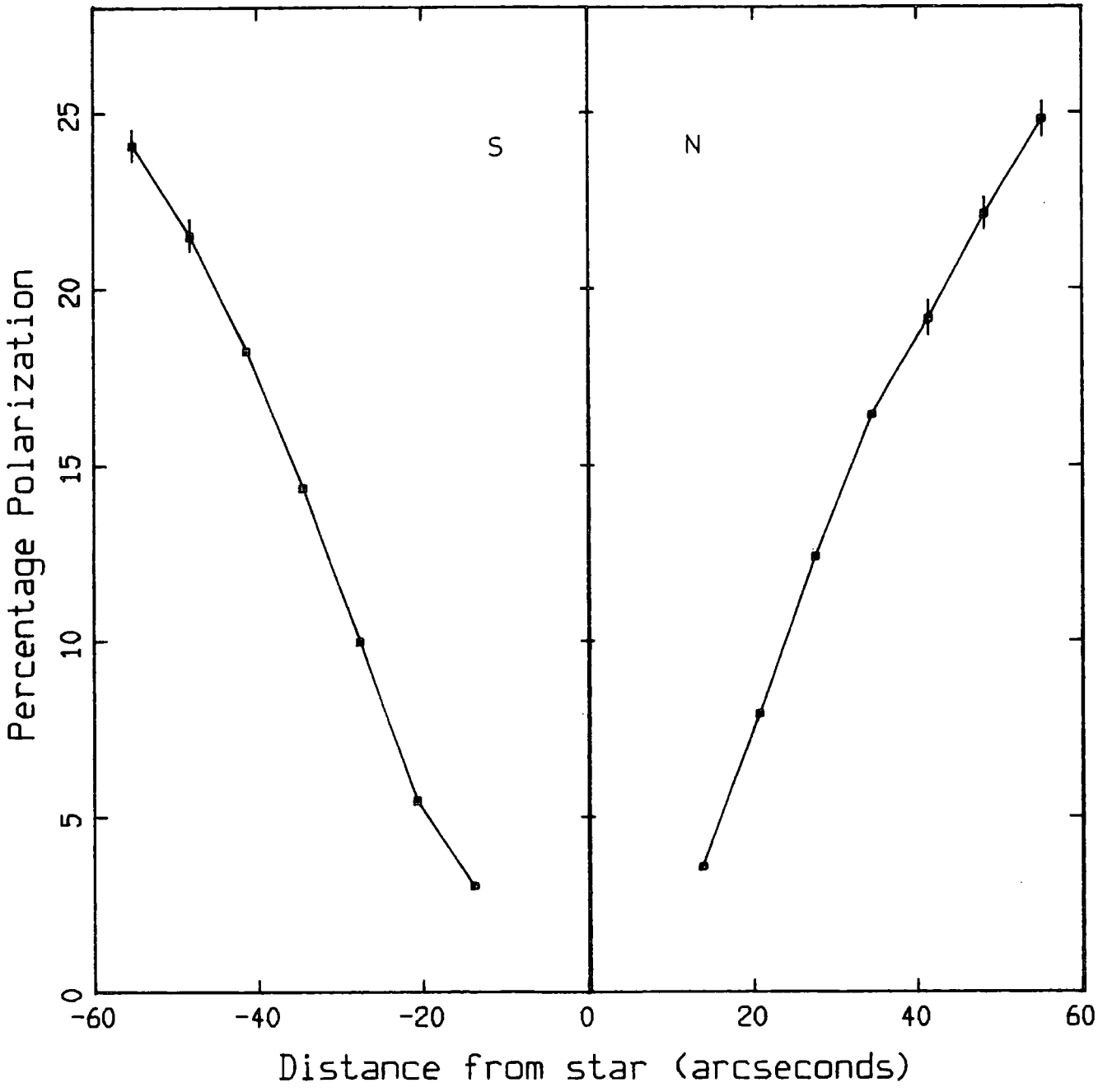

Figure 5.3

The polarization measurements used in model/data fitting procedures. The data points all lie along the axis of the nebula which runs N/S and passes through the central star. The data values measure the polarizations from a 10 arcsecond circular aperture centred on the specified coordinates.

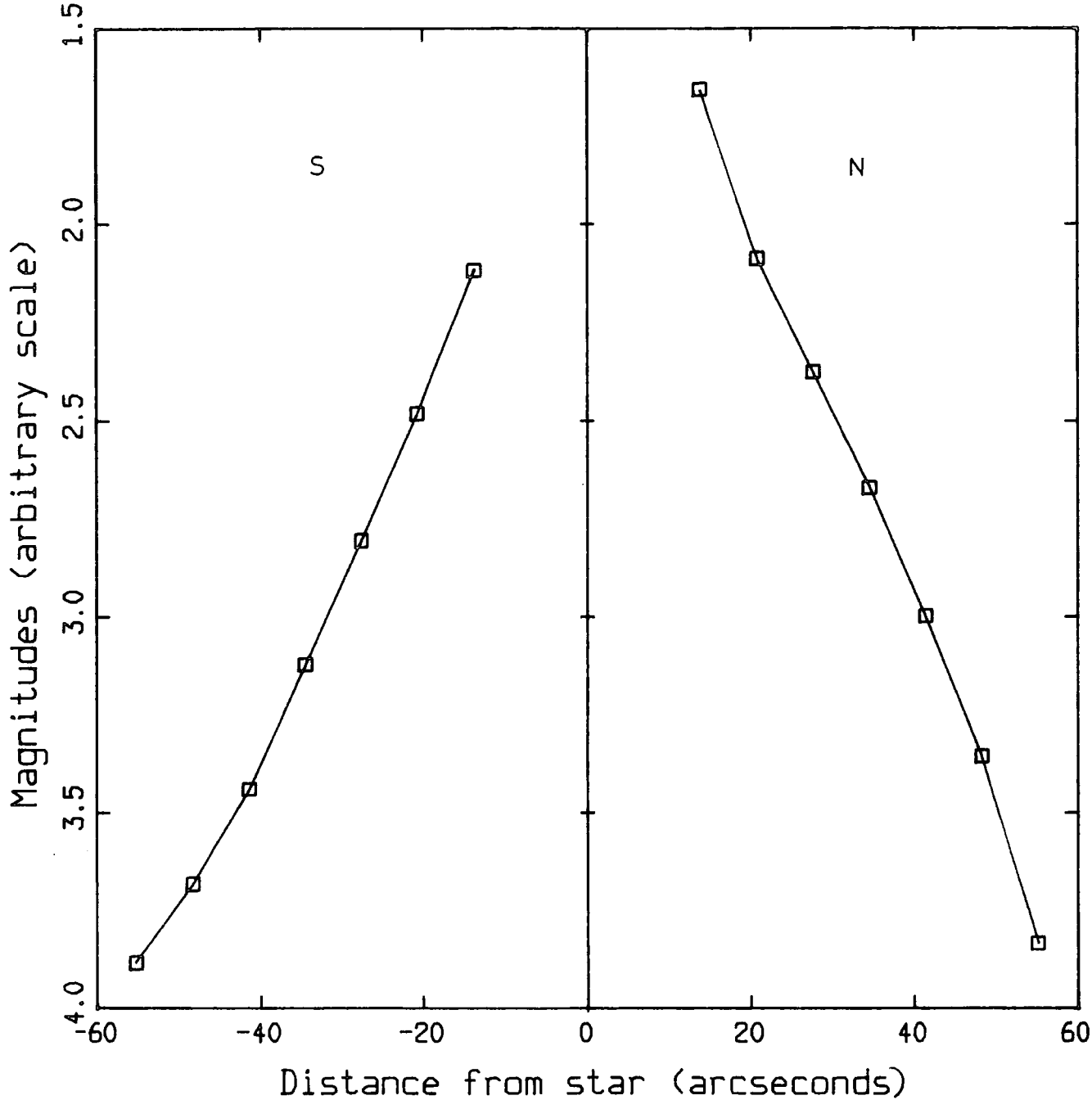

Figure 5.4

The brightness measurements, in magnitudes (scale is uncalibrated), used in model/data fitting procedures. The data values have been prepared from the corrected polarimetry images in the same way as for the polarization data presented in figure 5.3.

unity), since the surface brightness of the nebulosity as recorded by Khachikyan and Parsamyan (1965) is low compared to the star brightness. High optical depths would result in higher surface brightnesses than are observed, the integrated brightness of the nebulosity being at least comparable to that of the star brightness (Warren-Smith, 1983).

Little information is to be gained directly from the observational data concerning the grain parameters (i.e. the refractive index of the grains and the indices of the power-law functions which describe the grain size distribution and dust density variations) and it is difficult at this stage to place any contraints on their possible values. However, a lower limit must be placed on the sizes of the grains in order to remove the singularity in the distribution function at a=0. This limit is badly defined by the optical data to be used (which predominantly records scattered light), since the mean scattering cross-section of the dust is insensitive to the small sized grains, these being low in scattering efficiency. A value of 0.01 μ will be used.

The nebular form, seen projected in the plane of the sky, (figures 4.1 to 4.4), suggests that a simple geometric structure, such as a bicone, could be used to describe the nebulosity. The data certainly seem to preclude structures such as spherical dust clouds, or

clouds having an irregular geometry. Concerning any possible tilt of the nebular structure with respect to our line of sight, the data, on the basis of the observed symmetry in the two lobes, argue for a tilt which is less than 10^{0}.

Any nebular model must reproduce the centro-symmetry of the polarization pattern, and account for an increase in the polarization with offset distance from the star of ~ 0.54% per arcsecond. No attempt will be made to simulate data values further than 60 arcseconds from the star, since the polarization variations with offset distance are no longer smooth beyond this limit. It soon became clear that the rapid increase in the polarization with offset distance provides a very powerful constraint on the possible nebular models.

The brightness data show a fall in brightness of ~ 0.05 magnitudes per arcsecond. This needs to be accounted for, and if possible, so does the difference in the brightness distributions in the north and south nebular lobes. It was not possible, due to data-calibration difficulties (section 4.2), to model the brightness of the nebular lobes relative to the stellar brightness and instead, the calculated model brightnesses were normalized to the observational data, so modelling in effect, the gradients.

For each model considered, in order to make

efficient use of the computing resources available, the grain parameters were varied 'manually' over a wide range of values, and the fitting algorithm (described in section 5.1) optimized only the geometric parameters. This enabled the location of regions where a fit might be found. The grain and the geometric parameters were then optimized together. The procedure was subsequently repeated for a range of power-indices controlling radial density variations.

As a final check on all nebular models recorded in this text, it was ensured that the predicted nebular brightnesses (in magnitudes per square arcsecond) relative to a 12.74 magnitude star (with 2 magnitudes of extinction in the visual as calculated by Finkenzeller and Mundt, 1984) were not inconsistent with the range of brightnesses recorded by Khachikyan and Parsamyan (1965).

Several nebular models which have been considered as possible candidates will now be discussed in some detail, since even though many proved unsuitable, their study is profitable, as in many circumstances they have been found to clarify the interplay of the many parameters involved, and have highlighted those which are of greatest importance.

5.4 A STARTING POINT : THE DUST-FILLED BICONE

The simplest geometry that could be used to describe the nebulosity is that of a bicone, depicted in figure 5.5 and described by the equation

$$\underline{U}^{T}.\underline{A}.\underline{U} = 0 \qquad \ldots.(5.20)$$

The matrix $\underline{U}$ contains the principle axes of the bicone such that

$$\underline{U}^{T} = (u_1 , u_2 , u_3) \qquad \ldots.(5.21)$$

In this formulation, u_2 is taken to lie along the major axis of the cones. The matrix $\underline{A}$ is dependent only on the opening angle of the bicone, γ.

$$\underline{A} = \begin{bmatrix} 1 & 0 & 0 \\ 0 & -(\tan\gamma/2)^2 & 0 \\ 0 & 0 & 1 \end{bmatrix} \qquad \ldots.(5.22)$$

Figure 5.5 shows u_2 tilted by an angle β out of the plane of the sky. The major axis of the bicone may also be rotated in this plane. In order to be able to calculate the forward and backward scattering angles for any line of sight column (required for the integration limits in equations 5.11 and 5.14), for any orientation of the

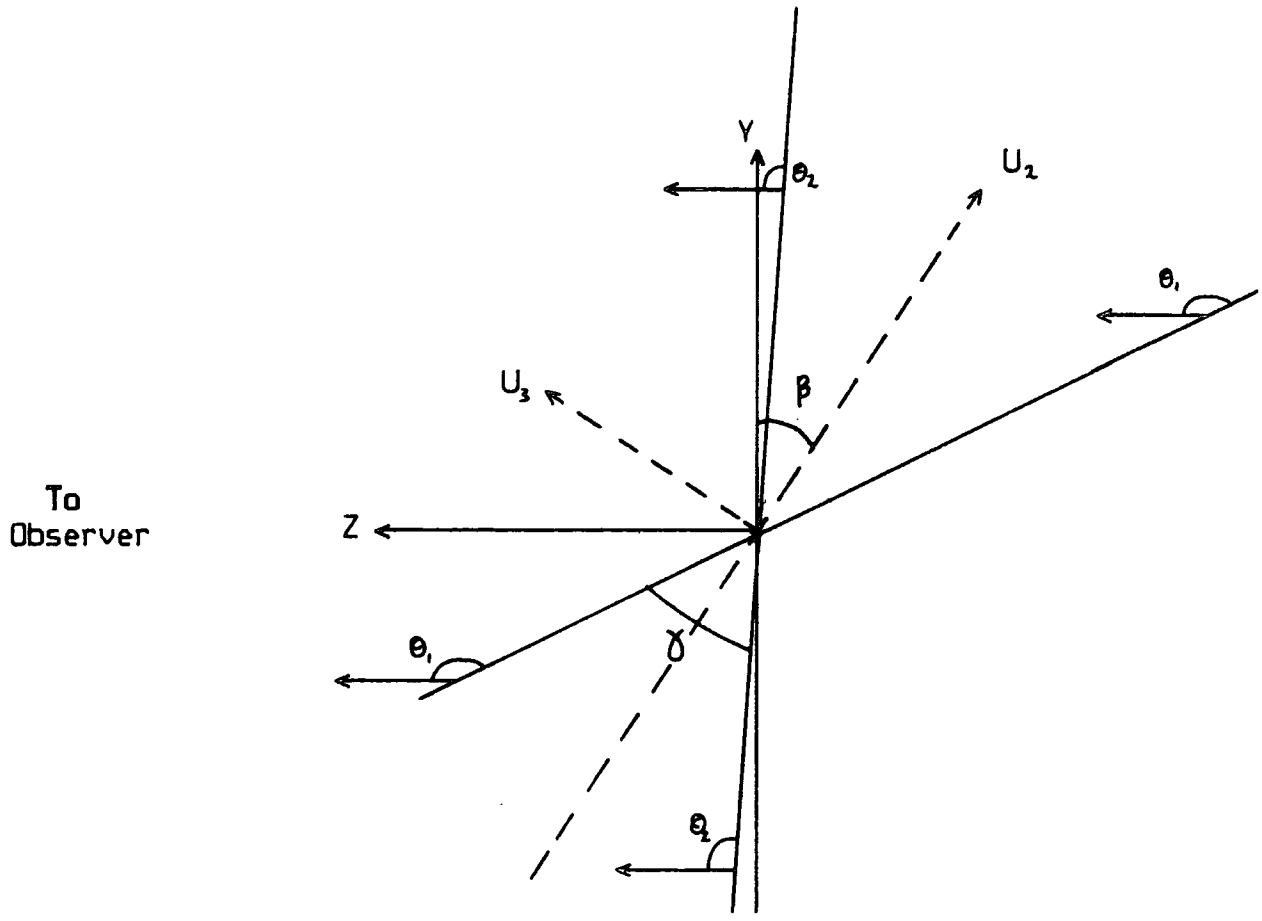

Figure 5.5

The biconical nebular geometry showing the nebula tilted by an angle β out of the plane of the sky (taken to lie perpendicular to both the plane of the paper and the z axis). The opening angle of the bicone is γ . The scattering angles at the front and back surfaces of the bicone are marked.

bicone, the general equation given above (5.20), was written in terms of the observers reference frame, depicted in figures 5.1 and 5.5. A simple transformation equation given by

$$\underline{U} = \underline{P}.\underline{X}, \qquad \ldots.(5.23)$$

($\underline{X}$ = (x , y , z) and refers to the observers reference frame), enables equation 5.20 to be rewritten as

$$\underline{X}^{T}.\underline{P}^{T}.\underline{A}.\underline{P}.\underline{X} = 0 \qquad \ldots.(5.24)$$

Calculation of the matrix $\underline{P}$ requires knowledge of the angle of rotation, α, of the major axis of the bicone in the plane of the sky, and β, the tilt of the major axis into or out of the plane of the sky (measured after the rotation angle). $\underline{P}$ is then given by

$$\underline{P} = \begin{bmatrix} \cos\alpha & \sin\alpha & 0 \\ -\sin\alpha\cos\beta & \cos\alpha\cos\beta & -\sin\beta \\ -\sin\alpha\sin\beta & \cos\alpha\sin\beta & \cos\beta \end{bmatrix} \qquad \ldots.(5.25)$$

The angles α and β are shown in figure 5.6. However, for the present case of investigation of the nebulosity around LkHα208, the observational data is orientated such that α=0.

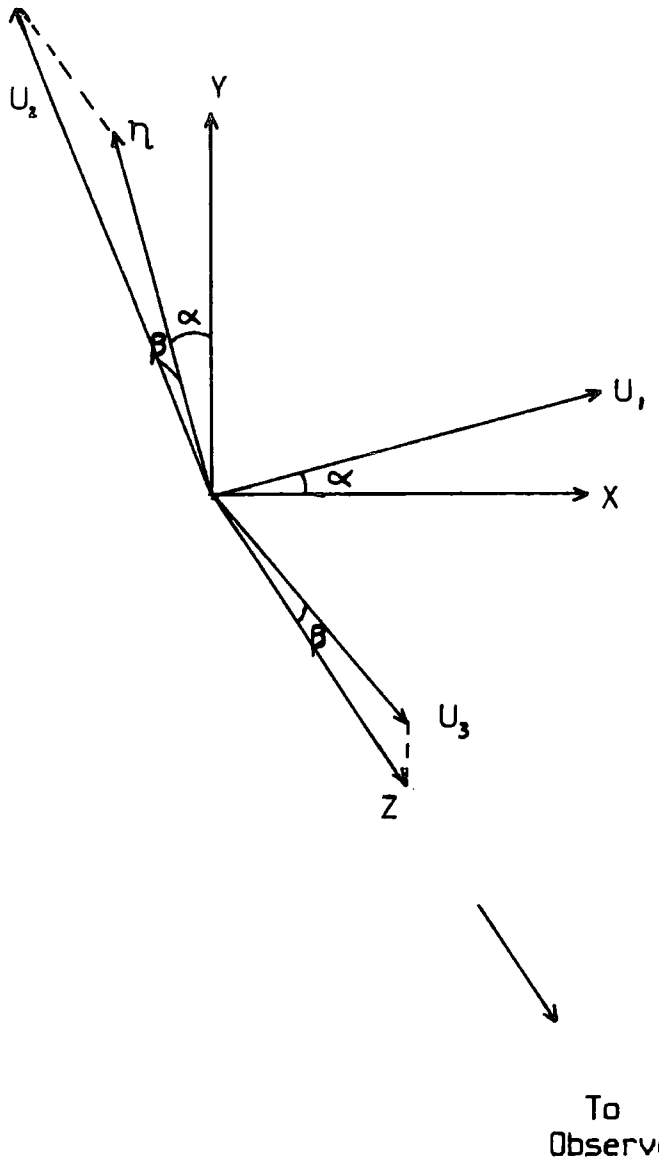

Figure 5.6

If the principal axes of a bicone are defined by U_1, U_2 and U_3, then the equation of the bicone can be written in terms of the XYZ axes, defined by figures 5.1 and 5.5, by invoking the appropriate transformation equation, which requires the measurement of α and β, as depicted above.

5.4.1 POLARIZATION AND BRIGHTNESS CALCULATIONS FOR A DUST-FILLED BICONE

Clearly, the scattering angles at the front and rear surfaces of any proposed nebular structure are of great importance, since they determine the limits of the integrations which must be evaluated in order to calculate the Stokes vectors of the scattered light (equation 5.11). Figure 5.7 shows that these limits are the same for all line of sight columns through an untilted, non-rotated bicone, resulting in uniform polarization throughout the nebula. (The only factor required for calculation of the Stokes vectors, which differs for different line of sight columns, is the extinction factor. Even so, its effect is negligible (provided that the optical depth is low), in the calculation of the percentage polarization.)

Figure 5.8 shows the percentage polarization that would be measured from the cones of an untilted, optically thin bicone, filled with silicate grains, as a function of the opening angle. This figure demonstrates an important point concerning the nebular structure. Broadly speaking, the percentage polarizations are lower, the wider the range of scattering angles (i.e. the greater the opening angle). The observational data therefore indicate that

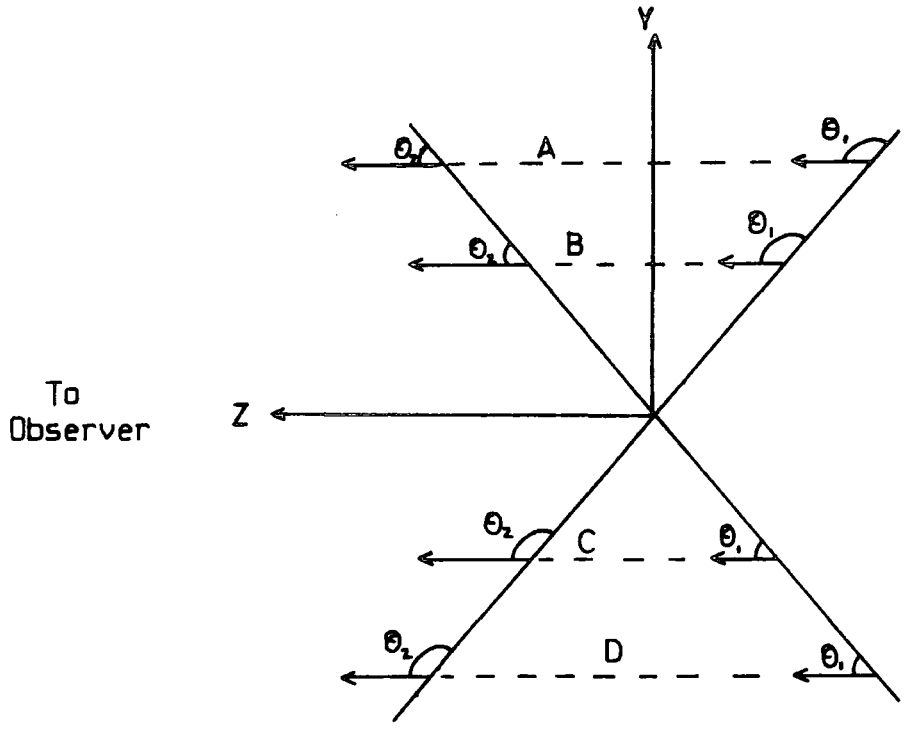

Figure 5.7

The biconical nebular geometry shown untilted in the plane of the sky (taken to lie perpendicular to both the plane of the paper and the z axis). The scattering angles at the front and back surfaces of the bicone are marked for several line of sight columns, A B, C and D.

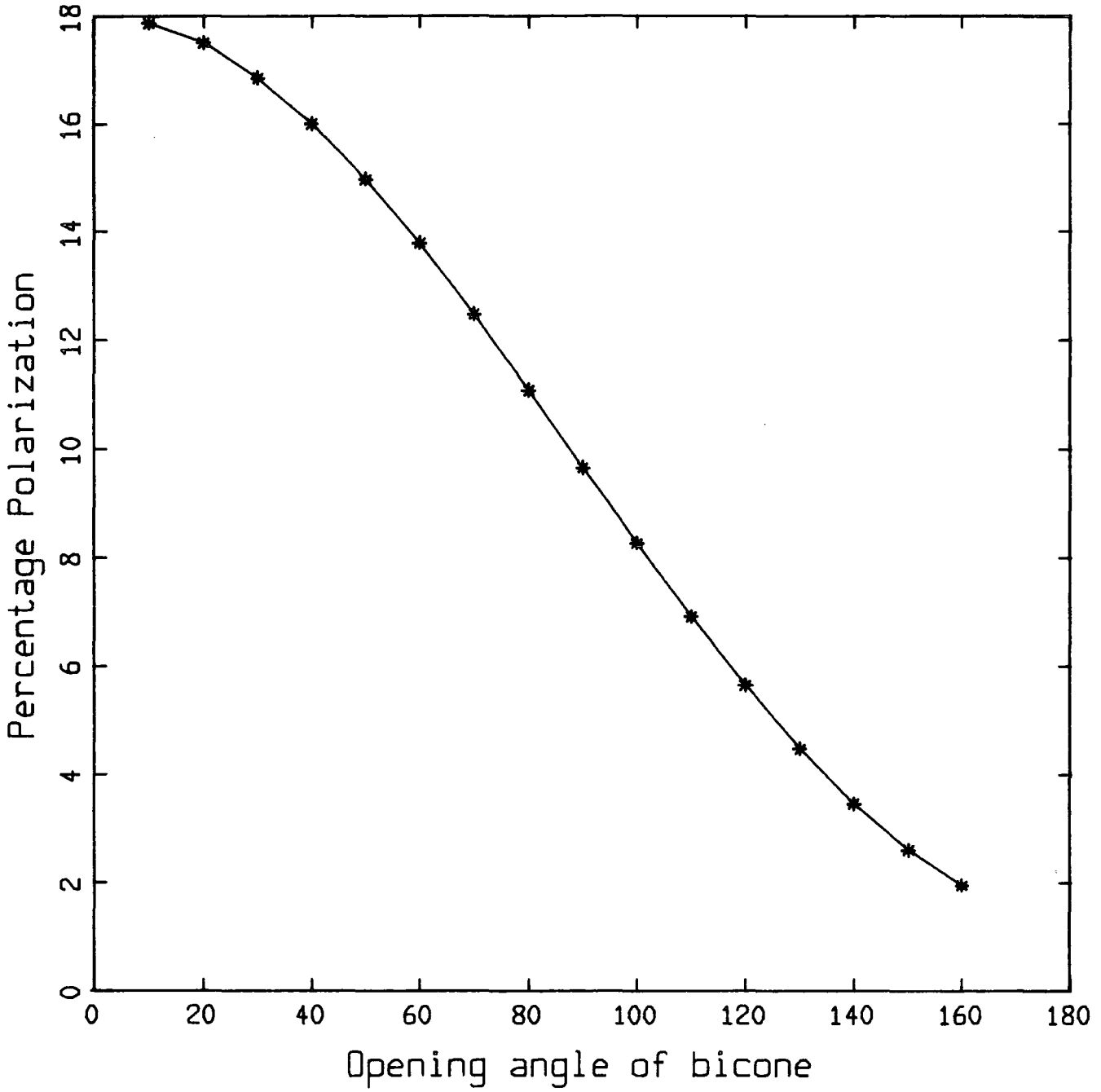

Figure 5.8

The percentage polarization that would be observed throughout an untilted, optically thin biconical nebula, as a function of the cone opening angle. The bicone is uniformly filled with silicate grains having a power-index in the dust size distribution function of -3.5. The shape of the curve remains the same for a wide range of grain parameters.

there must be a wide range of scattering angles close to the star, in order to achieve polarizations as low as 5% and that the nebular geometry must cause the range of scattering angles to decrease with offset distance from the star. Clearly, the uniformly dust-filled biconical nebular model cannot reproduce the polarization observations since the range of scattering angles is constant through the structure along any given axis.

Tilting the model nebula in the plane of the sky, as in figure 5.5, does not answer the problem since it simply results in the production of different levels of polarization in the two cones, the polarization within each cone being uniform throughout.

The model is capable, however, of adequately fitting the brightness data, and a wide range of parameters enabled reasonable model reproductions of the observations. Figure 5.9 presents the model calculations compared to the observational data for a bicone with a cone angle of 60^{0}. The bicone model required the northern lobe to be tilted by 5.7^{0} out of the plane of the sky and towards the observer. Silicate grains were taken to fill the nebula, and the required power-law index in the size distribution was -3.5.

Amongst other things, the above work highlights the fact that it is not difficult to reproduce the brightness measurements, but that it is considerably more

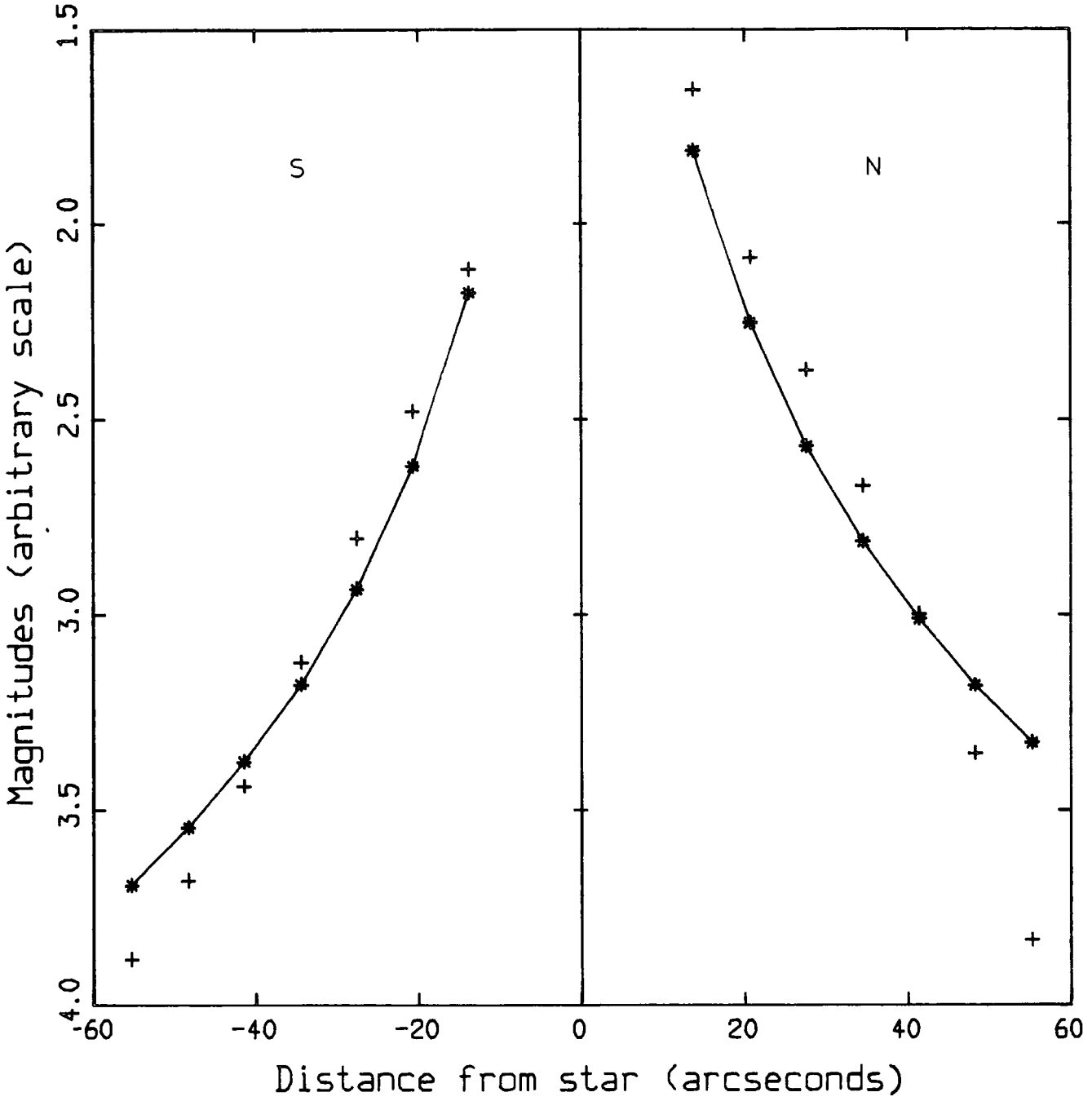

Figure 5.9

Nebular brightness calculations for the biconical model as a function of offset distance from the star. The nebular parameters are recorded in the text. The observational data points are indicated with + signs. No biconical model was found to be capable of reproducing the polarization observations.

difficult to simultaneously reproduce both sets of observations.

5.4.2 THE BICONICAL NEBULAR MODEL WITH A RADIAL DUST DENSITY DISTRIBUTION

The biconical nebular model which contains a uniform dust density distribution has been shown above to be inadequate. The effect of introducing a radial dust density variation to the model should now be investigated. It is expected for an untilted nebula, with a power-law fall-off in the dust density, that the percentage polarization will increase along all line of sight columns, since the distribution results in a concentration of dust around the 90° scattering angles.

The nebulosity is expected to become fainter with increasing offset distance more rapidly than the nebulosity of an equivalent, uniformly dust-filled structure, since the dust density at the front surface of the cones is a decreasing function of the radial distance from the star.

A specific case will be investigated consisting of an optically thin bicone which is filled with silicate grains, having a power-index in the grain size distribution of -3.5. The percentage polarization in the

cones and the average brightness gradients along the major axis were calculated for a wide range of opening angles. The power-index of the dust density distribution (defined in equation 5.18) was varied from 0 to 3. The results are recorded in figures 5.10 and 5.11.

Figure 5.10 demonstrates the dramatic impact that increasing the dust density power-index has on the average brightness gradients. They rise from an average variation of ~ 0.04 magnitudes per arcsecond with a uniform dust density distribution, to 0.145 magnitudes per arcsecond. The brightness gradients do not change significantly with increasing cone angle. The gradient observed along the major axis of the nebular lobes under investigation is ~ 0.047 and so favours the uniform dust density distribution.

The polarization calculations showed that introducing dust density variations into the model did not cause significant variations in the polarization along the major axis of the nebulosity. As expected, the level of the polarization was affected (figure 5.11), the increase in polarization being correspondingly greater for line of sight columns with a wide range of scattering angles than for those with a low range. For a bicone with an opening angle of 20^{0}, the scattering angles along each line of sight column on the major axis range from 80^{0} to 100^{0} and the total change in the polarization as the dust density

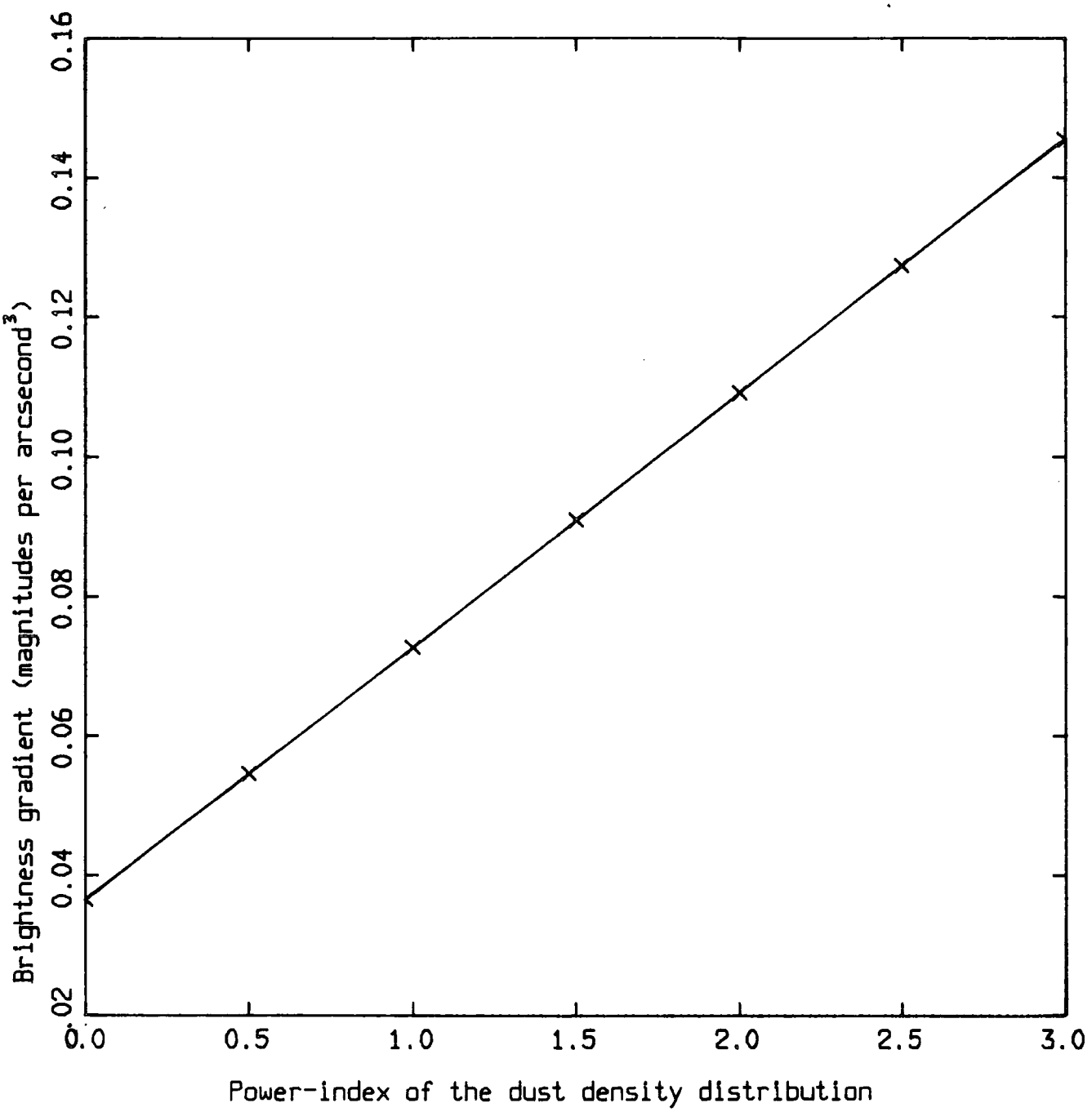

Figure 5.10

Calculation of the average brightness gradient along the major axis of the cones of anuntilted, biconical model nebula as a function of the power-index in the dust density distribution. The brightness gradients are the same for a wide range of cone angles. The nebular lobes are assumed to be filled with silicate grains.

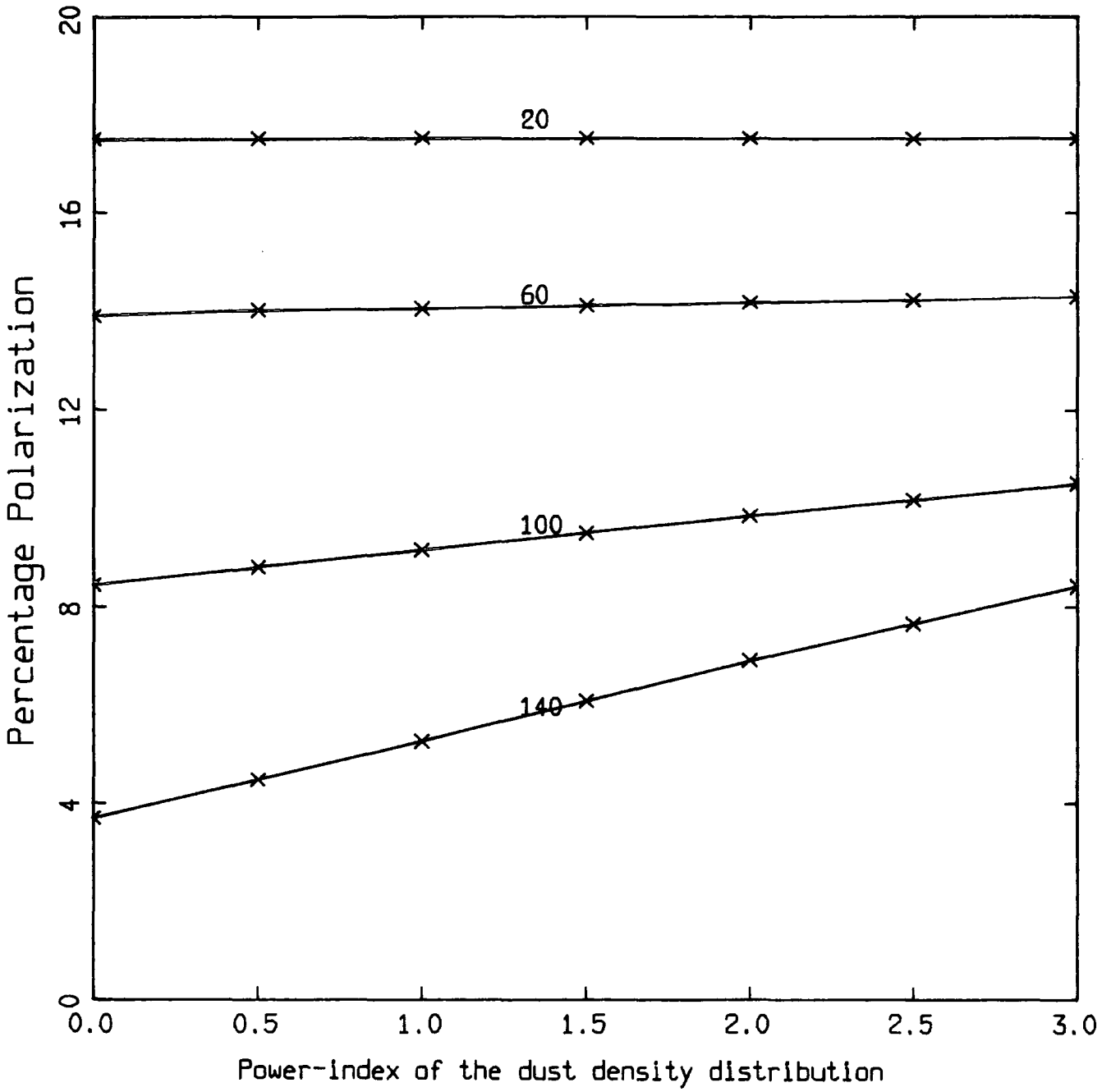

Figure 5.11

Calculation of the percentage polarization expected from the cones of anuntilted, biconical model nebula as a function of the power-index in the dust density distribution. Polarizations are given for a range of cone angles as indicated on each curve. The nebular lobes are assumed to be filled with silicate grains.

varies from having a power-index of 0 to 3, is only 0.07%, while for a bicone with an opening angle of 140°, with scattering angles ranging from 20° to 160°, the corresponding change is 4.73%.

In summary, investigation of radial dust density fall-offs has shown that their effect is seen predominantly in changes in the brightness gradients, with only limited effect on the percentage polarization. Even so, for the particular case of the bicone, it is still not possible to reproduce the polarization variations observed in the nebular lobes, and there are now few changes that could be made to this basic model which could in any way enable it to reproduce the observational data. A new geometry must be sought.

This study must place serious doubts as to the feasibility of the nebular model presented by Yusef-Zadeh et al., (1984) and described in section 3.6. Their model nebula is illuminated by radiation which escapes from an optically thick circumstellar dust disc, which results in two cones of light escaping from the disc. The nebular brightness and polarization is dominated by scattering at the surfaces of the two cones, since the region enclosed by the cones is specified as being empty. In view of the discussion above, it can be seen that while this model may be able to reproduce the nebular brightness, it is certainly not capable of reproducing the polarization

variations observed for these objects and recorded by Ney et al. (1975), Crampton et al. (1975), Herbig (1975) and Cohen et al. (1975).

5.5 THE PARABOIDAL MODEL

The investigation of biconical nebulae highlighted the fact that the real nebular geometry must, in some way, restrict the range of scattering angles along the line of sight columns as their offset distance from the star increases. A paraboidal nebular structure would, in principle provide such restrictions, as demonstrated in figure 5.12, and such a nebular model, consisting of two dust-filled paraboloids having a common major axis and origin as shown, was investigated.

The general equation of a paraboloid, written in terms of the principle axes, (u_1, u_2, u_3) is

$$u_1^2 + u_3^2 = 4.F.u_2 \qquad \ldots.(5.26)$$

u_2 is taken to lie along the major axis and the term denoted by F (with units of arcseconds), is known as the focus of the paraboloid. Using the transformation matrix $\underline{P}$ (described by equations 5.23 and 5.25), equation 5.26 may also be written in terms of the observers reference frame, $\underline{X}$, so enabling the scattering angles to be calculated for

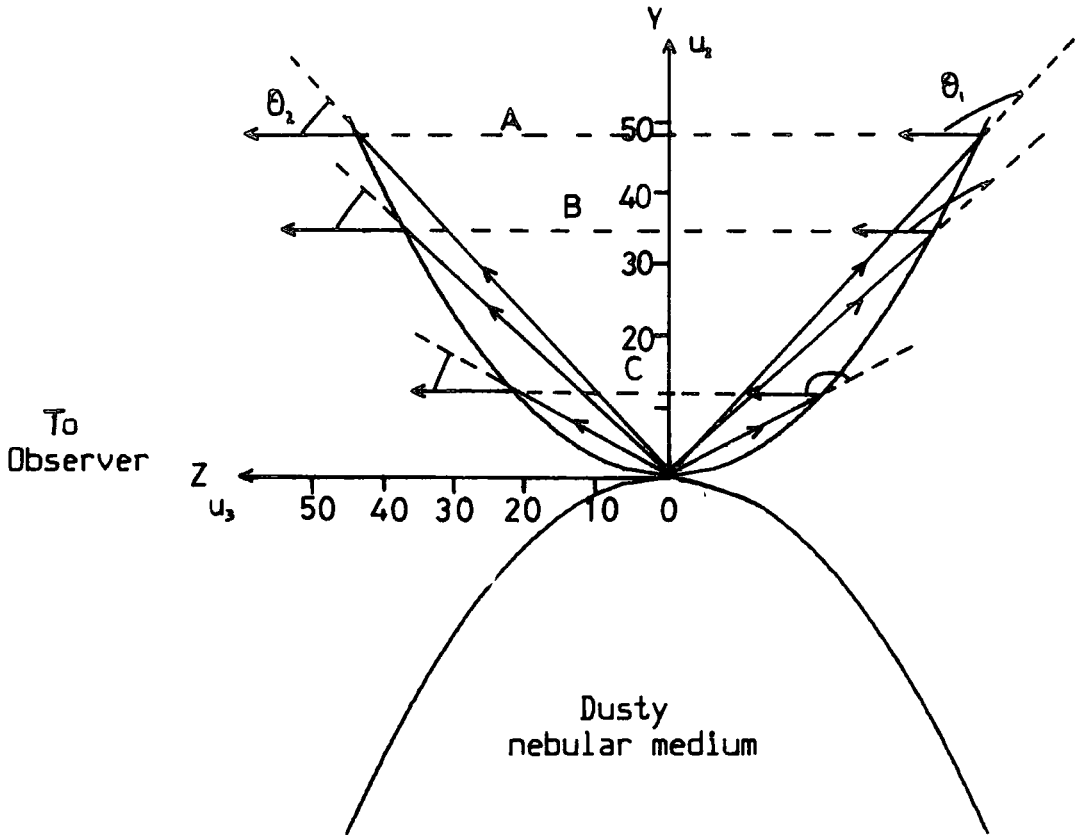

Figure 5.12

The paraboidal nebular geometry shown untilted in the plane of the sky. The scattering angles at the front and back surfaces of the paraboloid are marked for several line of sight columns and show how their range becomes restricted with increasing off-set distance from the star.

The focus of the paraboloid shown above in the yz plane is 10 units

any line of sight column through the nebulosity.

Prior to numerical modelling, an upper limit of 10^0 was placed on the possible tilt of the major axis of the nebula out of the plane of the sky, with the northern lobe being tilted towards the observer (discussed in section 4.4 and 5.3). Early results using the paraboidal model indicated that, as expected, this structure is able to reproduce the observational data more closely than previous models. However, it also became evident that a nebular tilt of more than 1^0 out of the plane of the sky results in an unacceptable difference in the polarizations calculated for the two lobes. Consequently, either the scattering mechanism must be different in the two nebular lobes or, they are similar in geometry but the southern lobe is obscured in some way relative to the northern lobe. If the scattering properties of the two lobes are different, then it is fortuitous indeed that the polarizations are so similar. In view of this, it is proposed that the southern lobe is obscured relative to the northern lobe along the major axis (as in section 4.4), although the exact nature of the obscuration is unclear. Such a low value for the tilt would certainly seem to preclude an extensive circumstellar ring as being the source.

Subsequent to these calculations, the model brightnesses were normalized only to the northern lobe

measurements and the major axis of the nebula was taken to lie in the plane of the sky. Optimization of the real part of the refractive index, the power-index of the grain size distribution, and the focus of the paraboloid, gave results which have been listed in table 5.1. Figures 5.13 and 5.14 show the optimized model calculations of nebular brightness and polarization compared to the observational data. During the final procedures, the imaginary part of the refractive index was set to zero, since previous calculations had demonstrated that the best model/observation fits were to be aquired where the grain albedo was greater than 0.75. The extinction length also was not optimized since it was badly defined by the data, although again previous calculations showed that the best fits were to be obtained for high extinction lengths ($t_0 > 70"$).

The paraboidal structure is certainly more able to reproduce the polarization observations than the biconical models, although it clearly experiences difficulty in fully accounting for the rapid increase in the polarization with increasing distance from the star. This results in the model predictions being too high for nebulosity in within ~ 30" from the star and too low for the rest of the nebula. An increase in the focus of the paraboloids has the effect of increasing the range of scattering angles along all line of sight columns and so

Table 5.1

Parameter	Value
Focus of Paraboloid (arcsecs)	40.96 ± 11.11
Re (Refractive Index)	1.18 ± 0.13
Power Index	-3.64 ± 1.02

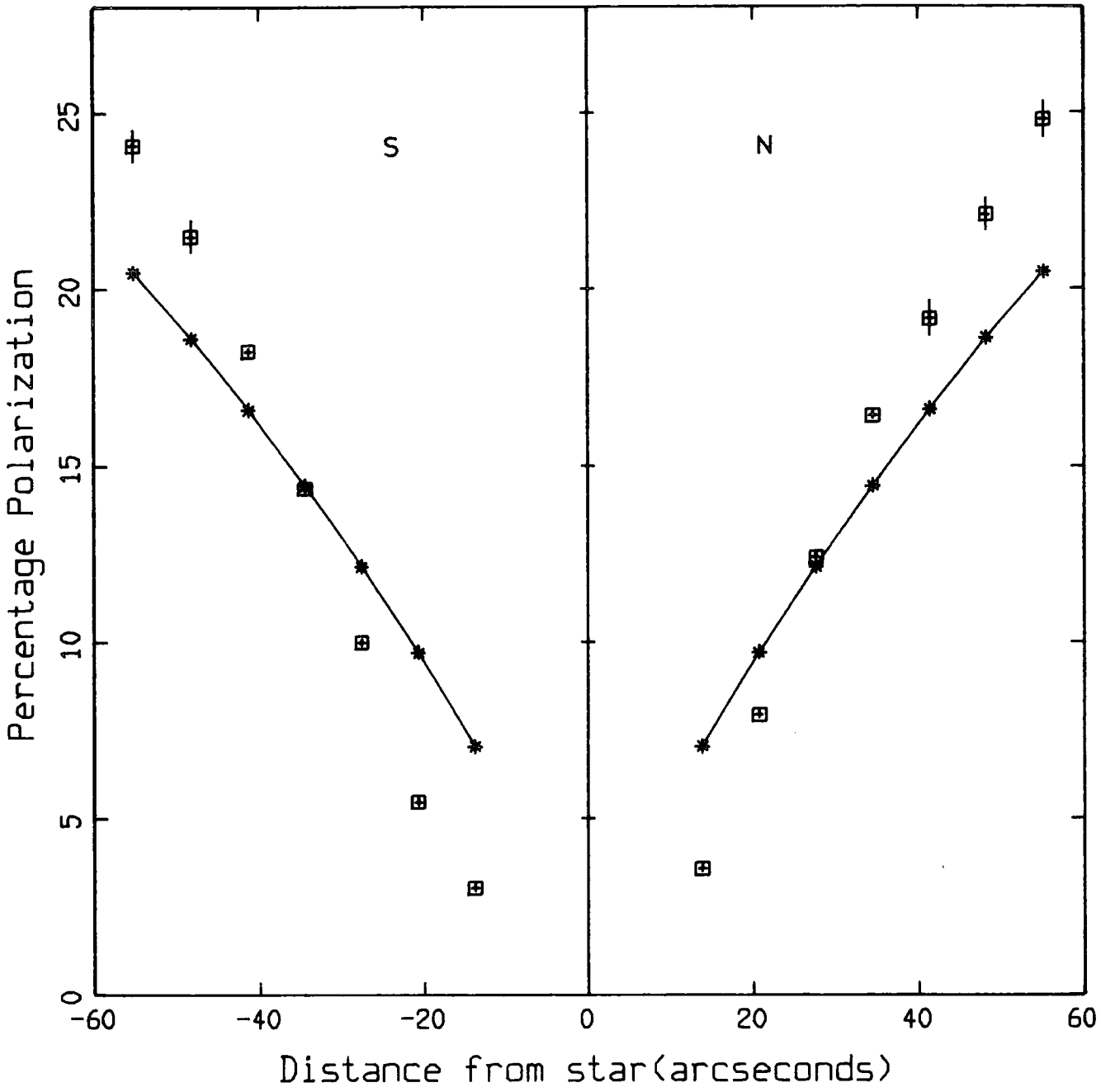

Figure 5.13

Polarization calculations for the paraboidal nebular model as a function of offset distance from the star. The model nebula is untilted and has a uniform dust density distribution. The optimized nebular parameters are recorded in the text. The observational data points are indicated with ⊞ signs.

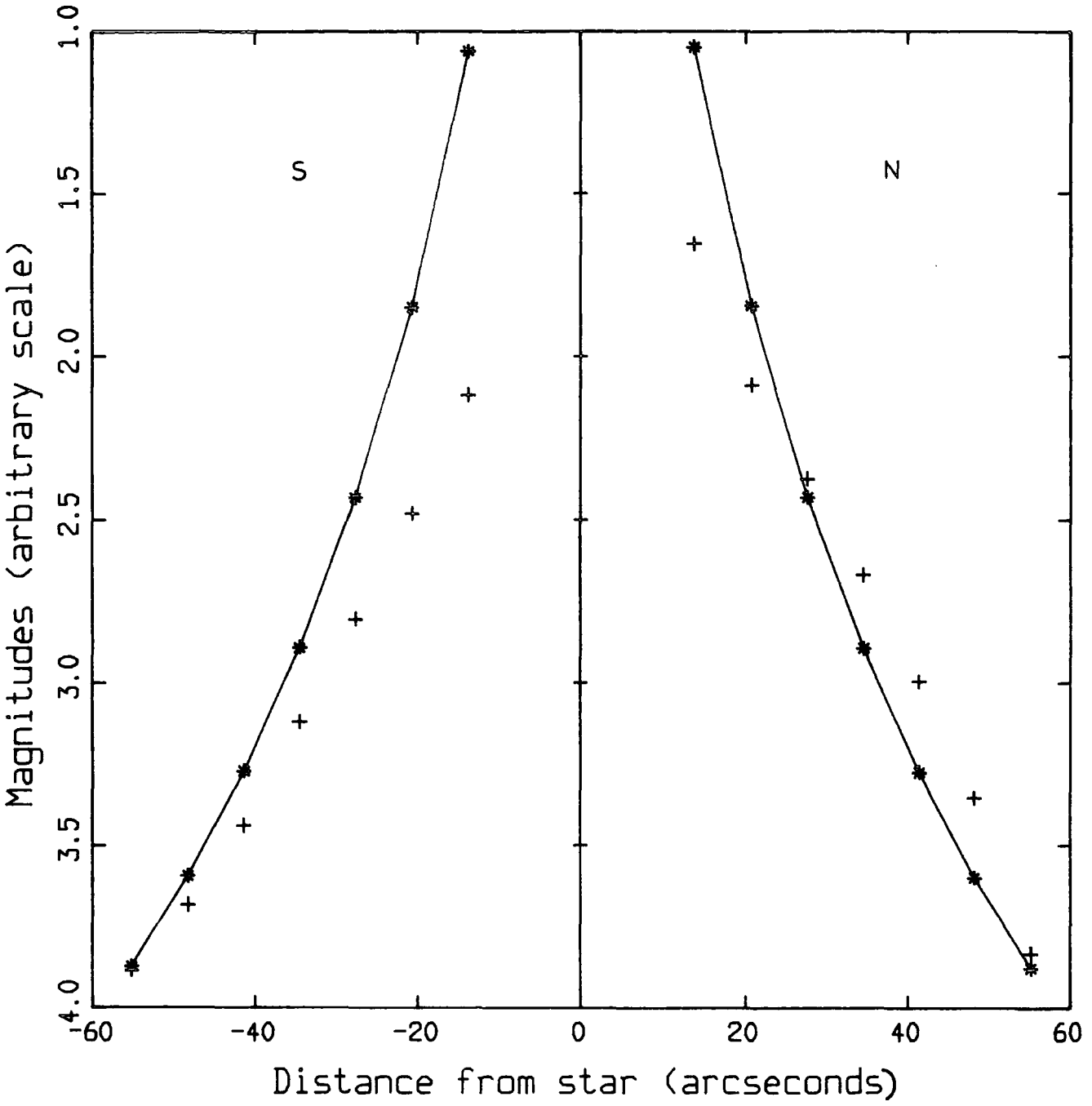

Figure 5.14

Brightness calculations for the paraboidal nebular model as a function of offset distance from the star. The brightnesses were normalized only to observational data from the northern lobe. The optimized nebular parameters are recorded in the text. The observational data points are indicated with + signs.

reduces the overall levels of polarizatio. The converse is also true and as a result, no combinations of foci and grain parameters enabled the correct simulation of the polarization data.

As with the biconical model, there was little difficulty in reproducing adequately, the observed brightness gradient for a wide range of nebular parameters.

Radial dust density distributions were investigated and again found to be inadequate. As shown in section 5.4.2, they have the effect of increasing the polarization along any given line of sight column with the increase being greater, the wider the range of scattering angles along that column (figure 5.11). The result for the present geometry, is that they decrease the rate of increase of polarization with increasing offset distance, while increasing the overall level of the polarization. There is, therefore, nothing to be gained by introducing a radial dust density variation into the nebular simulations.

5.5.1 THE PARABOIDAL MODEL WITH A CYLINDRICAL CORE.

The difficulty in fully accounting for the rapid increase in the polarization with increasing distance from the star led to an attempt to model the jet of dusty material in the north-western part of the nebula (other possible sources for the observed intensity and brightness enhancements were discussed in section 4.3). The jet was included into the model in the form of a cylindrical core of material, the axis of the cylinder being coincident with the nebular axis, as depicted in figure 5.15.

The optical path length in the core was included as a variable model parameter, together with the cylinder radius. Radial dust density variations throughout the nebula could be included in the model as required. Calculation of the Stokes parameters of the scattered light for a given line of sight column, required the separate calculation of the optical extinction along each light path included in the evaluation of the line of sight integral (equation 5.11).

This model proved capable of reproducing the observed gradients in the polarization variations with offset distance from the star, since the scattering angles become dominated by the core geometry (provided the dust

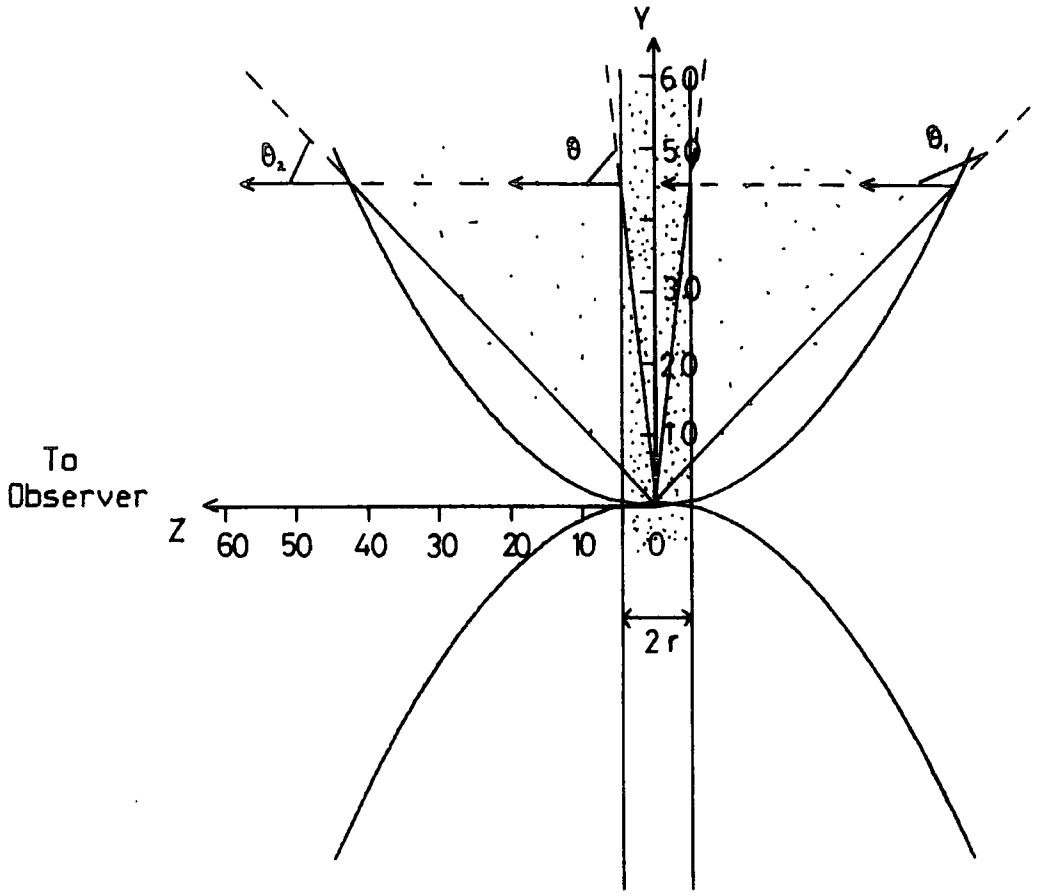

Figure 5.15

The paraboidal nebular model with a cylindrical core. The dust density of the core is much higher than that found in the rest of the nebula. Scattering angles are marked for one line of sight column. Clearly, the range of angles through the core are much less than along the entire column.

Focus of the paraboloid = 10 units

density in the core is significantly higher than in the surrounding nebular medium). The result is a rapid constriction of the scattering angles to around 90^0 as the distance from the star increases. However, the predicted polarizations were far in excess of those observed. The brightness variations along the major axis of the nebula were still dominated by scattering at the front surface of the nebula (ie. by the lowest possible scattering angles), and so brightness predictions were very similar to those of the filled paraboloid model.

5.5.2 SUMMARY OF THE DUST-FILLED PARABOIDAL MODELS

Even though the investigation did not result in a suitable nebular model, calculations with the uniformly dust-filled nebula in particular, were promising, yielding the most realistic simulations of the observational data so far. However, the requirement that the nebular structure should restrict the range of scattering angles along the line of sight columns at increasing offset distance from the star, has not been fully met. The need for very low scattering angles close to the star was emphasized.

Should the dust, instead of being distributed throughout the structure, be found only at the parabolic

surfaces, then the above conditions may well be met, since the light received by the observer will principally be scattered through a small range of angles at the front surface only.

5.6 THE CAVITY MODEL

This model consists of two paraboloids having slightly different foci and a common major axis and origin. All dusty material is to be found only in the intervening space between the paraboloids, and the remaining structure is assumed to be hollow. It nebular structure is depicted in figure 5.16 and is defined by two parameters, namely the foci of the inner and outer paraboloids.

The Stokes vector describing a beam of light, results from the simple addition of the Stokes vectors describing each individual wave (discussed in section 1.4). Similarly, calculation of the Stokes vector describing light scattered from a line of sight column through the present nebular structure, requires simply subtracting the vectors describing the scattered light from the same columns through two, dust-filled parabolic nebulae of appropriate foci. Such a procedure is valid under conditions of low optical depth (were the extinction

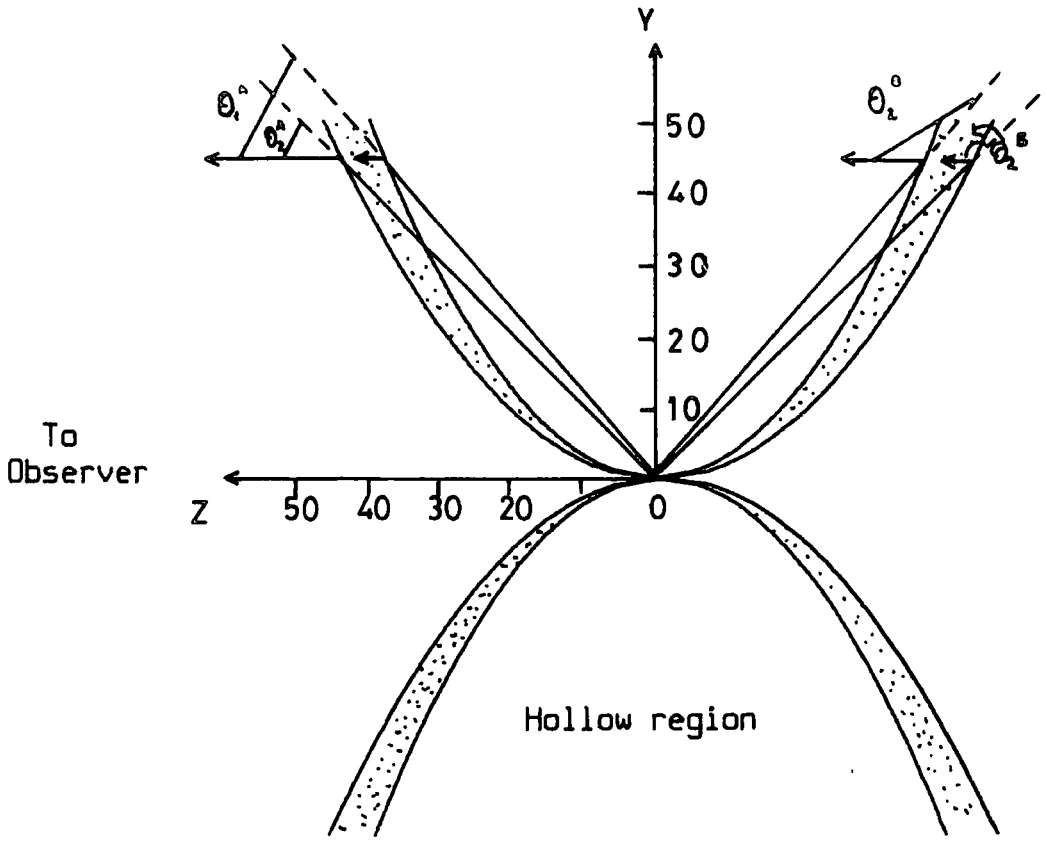

Figure 5.16

The cavity model, shown untilted in the plane of the sky. The range of scattering angles through the dust are marked for one line of sight column.

Focus of inner paraboloid = 10.97 units
Focus of outer paraboloid = 8 units

factor, described by equation 5.17, is close to unity) and uniform dust density distribution. It is valid for conditions of high optical depth if the dust is concentrated only on the surface of a paraboloid which is otherwise empty. Under such conditions, the light from the star will only suffer extinction when traversing the line of sight column, and if the dust is confined to a surface, then the extinction of the light is negligible and the extinction factor is unity. Equation 5.14 becomes

$$m_{NEB} = m_{STAR} - 2.5 \left(\log_{10} \frac{D^2 . \lambda^2 N}{8 . \pi^2 r \alpha^2} + \log_{10} \left(\int_{\theta_2}^{\theta_1} (F_1(\theta) + F_2(\theta)) . d\theta \right) \right) \quad \ldots . (5.28)$$

Clearly, the brightness gradients are now insensitive to the grain number density, N.

As with the dust-filled paraboidal nebular models, the model brightness predictions were normalized to the observational data of the northern lobe only. Preliminary calculations again showed that the nebular tilt must be restricted to less than ~ 1^0 out of the plane of the sky, and so it was fixed at zero degrees for all subsequent optimization procedures. It was found to be difficult to optimize both nebular foci simultaneously, and so the inner focus was varied 'manually' over a wide range of values, allowing the fitting algorithm (described in section 5.1) to optimize the outer focus and the grain parameters.

This nebular model proved able to reproduce the observational data far better than any of its predecessors. The polarization calculations were found to be very sensitive to the parabolic foci, resulting in the geometric parameters of the model being well defined by the observational data.

For the final optimization procedure, the imaginary part of the refractive index was again set to zero, since earlier work had shown that a grain albedo of > 0.8 was required if the nebular models were to accurately simulate the observations. The optimized nebular parameters are given in table 5.2, and figures 5.17 and 5.18 show the optimized model calculations of the nebular brightness and polarization compared to the observational data. Figure 5.19 shows the polarization behaviour of grains described by the parameters listed in table 5.2 as a function of scattering angle.

As a final check on the model parameters, surface brightnesses throughout the final nebular model were calculated (in magnitudes per square arcsecond) relative to a 12.74 magnitude star (with 1.9 magnitudes of extinction in the visual). They were then compared to the calibrated observational data recorded by Khachikyan and Parsamyan (1965). Grain number densities of 37 ± 7 m^{-3} are required at the parabolic surfaces in order to give agreement with the observations.

Table 5.2

Parameter	Value
Inner Focus of Paraboloid (arcsecs)	8.0
Outer Focus of Paraboloid (arcsecs)	10.97 ± 8.5
Re (Refractive Index)	1.25 ± 0.12
Power Index	-4.30 ± 0.22

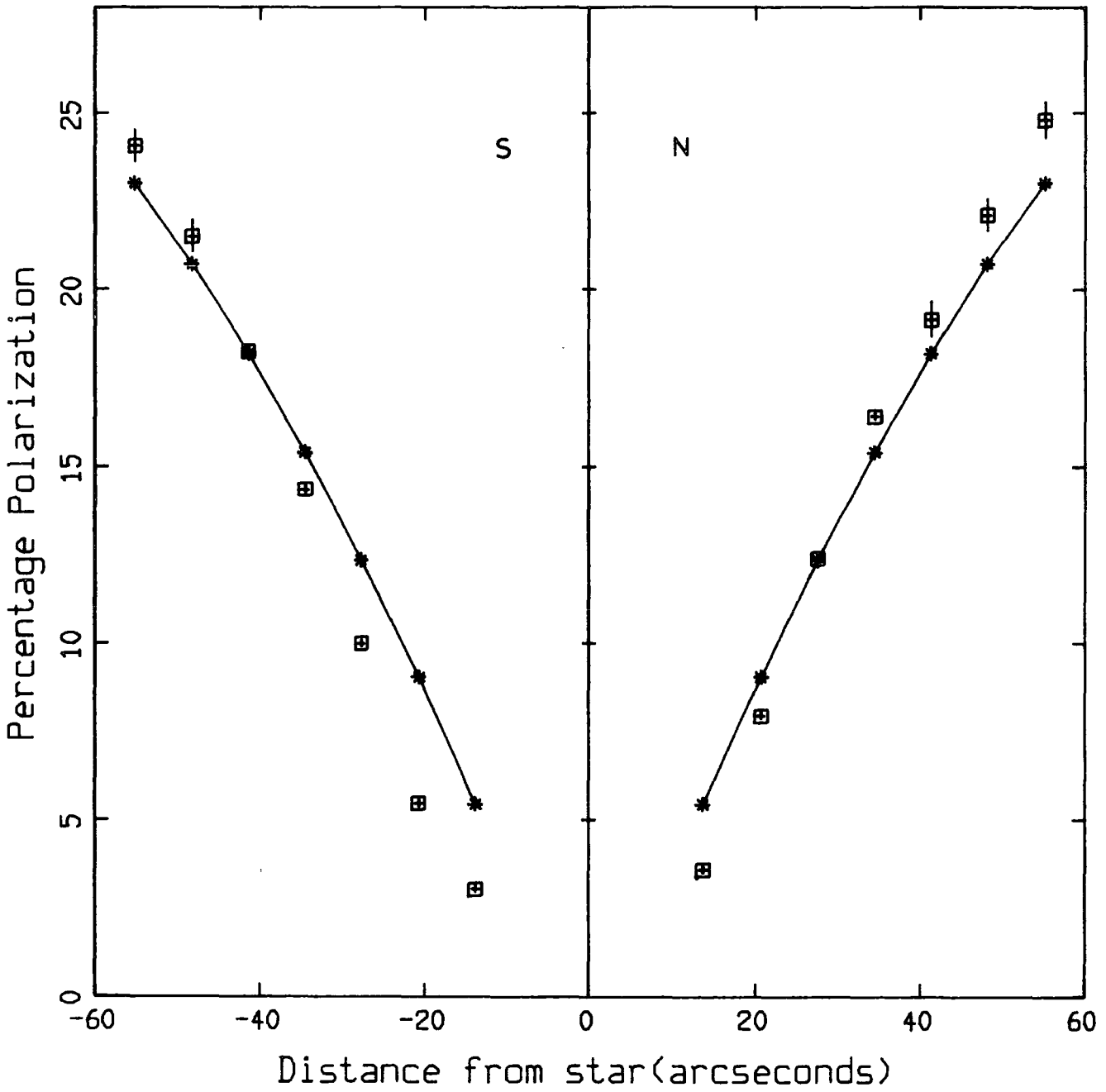

Figure 5.17

Polarization calculations as a function of offset distance from the star for a 'hollow' model nebula. The dust is concentrated at the parabolic surfaces of the structure. The optimized nebular parameters are recorded in the text. The observational data points are indicated with + signs.

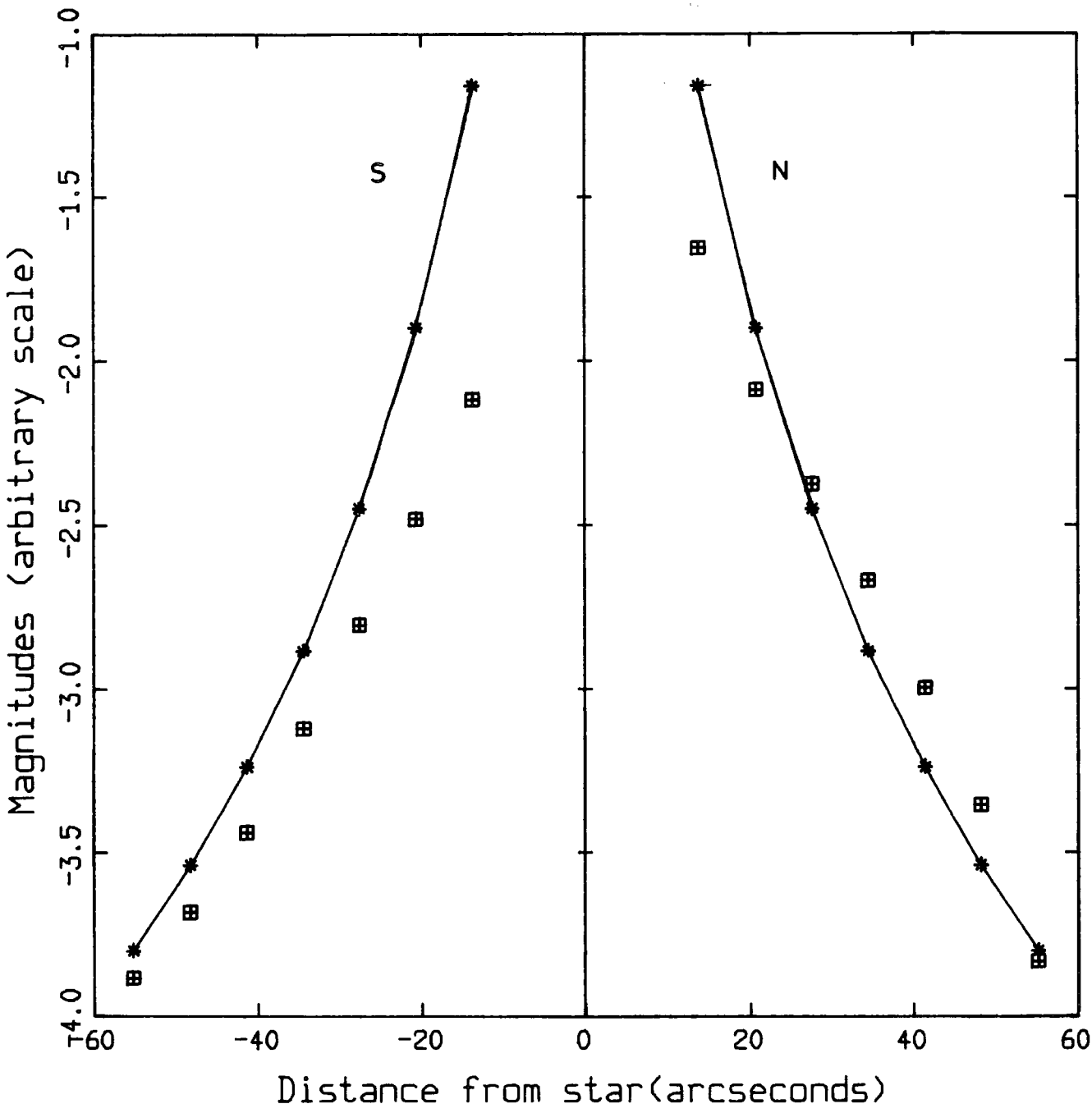

Figure 5.18

Brightness calculations as a function of offset distance from the star for a 'hollow' model nebula. The dust is concentrated at the parabolic surfaces of the structure. The brightnesses were normalized only to observational data from the northern lobe and the optimized nebular parameters are recorded in the text. The observational data points are indicated with + signs.

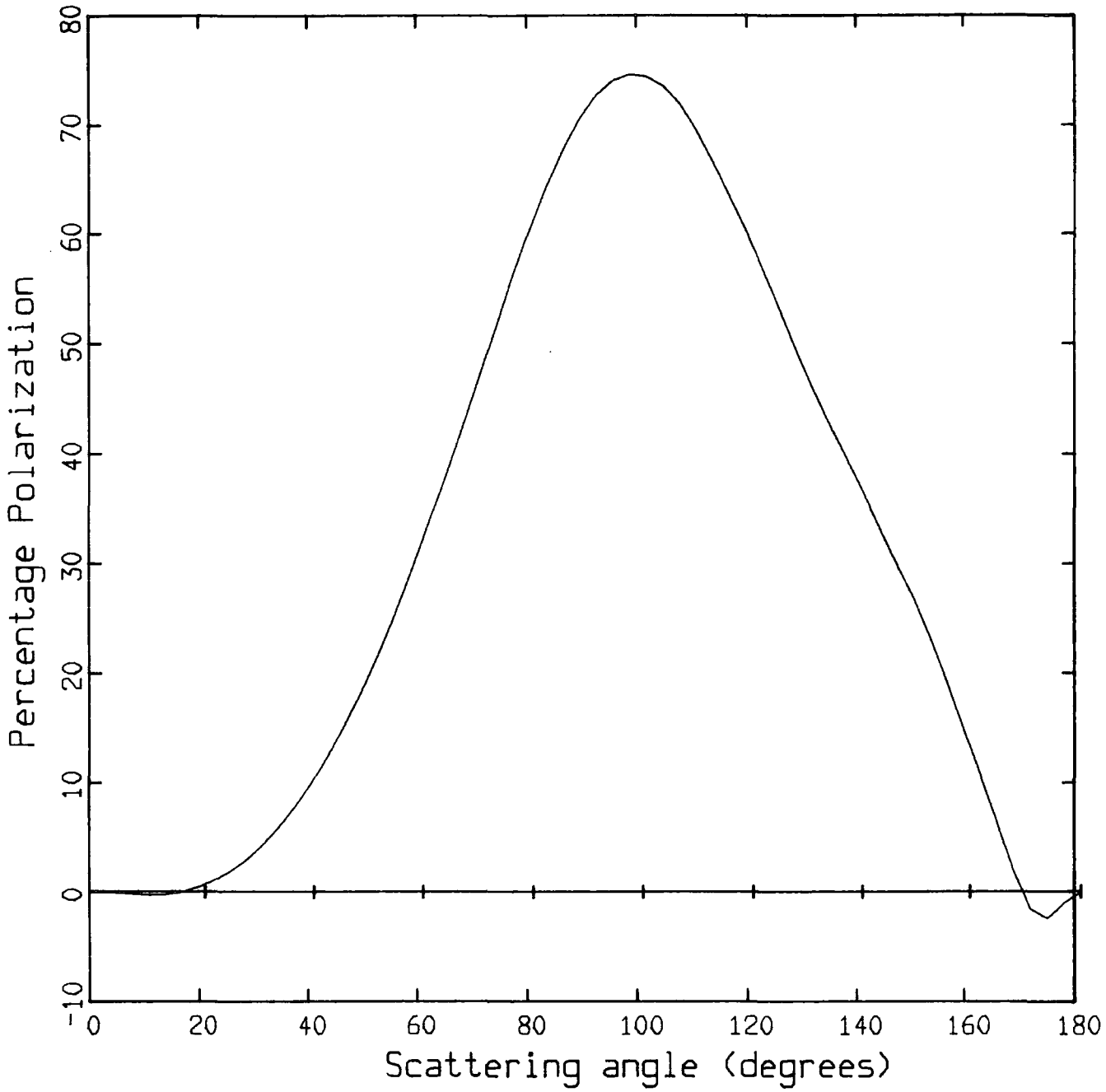

Figure 5.19

Percentage polarization as a function of scattering angle for a normalized power-law size distribution of grains. The index of the size distribution is -4.3. The refractive index of the grains is (1.25,0.0i)

Table 5.2

Parameter	Value
Inner Focus of Paraboloid (arcsecs)	8.0
Outer Focus of Paraboloid (arcsecs)	10.97 ± 8.5
Re (Refractive Index)	1.25 ± 0.12
Power Index	-4.30 ± 0.22

Simulated model images of the nebulosity are shown in plates 5 and 6 for comparison with the observed nebulosity shown in plates 1 to 4 (section 4.2).

5.7 DISCUSSION OF THE RESULTS

Figures 5.17 and 5.18 show clearly that this nebular model is well able to account for the observational data, although there is still some difficulty in fully accounting for the very low polarizations observed close to the star. The simulated intensity images of the nebulosity are quite realistic when compared to the observational images, although as shown in figure 5.18, the model nebular brightness falls off a little too sharply with offset distance from the star. The bright rims, which mark the inner and outer edges of the dust distribution on the plane of the sky, are not seen in the observational data. This is due to a combination of factors. The rims are very narrow and close to the seeing disc size. Also, in the numerical model, there is a sharp discontinuity in the dust distribution at the parabolic surfaces, resulting in the bright rims. In the real nebula, such discontinuities are not expected to exist.

The observed centro-symmetry of the polarization

pattern is well accounted for, since a centro-symmetric polarization pattern will always be predicted for models where the radiation undergoes only single scattering. This is simply because the plane of polarization of the scattered light always lies in the plane perpendicular to the scattering plane and the direction of propagation of the radiation, as demonstrated in figure 5.2.

5.7.1 DISCUSSION OF THE REFRACTIVE INDEX

The grains required by this model are of high albedo (> 0.8) and low refractive index (1.25 ± 0.12). Interestingly, this is also the case for the grains which comprise the nebula, NGC1999, which has been modelled by Warren-Smith (1983). This nebulosity is also associated with a young stellar object.

The refractive index and albedo found for any nebulosity must be representative of a combination of grain materials. There is no evidence from investigation of the interstellar medium to imply that its observable properties can all be explained in terms of a single grain composition. Mathis et al., (1977) found all of the grain mixtures that they considered, to require the presence of graphite in order to explain the observed ultra-violet extinction features. Cohen (1980) has identified the

presence of silicate grains in the spectrum of LkHα208. It seems likely then, that there will be a silicate and graphite content to the grain material. However, some other material must also be present, since neither of these compounds have a low index of refraction, and graphite is a highly absorbing material with a low albedo.

The only simple material which has a refractive index within the parameter range for this model is ice (refractive index = 1.33,0.0i), which is also highly refractory. On the basis of arguments presented in section 2.8.7, it seems unlikely that ice would exist in the nebula in the form of ice grains. An ice presence in the form of icy grain mantles is more consistent with present grain models, particularly when the youth of the star LkHα208 is considered. The identification of silicate grains in the circumstellar dust around the star, supports this hypothesis since silicates could have provided the necessary nucleation cores onto which mantles condensed in the early stages of the protostellar collapse. It is certainly conceivable that the icy grain mantles are subject to photolysis (discussed in section 2.8.7) which results in the formation of non-volatile mantles which themselves are highly refractory and of low refractive index. Confirmation of the presence of ice in the nebular medium will require spectral observations of the nebulosity in the 3.1 μ region to see if there is an ice

absorption feature.

5.7.2 DISCUSSION OF THE DUST SIZE DISTRIBUTION

As with the refractive index, the index of the power-law function which describes the grain size distribution was found to follow the trend set by the results from NGC1999 (power-index = -4.24 ± 0.18) . The power-indices found both for the grains comprising the nebulosity illuminated by LKHα208 (-4.3 ± 0.22) and NGC1999, are significantly lower than the indices of -3.3 to -3.6, which are required for the grains giving rise to the observed interstellar extinction (Mathis et al. (1977)). This seems to indicate that there are proportionally larger numbers of small grains in the nebular structures than in the general interstellar medium. As discussed in section 2.7.1, Mathis et al. carried out an empirical derivation of the grain size distribution by modelling the mean interstellar extinction curve.

Warren-Smith proposed that $[\partial \ln(n)/\partial \ln(a)]$ is, in fact, not a constant, but varies slowly with the grain size, the index of the distribution becoming more negative with increasing grain radius (n(a)da is the number density of particles with radii in the range a to a+da). This

would account for the low power-index found for NGC1999, since the polarization data are sensitive to grain sizes from 0.2 to 0.5 μ, whereas, the interstellar extinction data is sensitive to grain sizes in the region of 0.03 μ.

Since the nebular structure under the present investigation is also sensitive to grains sizes from 0.2 to 0.5 μ, the value calculated for the power-index here (-4.30 ± 0.22), would seem to confirm this hypothesis, although care should be taken since both NGC1999 and the nebulosity surrounding LkHα208 are associated with young stellar objects and the dust may not be representative of the general interstellar medium.

High velocity winds are known to be associated with Herbig Ae/Be stars and the destructive processes which have been, and indeed may well still be, in operation in the stellar and nebular environments, may have resulted in a size distribution of grains where there are more small grains than usual, so accounting for the low power-index. However, grains in the diffuse cloud medium originate in young stellar environments and when they are ejected into the diffuse cloud medium, they suffer only destruction processes and do not grow (discussed in section 2.7.1). It would therefore be difficult to account for the observed distributions of Mathis (1977), where there seem to be a higher number of large grains than has been calculated in the nebulae, if

the grains in the young stellar environments consist of a proportionally much higher number of small grains. In conclusion, the suggestion by Warren-Smith that $[\partial \ln(n)/\partial \ln(a)]$ is a slowly varying function is favoured.

5.7.3 DISCUSSION OF THE NEBULAR STRUCTURE

A consideration of the nature of Herbig Ae/Be stars, theoretical work on young stellar objects, and the available observational data, suggests that the object under study is a representative of the latter stages of stellar formation. In particular, it would seem to be a good example of the final stage of the stellar formation model proposed by Konigel (and described in section 3.9) where the stellar object is observed through a thick dust disk or torus, and illuminates one or two nebular lobes. Numerical modelling has shown that dust which gives rise to the nebulosity must be concentrated at the edges of a cavity. The geometric structure of the cavity region may be approximated by the surface of a paraboloid. Presumably, the cavity has been evacuated by the two supersonic jets, which were formed much earlier in the evolutionary process by the focusing of the stellar wind by the molecular cloud from which LKHα208 has condensed.

As mentioned above (section 5.6), the model data

were compared to the calibrated observational data recorded by Khachikyan and Parsamyan (1965) and it was found, in order to give agreement with the observations, that a grain number density of $37 \pm 7\ m^{-3}$ is required, which is ~ 1000 times greater than the number density of the grains in NGC1999. Taking the mass density of ice, $1000\ kgm^{-3}$, for the grains, it is possible to place a lower limit on the mass of grain material contained in the nebular structure. Integrating over the size spectrum of the grains and taking a value of 60 arcseconds for the N/S extent of each lobe, a mass of $10^{-2}\ M_{\odot}$ was calculated for material contained in each lobe.

While the hollow paraboidal model explains most of the observational features well, it cannot fully account for the very low polarizations measured close to the star. Also, the model nebular brightness falls off a little too sharply with offset distance from the star. Any numerical model is, at best, only an approximation to the real nebular structure and composition, and the observations of both brightness and polarization close to the star are likely to result from scattering not only from dust at the parabolic surfaces, but also from material which still remains from the molecular cloud and from dust connected to the dust disc. As a result, the forward scattering angles for light scattered close to the star will be much lower than from the paraboidal structure alone, so

accounting for the low polarization measurements and also resulting in a slower fall-off in the nebular intensity at low offset distance than is predicted by the hollow paraboidal model.

An interesting point concerning the nebular model of Yusef-Zadeh et al., (1984), is that if, instead of invoking a biconical cavity in a dust cloud, the cavity was curved, so as to be better approximated by a paraboloid, then the scattering geometry would be very similar to the hollow paraboidal model invoked above. The dust disc would again account for the low polarizations observed close to the star.

5.8 A SUMMARY OF THE CONCLUSIONS

Investigation of the photometric data revealed not only the classical hourglass appearance of the nebulosity, but also many asymmetries in the object about both the major axis of the nebular lobes and the plane of the dust disc. A jet-like feature, which appears to emanate from the central object, was observed in four colours in the north-western part of the northern lobe, and the percentage polarization is well correlated with the feature. The jet may simply be an illumination effect, such as a shaft of light penetrating the dust at some

appropriate angle, or it may be a jet of nebular material, probably connected with the supersonic jets which are proposed by Konigel (1982), to exist during the early stages of stellar formation.

The nebulosity lies at the edge of a dark cloud to the east, which is proposed to be responsible for the nebular lobes appearing to be swept towards the west, so giving the object a slight boomerang shape. The circumstellar dust disk is evidenced by the steep brightness gradients perpendicular to the major axis of the nebular lobes.

Numerical modelling of the nebular lobes has shown that the observations result from the scattering of radiation from dust which is concentrated at the edges of a cavity, the structure of which has been approximated by a paraboloid. This model is able to account for the observed centro-symmetry of the polarization data, the levels of polarization, and the symmetry in the observations along the major axis of the object.

The grains comprising the nebular are of high albedo (> 0.8) and low refractive index (1.25 ± 0.12). It is likely, on the basis of previous observations, that there is a silicate and graphite content to the grain material. On the basis of the present calculations, it is proposed that there is an ice presence in the nebular medium in the form of icy grain mantles, which may well

have undergone photo-processing to yield non-volatile, highly refractory grain mantles which are of low refractive index.

A power-law function has been used to describe the grain size distribution and the power-index which best accounts for the observational data is (-4.3 ± 0.22). This value is significantly lower than the indices found from modelling the interstellar extinction curve (Mathis et al. (1977) and the proposal by Warren-Smith (1983) that $[\partial \ln(n)/\partial \ln(a)]$ is not a constant, but varies slowly with the grain size, the index of the distribution becoming more negative with increasing grain radius, is favoured as the possible explanation.

The number density of dust grains at the surface of the cavity is 37 ± 7 m^{-3} which is ~ 1000 times greater than the value calculated for the nebulosity NGC1999 (Warren-Smith, 1983) and 10^{10} times greater than the typical value for the diffuse cloud medium (Greenberg, 1983). A mass of 10^{-2} $M_{\odot}$ is found for the dusty material contained in each lobe.

REFERENCES

The following abbreviations for journal titles have been used :

A.J.	:	Astronomical Journal
A. & A.	:	Astronomy and Astrophysics
Ap.J.	:	Astrophysical Journal
M.N.R.A.S.	:	Monthly Notices of the Royal Astronomical Society

Aannestad,P.D. and Purcell,E.M.,(1973),*Ann.Rev.A. & A.*,**11**,309

Aitken,D.K.,Roche,P.F.,Spencer,P.M. and Jones,B.,(1979), *A. & A.*,**76**,60

Aitken,D.K.,(1981),*I.A.U. Symp 96*,p207

Allamandola,L.J. and Norman,C.A.,(1978),*A. & A.*,**63**,L23

Allamandola,L.J. and Norman,C.A.,(1978),*A. & A.*,**66**,129

Allamandola,L.J.,Greenberg,J.M. and Norman,C.A.,(1979), *A. & A.*,**77**,66

Allen,D.A. (1973),*M.N.R.A.S.*,**161**,145

Ambartsumian,V.A.,(1947),*Stellar Evolution and Astrophysics (Acad.Sci.Armenian U.S.S.R.)*

Ambartsumian,V.A.,(1954),*Comm. Burakan Obs.*,No. 13

Andriesse,C.D.,(1977),*Vistas Astr*,**21**,107

Bally,J. and Lada,C.J.,(1983),*Ap.J.*,**265**,824

Barlow,M.J.,(1978)a,*M.N.R.A.S.*,**183**,367

REFERENCES

Barlow,M.J.,(1978)b,*M.N.R.A.S.*,**183**,397

Bar-Nun,A.,(1975),*Ap.J*,**197**,341

Barrel,J.F. and Canto.,J.,(1981),*Rev. Mexicana Astron. Afro.*,**5**,101

Bash,F.N.,(1979),*Ap.J*,**233**,524

Bellingham,J.G. and Rossano,G.S.,(1980),*A.J.*,**85**,555

Bergh,S. van den,(1966),*Ap.J.*,**71**,990

Bless,R.C. and Savage,B.D.,(1970),*I.A.U. Symp.*,**36**,28

Bless,R.C. and Savage,B.D.,(1972),*Ap.J*,**171**,293

Bohlin,R.C.,Savage,B.D. and Drake,J.F.,(1978),*Ap.J*,**224**,132

Boggess,A. and Borgman,J.,(1964),*Ap.J*,**140**,1636

Burke,J.R. and Silk,J.,(1976),*Ap.J*,**210**,341

Calvet,N. and Cohen,M.,(1978),*M.N.R.A.S.*,**182**,687

Cameron,A.G.W.,(1973),*Space Sci Rev*,**15**,121

Cameron,A.G.W.,(1973),*Icarus*,**18**,No 3,377

Canto,J. and Rodriguez,J.F.,(1980),*Ap.J.*,**239**,982

Canto,J.,Rodriguez,J.F.,Barral,F. and Carral.P.,(1981), *Ap.J.*,**244**,102

Cederbland,S.,(1946),*Lund. Obs. Medd. Ser.II*,No. 119

Chylek,P.,Grams,G.W. and Pinick,R.G.,(1976),*Science*,**193**,480

Clayton,D.D. and Hoyle,F.,(1976),*Ap.J.*,**203**,490

Cohen,M.,(1973),*M.N.R.A.S.*,**161**,105

Cohen,M.,(1975),*Ap.J.*,**196**,179

Cohen,M. and Kuhi,L.V.,(1977),*Ap.J.*,**213**,79

Cohen,M. and Schwartz,R.D.,(1979),*Ap.J.*,**233**,L77

Cohen,M. (1980),*M.N.R.A.S.*,**191**,499

REFERENCES

Cohen,M. and Schwartz,R.D.,(1983),*Ap.J.*,**265**,877

Coyne,G.V.,Gehrels,T. and Serkowski,K.,(1974),*A.J.*,**79**,581

Crampton,D.,Cowley,A.P. and Humphreys,R.M.,(1975),*Ap.J.*,**198**,L135

Cudworth,K.M. and Herbig,G.H.,(1979),*A.J.*,**84**,548

Dabai,E.A.,(1969),*Astrofizika*,**5**,115

Daniels,P.A. and Hughes,D.W.,(1981),*M.N.R.A.S.*,**195**,205

Danielson,E.R.,Wolf,J.N. and Gaustad,E.J.,(1965),*Ap.J*,**141**,116

Davies,L. and Greenstein,J.L.,(1951),*Ap.J*,**114**,206

Davis,R.,Strom,S.E.,Strom,K.M.,(1983),*Ap.J.*,**88**,1644

De Boer,K.S.,(1980),*Ap.J*,**224**,848

Dopita,M.A.,(1978),*Ap.J. Suppl*,**37**,117

Dorschner,J. and Gurtler,J.,(1966),*A.J.*,**289**,57

Dorschner,J.,Friedmann,C. and Gurtler,J.,(1977),*A. & A.*,**58**,201

Dorschner,J.,Friedmann,C. and Gurtler,J.,(1980),*Astrop. Space Sci*,**68**,159

Douglas,A.E.,(1977),*Nature*,**269**,130

Draine,B.T.,(1979),*Ap.J*,**230**,106

Duley,W.W.,Millar,T.J. and Williams,D.A.,(1979),*Ap. Space Sci.*,**65**,69

Duley,W.W. and Williams,D.A.,(1979),*Nature*,**277**,40

Duley,W.W. and Williams,D.A.,(1981),*M.N.R.A.S.*,**196**,269

Dwek,E.,Sellgren,K.,Soifer,B.T. and Werner,M.W.,(1980), *Ap.J.*,**238**,140

Dyck,H.M. and Lonsdale,C.J.,(1981),*I.A.U. Symp*,**91**

Ebert,R.,(1957),*Z. Astrophys.*,**42**,263

Eiroa,C. and Elsasser,H.,(1979),*A. & A.*,**74**,89

REFERENCES

Erickson,N.R. and Lada,C.J.,(1982),*Ap.J.*,**261**,L103

Field,G.B.,(1974),*Ap.J.*,**187**,453

Finkenzeller,U. and Mundt,R.,(1984),*A. & A. Suppl.*,**55**,109

Forrest,W.J., McCarthy,J.F. and Houck,J.R.,(1979),*Ap.J*,**233**,611

Gehrels,T.,(1960),*A .J.*,**65**,470

Geisel,S.L., Kleinmann,D.E. and Low,F.J.,(1970),*Ap.J.*,**161**,L101

Gillett,F.C. and Stein,W. (1971),*Ap.J.*,**164**,77

Gillett,F.C. and Forrest,W.J.,(1973),*Ap.J*,**179**,483

Gillett,F.C., Forrest,W.J. and Merrill,K.M.,(1973),*Ap.J*,**183**,87

Gillett,F.C.,Jones,T.W.,Merrill,K.M. and Stein,W.A.,(1975),
A. & A.,**45**,77

Gillett,F.C.,Kleinmann,D.E., Wright,E.L. and Cappes. R.W.,
(1975),*Ap.J*,**198**,L65

Gilra,D.P.,(1972),*Collective excitations and dust particles in space*,ed. A.D.Code

Gilra,D.P.,(1973),*I.A.U. Symp.*,**52**

Grasdalen,G.L. and Joyce,R.R.,(1976),*Ap.J.*,**205**,L11

Greenberg,J.M.,(1960),*Ap.J.*,**132**,672

Greenberg,J.M.,(1968),*Stars and Stellar Systems*,
(Univers. of Chicago Press)

Greenberg,J.M. and Shah,G.A.,(1969), *Physica*,**41**,92

Greenberg,J.M.,(1971),*A. & A.*,**12**,240

Greenberg,J.M.,(1973),*Molecules in the Galactic Environment*,
ed. Gordon & Snyder,(Wiley and Sons)

Greenberg,J.M.,(1974),*Ap.J.*,**189**,L81

Greenberg,J.M.,(1978),*Cosmic Dust*,ed. McDonnell,(Wiley
& Sons Ltd.)

REFERENCES

Greenberg,J.M.,(1978), *Infrared Astron.*, ed. Setti & Fazio,(Reidel),51-97

Greenberg,J.M.,(1982),*Comets*,ed. Wilkening,(Univers. of Arizona Press)

Greenberg,J.M.,(1983),*Adv. Space Res.*,**vol.3,no.9**,19

Greenberg,J.M.,(1983),*Poceedings of the Workshop on Laboratory and Observational Infrared Spectra of Interstellar Dust*,**Hilo Workshop Hawaii**

Greenberg,J.M. and Chlewicki,G.,(1983),*Ap.J*,**272**,563

Hall,J.S.,(1937),*Ap.J.*,**85**,145

Hall,J.S.,(1949),*Science*,**109**,166

Hall,R.C.,(1965),*Publ.Astron.Soc.Pac*,**77**,158

Hagen,W.,Allamandola,L.J. and Greenberg,J.M.,(1979),*Astrop. and Space Sci.*,**65**,215

Hagen,W.,Allamandola,L.J. and Greenberg,J.M.,(1980), *A. & A.*,**86**,L3

Hagen,W.,Tielens,A.G.G.M. and Greenberg,J.M.,(1983), *A. & A.*,**177**,132

Haro,G.,(1952),*Ap.J.*,**113**,697

Haro,G.,(1952),*Ap.J.*,**115**,572

Haro,G. and Herbig,G.H.,(1955),*Bol. Obs. Toriantzilla y Tacubaya*,**12**,33

Hartmann,W.K.,(1969),*Icarus*,**10**,201

Hayes,D.S.,Mavko,G.E.,Radick,P.R.,Rex,K.H. and Greenberg,J.M., (1973),*I.A.U. Symp.no 52*

REFERENCES

Herbig,G.H.,(1951),*Ap. J.*,**113**,697

Herbig,G.H.,(1960),*Ap. J. Suppl*,**4**,337

Herbig,G.H., (1962) *Adv.Astr.Ap.*,**1**,47.

Herbig,G.H. and Rao,N.K.,(1972),*Ap. J.*,**174**,401

Herbig,G.H., (1975),*Ap. J.*,**196**,129

Herbig,G.H., (1975),*Ap. J.*,**200**,1

Herbig,G.H., (1977),*Ap. J.*,**217**,693

Herbig,G.H. and Jones,B.F.,(1981),*A. J.*,**86**,1232

Henyey,L.G. and Greenstein,J.L.,(1941),*Ap J.*,**93**,70

Hellyer,B.,(1970),*M.N.R.A.S.*,**148**,383

Hiltner,W.A.,(1949),*Science*,**109**,165

Hiltner,W.A.,(1956),*Ap. J. Suppl*,**2**,389

Hong,S.S. and Greenberg,J.M.,(1980),*A. & A.*,**88**,189

Hoyle,F. and Wickramasinghe,N.C.,(1962),.*M.N.R.A.S.*,**142**,417

Hoyle,F. and Wickramasinghe,N.C.,(1970),*Nature*,**226**,62

Hoyle,F. and Wickramasinghe,N.C.,(1980),*Astrop. Space Sci*,**72**,247

Hubble,E.P.,(1922),*Ap. J.*,**56**,400

Huffman,D.R.,(1977),*Advances in Physics*,**26**,129

Huffman,D.R. and Stapp,J.L.,(1971),*Nature Phys. Sci.*,**229**,45

Hulst,H.C.van de,(1943),*Ned. Tijdschr. vor Natuurkunde*,**10**,25

Hulst,H.C.van de,(1949),*Rech.Astr.Obs.Utrecht*,**11**,

Hulst,H.C.van de,(1957),*Light Scattering by Small Particles* (Wiley and Sons)

Hulst,H.C.van de,(1981),*Light Scattering by Small Particles* (Dover Publications)

REFERENCES

Innanen,K.A.,(1969),*J.R.A.S. Canada*,**63**,260

Jones,B.F. and Herbig,G.H., (1982),*A.J.*,**87**,1223

Joy,A.H.,(1942),*Pub. Ast. Soc. Pac.*,54,15

Joy,A.H.,(1945),*Ap.J.*,**102**,168

Joy,A.H.,(1949),*Ap.J.*,**110**,424

Kaplan,S.A.,Pikelner,S.B.,(1970),*The Interstellar Medium*, (Harvard Univ. Press)

Khachikyan,E.E. and Parsamyan,E.S.,(1965),*Astrofizika*, **Vol.1 No.4**,417

Kleinmann,S.G., Sargent,D.G.,Gillett,F.C.,Grasdalen,G.L. and Joyce,R.R., (1977),*Ap.J.*,**215**,L79

Knacke,R.F.,Cudaback,D.D. and Gaustad,J.E.,(1969),*Ap.J*,**158**,151

Konigel,A.,(1982),*Ap.J.*,**261**,115

Krelowski,J. and Strobel,A.,(1983),*A. & A.*,**127**,271

Kuhi,L.V.,(1983),*Rev. Mexicana Astron. Astro.*,**7**,127

Kwan,J.,(1979),*Ap.J*,**229**,567

Lada,C.J.,Elmegreen,B,G and Cong,H.J.,(1978),*Ap.J*,**226**,L39

Larson,R. (1969),*M.N.R.A.S.*,**145**,271

Lillie,C.F. and Witt,A.N.,(1976),*Ap.J.*,**208**,64

Lindbland,B.,(1935),*Nature*,**135**,133

Martel,M.T.,(1958),*Suppl. Ann. d'Astrop.*,**No.7**

Mathewson,D.S. and Ford,V.L.,(1970),*Mem.R.A.S.*,**74**,139

Mathis,J.S.,Rumpl,W. and Nordsieck,K.H.,(1977),*Ap.J.*,**217**,425

Massa,D.,Savage,B.D. and Fitzpartick,E.L.,(1983),*Ap.J*,**266**,662

Mavko,G.E.,Hayes,D.S.,Greenberg,J.M.,and Hiltner,W.A., (1974),*Ap.J.*,**187**,L117

REFERENCES

Merrill,K.M., Russell,R.W. and Soifer,B.T.,(1976),*Ap.J.*,**207**,763

Merrill,P.W.,(1934),*Publ.Astron.Soc.Pac.*,**46**,206

Meyer,D.M. and Savage,B.D.,(1981),*Ap.J.*,**248**,545

Mie,G.,(1908),*Ann de Phys.*,**25**,377

Morton,D,C. and Smith,W.H.,(1973),*Ap.J.Suppl.*,**26**,333

Morton,D,C,(1974),*Ap.J.*,**193**,L35

Mundt,R.,Stocke,J. and Stockman,H.S.,(1983),*Ap.J.*,**265**,L71

Nandy,K.,Thompson,G.I.,and Jamar,C.,(1975),*A. & A.*,44,195

Neckel,T. and Staude,H.J.,(1984),*A. & A.*,**131**,200

Ney,E.P.,Merrill,K.M.,Becklin,E.E. and Neugebauer,G,(1975),
Ap.J.,**198**,L129

Oort,J.H. and van de Hulst,H.C.,(1946),*B.A.N.*,**10**,187

Peckham,G.,(1970),*Computor J.*,**164**,425

Perkins,H.G.,King,D.J. and Scarrott,S.M.,(1981),
M.N.R.A.S.,**196**,403

Perkins,H.G.,King,D.J. and Scarrott,S.M.,(1981),
M.N.R.A.S.,**196**,7P

Purcell,E.M.,(1969),*Ap.J*,**158**,433

Purcell,E.M. and Shapiro,P.R.,(1977),*Ap.J*,**214**,92

Racine,R.,(1968),*A .J.*,**73**,233

Raymond,J.C.,(1979),*Ap.J. Suppl*,**39**,1

Roberts,M.S.M.,(1957),*Pub. Astr. Soc. Pac.*,**69**,59

Rodriguez,L.F.,Moran,J.M.,Ho,P.T.P., and Gottlieb,E.W.,(1980),
Ap.J.,**235**,845

Rodriguez,L.F.,Ho,P.T.P. and Moran,J.M.,(1980),*Ap.J.*,**240**,L149

Rodriguez,L.F.,Carral,P.,Ho,P.T.P. and Moran,J.M.,(1982),
Ap.J.,**260**,635

REFERENCES

Rogerson,J.B.,York,D.G.,Drake,J.F.,Jenkins,E.B.,Morton,D.C.,
Spitzer,L., (1973),*Ap. J.*,**181**,L110

Russell,R.W., Soifer,B.T. and Willner,S.P.,(1978),*Ap. J*,**220**,568

Savage,B.D.,(1975),*Ap. J.*,199,92

Savage,B.D. and Mathis,J.S.,(1979),*Ann. Rev. A. & A.*,**17**,73

Scarrott,S.M.,Warren-Smith,R.F.,Pallister,W.S. and Axon.D.J.,
(1983),*M.N.R.A.S.*,**204**,1163

Schwartz,R.D.,(1977),*Ap. J. Suppl*,**35**,161

Schwartz,R.D.,(1978),*Ap. J.*,**223**,884

Scoville,N.Z. and Hersh,K.,(1979),*Ap. J*,**229**,578

Seab,C.G. and Snow,C.P. (1984),*Ap. J.*,**277**,200

Serkowski,K.,Mathewson,D.S. and Ford,V.L.,(1975),*Ap. J.*,**196**,261

Sharpless,S.,(1959),*Ap. J. Suppl.*,**4**,257

Shirt,J.V.,Warren-Smith,R.F.,Scarrott,S.M.,(1983),
.M.N.R.A.S.,**204**,1257

Slipher,V.M.,(1912),*Lowell Obs. Bull.*,**No 2**

Smith,W.H.,Snow,T.P. and York,D.G.,(1977),*Ap. J*,**218**,124

Snell,R.L.,Loren,R.B. and Plambeck,R.L.,(1980),*Ap. J.*,**238**,L17

Snow,C.P. and Seab,C.G.,(1980),*Ap. J.*,**242**,L83

Snyder,L.E.,Buhl,D.,Zuckerman,B. and Palmer,S.,(1969),
Phys. Rev. Letters,**22**,679

Soifer,B.T.,Puetter,R.C.,Russell,R.W. and Gillett,F.C.,
(1979),*Ap. J*,**232**,L53

Spitzer,L.,(1954),*Ap. J.*,**120**,1

Stecher,T.P.,(1965),*Ap. J*,**142**,1683

REFERENCES

Strom,S.E.,Strom,K.M and Yost,J.,(1972),*Ap.J.*,**173**,353

Taylor,K.N.R. and Scarrott,S.M.,(1980),*M.N.R.A.S.*,**193**,321

Trumpler,R.J.,(1930),*Lick Obs. Bulletin*,14,154

Vrba,F.,Schmidt,G.D. and Hintzen,P.M.,(1979),*Ap.J.*,**227**,185

Vogel,S.N. and Kuhi,L.V.,(1981),*Ap.J.*,**245**,960

Walker,M.F.,(1956),*Ap.J.suppl.*,**2**,365

Warren-Smith,R.F.,(1979),*PhD Thesis* Durham
University, England

Warren-Smith,R.F.,Scarrott,S.M.,Murdin,P.,Bingham,R.G.,
(1979),*M.N.R.A.S.*,**187**,761

Warren-Smith,R.F.,Scarrott,S.M.,Taylor,K.N.R.,Bingham,R.G.,
and Murdin,P.,(1980),*M.N.R.A.S.*,**192**,339

Warren-Smith,R.F.,(1983),*M.N.R.A.S.*,**205**,337

Warren-Smith,R.F.,(1983),*M.N.R.A.S.*,**205**,348

Welin,G.,(1971),*A. & A.*,**12**,312

Wenzel,W. and Gessner,H.,(1975),*Mitt. Ver. Sterne*,**7**,23

Whitford,A.E.,(1948),*Ap.J.*,**107**,102

Whitford,A.E.,(1958),*A.J.*,**63**,201

Whittet,D.C.B. and Blades,J.C.,(1980),*M.N.R.A.S.*,**191**,309

Whittet,D.C.B.,(1981),*Q.Jl.R.A.S.*,**22**,3

Wickramasinghe,N.C.,(1973),*Light Scattering Functions
for Small Particles with Applications in
Astronomy*,(Hilger,London)

Wickramasinghe,N.C. and Allen.D.A.,(1980),*Nature*,**287**,518

Wilking,B.A.,Lebofsky,M.J.,Martin,P.G.,Reike,G.H.,Kemp,J.C.,
(1980),*Ap.J.*,**235**,905

REFERENCES

Willner,S.P.,Russell,R.W.,Puetter,R.C.,Soifer,B.T. and Harvey,P.M.,(1979),*Astrop. Space Sci.*,**65**,95

Willner,S.P.,Russell,R.W.,Puetter,R.C.,Soifer,B.T. and Harvey,P.M.,(1979),*Ap. J.*,**229**,L65

Willner,S.P.,Russell,R.W.,Puetter,R.C.,Soifer,B.T. and Harvey,P.M.,(1980),*I.A.U. Symp.*,**87**,381

Witt,A.N. and Lillie,C.F.,(1973),*A. & A.*,**25**,397

Woodward,P.R.,(1978),*Annual Rev A. & A.*,**16**,555

Woolf,N.J. and Ney,E.P.,(1969),*Ap. J.*,**155**,L18

Woolf,N.J.,Stein,W.A. and Strittmatter,P.A.,(1970),*A. & A.*,**9**,252

Worden,S.P.,Schneeberger,T.J. and Africano,J.L.,(1981),*Ap. J.*,**244**,520

Wu,C.C.,York,D.G. and Snow,T.P.,(1981),*A J*,**86**,755

Yusef-Zadeh,F.,Morris,M.,White,R.L.,(1984),*Ap. J.*,**278**,186

Zellner,B.,(1973),*I.A.U. Symp.*,**52**

Zerull,R. and Giese,R.H.,(1974),*Planets , Stars and Nebulae Studied with Photopolarimetry* ed. Gehrels, (University of Arizona Press)

Zuckerman,B.,Kuiper,T.B.H. and Kuiper,E.N.R.,(1976),*Ap. J.*,**209**,L137

ACKNOWLEDGEMENTS

The author would like to thank her academic supervisor, Dr S.M.Scarrott and also Dr R.F.Warren-Smith, for their support in carrying out the research described in this text. In particular, Dr Warren-Smith is to be thanked for his invaluable help concerning the use of simulation techniques and his help in many other areas of the work.

The author would also like to thank Mr A.P.Lotts for his help whenever needed, in the use of the Starlink Vax at Durham. Thanks go to many other members of the Physics department, in particular David Berry,the author's contemporary, who have provided both help and encouragement.

The author is grateful to the staff at the Wise Observatory of the University of Tel Aviv, the Anglo-Australian Telescope, Siding Springs and the Royal Greenwich Observatory for the use of their facilities and their assistance. The University of Durham and the Science Research Council are acknowledged for their financial support both in Durham and during visits abroad.

Richard Myers and Margaret Stout are to be thanked for their precise checking of this manuscript.The author's parents have provided great support throughout the entire research period and it is to them, that this work is dedicated.